

# UC Berkeley

## Dissertations

### Title

Commercial Vehicle Classification System using Advanced Inductive Loop Technology

### Permalink

<https://escholarship.org/uc/item/92x23786>

### Author

Tok, Yeow Chern Andre

### Publication Date

2008-12-01

---

University of California Transportation Center  
UCTC Dissertation No. 161

**Commercial Vehicle Classification System using  
Advanced Inductive Loop Technology**

Yeow Chern Andre Tok  
University of California, Irvine  
2008

UNIVERSITY OF CALIFORNIA  
IRVINE

Commercial Vehicle Classification System using  
Advanced Inductive Loop Technology

DISSERTATION

Submitted in partial satisfaction of the requirements  
for the degree of

DOCTOR OF PHILOSOPHY

in Civil Engineering

by

Yeow Chern Andre Tok

Dissertation Committee:  
Professor Stephen G. Ritchie, Chair  
Professor Wilfred W. Recker  
Professor Amelia C. Regan

2008



The dissertation of Yeow Chern Andre Tok  
is approved and is acceptable in quality and form for  
publication on microfilm and in digital formats:

---

---

---

Committee Chair

University of California, Irvine  
2008

# TABLE OF CONTENTS

	<i>Page</i>
<b>LIST OF FIGURES.....</b>	<b>viii</b>
<b>LIST OF TABLES.....</b>	<b>xiii</b>
<b>ACKNOWLEDGEMENTS .....</b>	<b>xv</b>
<b>CURRICULUM VITAE .....</b>	<b>xvii</b>
<b>ABSTRACT OF THE DISSERTATION .....</b>	<b>xxiii</b>
<b>CHAPTER 1 INTRODUCTION.....</b>	<b>1</b>
1.1 INFLUENCE OF COMMERCIAL VEHICLES .....	1
1.1.1 Economic.....	1
1.1.2 Air Quality .....	1
1.1.3 Traffic Performance .....	2
1.1.4 Pavement .....	2
1.1.5 Safety.....	3
1.2 SURVEILLANCE NEEDS .....	4
1.3 CURRENT VEHICLE SURVEILLANCE DEPLOYMENT .....	5
1.3.1 Limitations and Implications.....	7
1.4 PROPOSED SOLUTION.....	10
1.5 ORGANIZATION .....	11
<b>CHAPTER 2 BACKGROUND .....</b>	<b>15</b>
2.1 THE VEHICLE CLASSIFICATION PROBLEM .....	15
2.2 REVIEW OF VEHICLE CLASSIFICATION STUDIES .....	15
2.2.1 State of the Practice.....	15

2.2.2	Review of other technologies and algorithms .....	17
2.2.3	Critique of studies and results .....	21
2.2.4	Critique summary .....	23
2.3	HIGH FIDELITY INDUCTIVE SENSORS .....	24
2.3.1	Advanced Inductive Loop Detectors .....	24
2.3.2	Blade™ Inductive Sensors.....	29
2.3.3	Previous studies on Blade™ Inductive Sensors.....	32
<b>CHAPTER 3 STUDY SITES AND DATA DESCRIPTION .....</b>		<b>34</b>
3.1	UNIVERSITY OF CALIFORNIA, IRVINE AT BISON AVE .....	34
3.1.1	Site Description .....	34
3.1.2	Surveillance System Set-up.....	35
3.1.3	Data Description.....	37
3.2	SOUTHBOUND SAN ONOFRE TRUCK WEIGH AND INSPECTION FACILITY.....	37
3.2.1	Site Description .....	37
3.2.2	Surveillance System Set-up.....	39
3.2.3	Data Description.....	42
3.2.4	Data ground truth system design .....	44
<b>CHAPTER 4 SPEED PROFILE INTERPOLATION TEMPORAL-SPATIAL TRANSFORMATION .....</b>		<b>47</b>
4.1	BACKGROUND .....	47
4.2	THE SPEED PROFILE SIGNATURE TRANSFORMATION PROBLEM .....	48
4.2.1	Theoretical Framework .....	48
4.2.2	Proposed Sensor Technology .....	53
4.3	DATA ORGANIZATION .....	56
4.4	SIGNATURE PRE-PROCESSING.....	56
4.4.1	Signature Interpolation and Noise Filtering .....	56

4.4.2	Magnitude Normalization.....	57
4.5	METHODOLOGY .....	61
4.5.1	Speed Profile Estimation .....	61
4.5.2	Temporal-Spatial Transformation .....	68
4.6	RESULTS ANALYSIS .....	74
4.6.1	Evaluation of Control Vehicles in Test Dataset .....	74
4.6.2	Length Statistics within Vehicle Classes.....	75
4.6.3	Consistency of Signatures .....	78
4.7	DISCUSSIONS.....	80
<b>CHAPTER 5 GENERAL VEHICLE CLASSIFICATION .....</b>		<b>81</b>
5.1	CLASSIFICATION SYSTEM FRAMEWORK .....	81
5.2	DATA ORGANIZATION .....	82
5.3	SIGNATURE PRE-PROCESSING.....	82
5.4	MODEL DEVELOPMENT.....	83
5.4.1	Feature Extraction .....	83
5.4.2	Statistical Analysis of Input Features .....	85
5.4.3	Model Architecture .....	89
5.5	RESULTS ANALYSIS .....	93
<b>CHAPTER 6 COMMERCIAL VEHICLE AXLE CONFIGURATION CLASSIFICATION .....</b>		<b>95</b>
6.1	THE VEHICLE AXLE CONFIGURATION CLASSIFICATION PROBLEM .....	95
6.2	AXLE CONFIGURATION CLASSIFICATION SCHEME.....	96
6.3	DATA ORGANIZATION .....	96
6.4	METHODOLOGY .....	99
6.4.1	Wheel spike location determination .....	99
6.4.2	Axle assembly location and configuration determination .....	104
6.4.3	Axle Configuration Classification by Decision Trees .....	106



6.5	RESULTS ANALYSIS .....	110
<b>CHAPTER 7 COMMERCIAL VEHICLE BODY CLASSIFICATION.....</b>		<b>113</b>
7.1	CLASSIFICATION SCHEMES.....	113
7.1.1	Drive Unit Classification.....	113
7.1.2	Trailer Unit Classification .....	114
7.2	METHODOLOGY .....	116
7.2.1	Body Signature Extraction .....	116
7.2.2	Feature Extraction .....	117
7.2.3	Model Architecture .....	118
7.2.4	Data Description and Organization .....	122
7.3	RESULTS ANALYSIS .....	123
7.3.1	Drive Unit Classification Results .....	123
7.3.2	Trailer Unit Classification Results .....	126
7.4	COMBINED CLASSIFICATION PERFORMANCE .....	128
7.5	DISCUSSIONS.....	129
<b>CHAPTER 8 APPLICATIONS .....</b>		<b>130</b>
8.1	ACCURATE COMMERCIAL VEHICLE TRAVEL STATISTICS .....	130
8.1.1	Understanding Commercial Vehicle impacts from Port Activities .....	130
8.1.2	Non-port Related Freight Movement .....	132
8.2	VEHICLE RE-IDENTIFICATION IN UNSTABLE TRAFFIC CONDITIONS.....	134
8.2.1	Background .....	134
8.2.2	Feature Extraction .....	136
8.2.3	Repeatability Analysis.....	136
8.2.4	Discussion .....	142
8.3	PORTABLE TRAFFIC SURVEILLANCE SYSTEM .....	142
8.3.1	The need for temporary portable traffic surveillance .....	142

8.3.2	Proposed solution with surface mounted Blade™ inductive sensors.....	142
<b>CHAPTER 9 CONCLUDING REMARKS.....</b>		<b>144</b>
9.1	CONTRIBUTIONS .....	144
9.2	FUTURE RESEARCH .....	146
9.2.1	Investigation of Permanent Blade™ Inductive Sensors.....	146
9.2.2	Arterial Re-identification with Blade™ Inductive Sensors .....	146
<b>BIBLIOGRAPHY .....</b>		<b>147</b>

# LIST OF FIGURES

	<i>Page</i>
Figure 1.1. Typical Load Equivalency Factors (Source: WAPA, 2002) .....	3
Figure 1.2. Examples of different commercial vehicles with same axle configuration .....	8
Figure 1.3. Typical configuration of Automatic Vehicle Classifiers (AVCs).....	10
Figure 1.4. Relationship between major models in dissertation framework .....	13
Figure 2.1. Samples of Inductive Vehicle Signatures obtained from a 1.8m Round Inductive Loop Sensor .....	25
Figure 2.2. Advanced inductive loop detector cards installed in a traffic cabinet.....	26
Figure 2.3. Normal vs. distorted round inductive loop signatures.....	29
Figure 2.4. Example of Round and Blade™ inductive loop sensor signatures from a tractor with semi-trailer .....	31
Figure 2.5. Characteristics of a Blade™ inductive signature .....	32
Figure 3.1. Study site location in University of California, Irvine .....	35
Figure 3.2. Traffic flow at Bison Ave during data collection.....	38
Figure 3.3. Installation of double surface-mounted Blade™ inductive sensors at the San Onofre study site .....	39
Figure 3.4. Southbound San Onofre data collection study site.....	40
Figure 3.5. Sensor and equipment layout at San Onofre detector station.....	41
Figure 3.6. Wiring diagram of equipment setup at San Onofre.....	41

Figure 3.7. Traffic flow in San Onofre dataset .....	43
Figure 3.8. Speed distribution of vehicles in San Onofre dataset.....	43
Figure 3.9. Vehicle Classification Signature Data Query input .....	45
Figure 3.10. Commercial vehicle classification ground truth data entry system.....	46
Figure 4.1. Extracting time measures at equal intervals along a vehicle signature .....	50
Figure 4.2. Obtaining the speed profile from sampled speeds spanning a vehicle signature .....	51
Figure 4.3. Speed profile transformation of vehicle signature .....	53
Figure 4.4. Double Blade™ Inductive Sensors on Bison Ave in the University of California, Irvine.....	54
Figure 4.5. Comparison of double conventional round and Blade™ inductive signatures.....	55
Figure 4.6. Comparison of raw vs. interpolated and filtered Blade™ inductive signatures.....	58
Figure 4.7. Comparison between conventional magnitude normalization and MNR magnitude normalization.....	60
Figure 4.8. Error Sensitivity with respect to Signature Gradients.....	62
Figure 4.9. Analysis of slopes computed from normalized and smoothed Blade™ inductive signature .....	63
Figure 4.10. Estimation of vehicle speed profile.....	66
Figure 4.11. Sample of Blade™ Inductive Signatures with Corresponding Speed Profiles .....	67

Figure 4.12. Obtaining signature headway for Conventional Speed-trap Temporal-Spatial (COSTS) transformation .....	69
Figure 4.13. Comparison of vehicle signatures and estimated vehicle lengths obtained via SPRINTS vs. COSTS Transformation .....	70
Figure 4.14. Control vehicle inductive signatures under different driving conditions .....	73
Figure 4.15. Comparison of standard deviation changes with Maximum Time Segment values.....	74
Figure 4.16. Comparison of signature distortion before and after SPRINTS transformation .....	79
Figure 5.1. Extracting NOMAD features from a Blade inductive signature .....	84
Figure 5.2. Artificial neuron with activation function.....	90
Figure 5.3. General Vehicle Classification (G-VeC) model Multi-Layer Feedforward (MLF) neural network architecture.....	91
Figure 6.1. Drive unit axle sub-classification.....	97
Figure 6.2. Trailer unit axle sub-classification .....	97
Figure 6.3. Sample double Blade™ inductive vehicle signatures with three non- negative domain wheel spikes.....	100
Figure 6.4. False wheel spike wrongly detected in Blade™ inductive signature .....	102
Figure 6.5. Sensitivity Analyses of Gradient Threshold (GT) and Peak Width Threshold (PWT) on Average Axle Count Errors.....	103
Figure 6.6. Sensitivity Analyses of Slope and Spike Width Threshold on Axle Count Accuracy (ACA).....	104

Figure 6.7.	Detected Wheels Spikes and Axle Assemblies (Clusters) in a Blade™ signature .....	106
Figure 6.8.	Sample double Blade™ inductive signatures with indistinct steering wheel spikes .....	108
Figure 6.9.	Axle Configuration Classification Model .....	109
Figure 7.1.	Drive unit body classification .....	114
Figure 7.2.	Trailer unit body classification.....	115
Figure 7.3.	Sample of extracted of drive and trailer unit body signatures.....	116
Figure 7.4.	Extraction of drive unit body signature features .....	119
Figure 7.5.	Extraction of trailer unit body signature features.....	120
Figure 7.6.	Assignment of vehicles to drive unit body classification sub-models by axle classification .....	121
Figure 7.7.	Sample output from the Commercial Vehicle Vector Classification System .....	128
Figure 8.1.	Travel patterns of port-related commercial vehicles by trailer type .....	131
Figure 8.2.	Travel patterns of 40' box trailers by drive unit type.....	132
Figure 8.3.	Travel patterns of non-port related freight trucks .....	133
Figure 8.4.	Comparison of Signature Repeatability (SRI) Index for each control vehicle ordered by duration standard deviation .....	138
Figure 8.5.	Comparison of 30-point interpolated control vehicle signature samples before (left) and after SPRINTS transformation (right) of control vehicles BMW 325is-1 and BMW 325is-2.....	140

Figure 8.6. Comparison of 30-point interpolated control vehicle signature samples before (left) and after SPRINTS transformation (right) of control vehicles Alfa Romeo Spider and Acura Integra..... 141

Figure 8.7. Components of a portable advanced inductive loop detector system ..... 143

## LIST OF TABLES

		<i>Page</i>
Table 1.1.	FHWA Scheme F Classification .....	7
Table 2.1.	California-Modified FHWA Vehicle Classification Scheme.....	16
Table 4.1.	Comparison of Estimated Control Vehicles Lengths in Calibration Dataset (March 7 2008).....	71
Table 4.2.	Length statistics from control vehicles in test dataset (April 15 2008).....	75
Table 4.3.	Comparison of Estimated Lengths by Vehicle Types from Mar 7 2008 Calibration Dataset .....	77
Table 4.4.	Comparison of Estimated Lengths by Vehicle Types from Apr 15 2008 Test Dataset .....	77
Table 5.1	General Vehicle Classification (G-VEC) Scheme .....	81
Table 5.2.	Pearson’s correlation analysis on extracted Blade™ inductive signature features.....	86
Table 5.3.	Levene’s homogeneity-of-variance test on extracted Blade™ inductive signature features.....	87
Table 5.4.	Rank results by vehicle class for each input feature .....	88
Table 5.5.	Kruskal-Wallis one-way analysis of variance test on extracted Blade™ inductive signature features.....	88
Table 5.6	Trained G-VEC model cross-classification results on training dataset.....	93
Table 5.7.	Trained G-VEC model cross-classification results on test dataset .....	94



Table 6.1.	Expanded Axle Configuration Classification Scheme .....	98
Table 6.2.	Axle Configuration Classification Results .....	111
Table 6.3.	Axle Configuration Test Data Cross-Classification Results .....	112
Table 7.1.	Type I Drive Body Configuration classification results.....	124
Table 7.2.	Type I Drive Body Configuration test data cross classification results .....	125
Table 7.3.	Type II Drive Body Configuration classification results .....	125
Table 7.4.	Type II Drive Body Configuration test data cross classification results .....	126
Table 7.5.	Trailer Body Configuration classification results .....	127
Table 7.6.	Trailer Body Configuration test data cross classification results .....	127
Table 8.1.	Signature Repeatability Index (SRI) results for control vehicles.....	138

## ACKNOWLEDGEMENTS

I would like to express the deepest appreciation to my committee chair, Professor Stephen Ritchie, who has been a mentor par excellence. He has provided me with the most insightful critiques of my research and helped me develop a larger perspective of my research goals and interests. I could not have had a more fulfilling experience earning my doctorate under anyone else.

I would like to thank my committee members, Professor Wilfred Recker and Professor Amelia Regan for their support and guidance.

I would like to thank my colleagues at the University of California, Irvine Institute of Transportation Studies, past and present, who have helped me in my professional development and have made my graduate student experience such an enriching one.

I extend my gratitude to the California Department of Transportation field staff that has helped me with my data collection efforts, with special mention to John Slonaker from the Department of Research and Innovation and Nadine Martins from District 11, for their assistance in field logistics that often transcended their call-of-duty.

I also appreciate Steven Hilliard and Geoff Yerem of Inductive Signature Technologies (IST) for providing the Blade™ inductive sensors and technical support.

In addition, I would like to thank the California Highway Patrol officers and inspectors at the San Onofre Truck Weigh and Inspection Facility. They have been instrumental in their assistance with traffic control and operations to ensure smooth and uneventful sensor installations and data collections.

I extend my appreciation to the University of California, Irvine Parking and Transportation Services for graciously allowing me to conduct the data collection experiments at Bison Ave in the University of California, Irvine as well as providing the necessary traffic diversion operations during sensor installation.

I am especially grateful to my parents for showing me unwavering support and belief.

Lastly, I reserve my most heartfelt appreciation and gratitude to my wife – the love of my life. She has offered incredible patience, and maintained steadfast belief and trust, even in times when I started to lose hope. She has provided the emotional and physical support, and has turned the otherwise hectic and stressful final lap of this dissertation into such a wonderful, positive experience. This accomplishment would pale in insignificance without having her to share it with. I'm tremendously grateful to share my life with such a phenomenal person.

Financial support was provided by the University of California Transportation Center (UCTC), California Partners for Advanced Transit and Highways (PATH) and California Department of Transportation (CalTrans).

# CURRICULUM VITAE

**Yeow Chern Andre Tok**

## EDUCATION

**Ph.D., Civil Engineering, 2008**

University of California, Irvine

Dissertation: Commercial Vehicle Classification System using Advanced Inductive Loop Technology

**M.S., Civil Engineering, 2004**

University of California, Irvine

**B. Eng., Civil Engineering (Honors), 2002**

National University of Singapore

Thesis: Expressway Incident Detection Using Advanced Algorithms

## RESEARCH EXPERIENCE

**Graduate Student Researcher, 2002-2008**

University of California, Irvine

**A New Approach to Real-Time Commercial Vehicle Monitoring, 2007-2008**

- Designed sensor configurations of permanent Blade™ inductive sensors and Sensys™ wireless magnetometer sensors for testbed installation
- Prepared permit application to Caltrans for installation of permanent Blade™ inductive sensors and Sensys™ wireless magnetometer sensors
- Coordinated installation of permanent Blade™ inductive sensors and Sensys™ wireless magnetometer sensors
- Investigated optimal configuration of permanent Blade™ inductive sensors for advanced commercial vehicle surveillance
- Investigated feasibility of Sensys™ wireless magnetometer sensors for advanced commercial vehicle surveillance

**User-based Segmentation of the US Market for Urban Traffic Control Systems, 2007**

- Analyzed socio-demographic statistical data as well as data describing ITS spending levels using advanced statistical methods
- Performed phone and face to face interviews to 12 city agencies (48 in total for the whole team)
- Analyzed resulting intelligence to generate market segments.

### **Testbed Technical Assistance and Development Program, 2006-2008**

- Designed sensor configurations of surface-mounted Blade™ inductive sensors for testbed installation
- Coordinated Installation of surface-mounted Blade™ inductive sensors
- Formulated the vehicle speed profile transformation problem
- Developed vehicle speed profile transformation model for correcting inductive loop signatures distorted by acceleration effects based on surface-mounted Blade™ inductive sensors
- Developed improved single loop speed estimation model using inductive loop signatures from single round inductive loop sensors

### **Corridor Deployment and Investigation of Anonymous Vehicle Tracking for Real-Time Traffic Performance Measurement, 2004-2006**

- Designed and conducted vehicle signature data collection for freeway traffic in Irvine and Anaheim
- Designed and conducted vehicle signature data collection for commercial vehicles at San Onofre Truck Weigh and Inspection Facility
- Developed vector classification framework for commercial vehicles
- Developed commercial vehicle classification model based on surface-mounted Blade™ inductive sensors
- Developed Interactive Real-Time Performance Measurement System Database framework and Website based on Anonymous Vehicle Tracking

### **Anonymous Vehicle Tracking for Real-Time Freeway and Arterial Street Performance Measurement, 2003-2004**

- Designed and conducted vehicle signature data collection for freeway traffic in Irvine
- Developed Real-Time Freeway Level-of-Service Performance Measurement System

### **Field Investigation of Advanced Vehicle Reidentification Techniques and Detector Technologies – Phase 2, 2002-2004**

- Performed volume accuracy analysis of vehicle inductive signature and V2SAT vehicle image data

## **TEACHING EXPERIENCE**

### **Teaching Assistant, 2003-2004**

University of California, Irvine

### **Transportation Systems I: *Highway Design and Analysis*, Fall 2004**

- Led discussion and lab groups
- Taught in lecture
- Organized field trip

### **Civil Engineering Practicum I: *Introduction to AutoCAD*, Spring 2004**

- Led lab groups

- Taught in lecture

**Civil Engineering Practicum II: *Introduction to Civil Engineering*, Winter 2004**

- Led discussion groups
- Designed lab and homework assignments
- Taught in lecture

**Transportation Systems I: *Highway Design and Analysis*, Fall 2003**

- Led discussion and lab groups

**Civil Engineering Practicum II: *Introduction to Civil Engineering*, Spring 2003**

- Led discussion groups
- Designed lab and homework assignments
- Taught in lecture

**Civil Engineering Practicum I: *Introduction to AutoCAD*, Winter 2003**

- Led lab groups

**PUBLICATIONS**

**Journal Articles**

**C. Oh, A. Tok, S. G. Ritchie, 2005. Real-Time Freeway Level of Service Based on Anonymous Vehicle Reidentification**

IEEE Transactions on Intelligent Transportation Systems, Vol. 6(2) pp 138 – 146.

**A. Tok, S. G. Ritchie, 2008. Commercial Vehicle Vector Classification through New High Fidelity Inductive Sensors**

Transportation Research C, in preparation.

**Proceedings Papers**

**A. Tok, S. G. Ritchie, S. Jeng, 2007. Understanding Commercial Vehicle Travel through New High Fidelity Inductive Sensors**

In proceedings of the 86<sup>th</sup> Annual Meeting of the Transportation Research Board (CD-ROM), Washington D.C.

**S. Jeng, S. G. Ritchie, A. Tok, 2007. Freeway Corridor Performance Measurement Based on Vehicle Reidentification**

In proceedings of the 86<sup>th</sup> Annual Meeting of the Transportation Research Board (CD-ROM), Washington D.C.

**C. Oh, A. Tok, S. G. Ritchie, 2004. Real-Time Freeway Level of Service Based on Anonymous Vehicle Reidentification**

In proceedings of the 83<sup>rd</sup> Annual Meeting of the Transportation Research Board (CD-ROM), Washington D.C.

## **Reports**

**S. G. Ritchie, S. Jeng, A. Tok, 2007. Corridor Deployment and Investigation of Anonymous Vehicle Tracking for Real-Time Traffic Performance Measurement**

California PATH Research Report.

**S. G. Ritchie, S. Park, C. Oh, S. Jeng, A. Tok, 2005. Anonymous Vehicle Tracking for Real-Time Freeway and Arterial Street Performance Measurement**

California PATH Research Report, UCB-ITS-PRR-2005-9.

**S. G. Ritchie, S. Park, C. Oh, S. Jeng, A. Tok, 2005. Field Investigation of Advanced Vehicle Reidentification Techniques and Detector Technologies – Phase 2**

California PATH Research Report, UCB-ITS-PRR-2005-8.

## **PRESENTATIONS**

**A. Tok, S. Jeng, H. Liu, S. G. Ritchie, 2008. Design and Initial Implementation of an Inductive Signature-Based Real-Time Traffic Performance Measurement System**

Accepted for presentation at the 11th International IEEE Conference on Intelligent Transportation Systems (ITSC2008), Beijing, China.

**A. Tok, S. G. Ritchie, 2008. Commercial Vehicle Classification System Using Advanced Inductive Loop Technology**

Presented at the Western Traffic Data Conference, Irvine, CA.

**A. Tok, S. G. Ritchie, 2008. Commercial Vehicle Classification System Using Advanced Inductive Loop Technology**

Presented at the 14<sup>th</sup> Annual University of California Transportation Research Conference, Santa Barbara, CA

**H. Liu, S. G. Ritchie, A. Tok, 2008. Visualization of Real-time Traffic Performance Measurements on Google Maps**

Presented at the 14<sup>th</sup> Annual University of California Transportation Research Conference, Santa Barbara, CA

**A. Tok, S. G. Ritchie, S. Jeng, 2007. Understanding Commercial Vehicle Travel through New High Fidelity Inductive Sensors**

Presented at the 86<sup>th</sup> Annual Meeting of the Transportation Research Board, Washington D.C.

**S. Jeng, S. G. Ritchie, A. Tok, 2007. Freeway Corridor Performance Measurement Based on Vehicle Reidentification**

Presented at the 86<sup>th</sup> Annual Meeting of the Transportation Research Board, Washington D.C.

**C. Oh, A. Tok, S. G. Ritchie, 2004. Real-Time Freeway Level of Service Based on Anonymous Vehicle Reidentification**

Presented at the 83<sup>rd</sup> Annual Meeting of the Transportation Research Board, Washington D.C.

**C. Oh, A. Tok, S. G. Ritchie, 2004. Real-Time Freeway Level of Service Based on Anonymous Vehicle Reidentification**

Presented at the 10<sup>th</sup> Annual University of California Transportation Research Conference, Davis, CA.

**A. Tok, R. L. Cheu, 2003. Expressway Incident Detection Using Advanced Algorithms**

Presented at the 9<sup>th</sup> Annual University of California Transportation Research Conference, Los Angeles, CA.

### **WORKING PAPERS**

**A. Tok, S. G. Ritchie, 2008. Better Distinction of Vehicle Types through the Correction of Acceleration-distorted Inductive Signatures in Arterial Traffic**  
UCI-ITS Working Paper

**A. Tok, S. Hernandez, S. G. Ritchie, 2008. Accurate individual vehicle speeds from single inductive loop signatures**

Submitted for presentation at the 88<sup>th</sup> Annual Meeting of the Transportation Research Board, Washington D.C.

**H. Liu, S. Jeng, A. Tok, S. G. Ritchie, 2008. Commercial Vehicle Classification using Vehicle Signature Data**

Submitted for presentation and publication at the 88<sup>th</sup> Annual Meeting of the Transportation Research Board, Washington D.C.

### **HONORS**

**Dissertation Grant Award, 2007**

University of California Transportation Center

**Most Promising Future Faculty Member Nomination, 2004 & 2005**

Henry Samueli School of Engineering, University of California, Irvine

### **COMPUTER SKILLS**

Programming Languages: MATLAB, Java, Visual Basic

Traffic Simulation: PARAMICS, TransCAD, TranPlan, Synchro

Optimization Modeling: C-Plex

Mapping: ArcGIS

CAD/CAM: AutoCAD

Database: Oracle, Access



Web Development: JDeveloper

### **PROFESSIONAL MEMBERSHIPS**

Institute of Transportation Engineers (ITE)	Student Member
Transportation Research Board (TRB)	Student Member
TRB Freight Transportation Data Committee	Friend

### **REFERENCES**

Professor Stephen Ritchie, Director of Institute of Transportation Studies, University of California, Irvine. (949) 824-4214, sritchie@uci.edu.

Professor Wilfred Recker, Department of Civil Engineering, University of California, Irvine. (949) 824-5642, wwrecker@uci.edu

Associate Professor Amelia Regan, Department of Computer Science, University of California, Irvine. (949) 824-1871, aregan@uci.edu.

Associate Professor R. Jayakrishnan, Department of Civil Engineering, University of California, Irvine. (949) 824-2172, rjayakri@uci.edu.

# **ABSTRACT OF THE DISSERTATION**

Commercial Vehicle Classification System using  
Advanced Inductive Loop Technology

By

Yeow Chern Andre Tok

Doctor of Philosophy in Civil Engineering

University of California, Irvine, 2008

Professor Stephen G. Ritchie, Chair

Commercial vehicles typically represent a small fraction of vehicular traffic on most roadways. However, their influence on the economy, environment, traffic performance, infrastructure, and safety are much more significant than their diminutive numerical presence suggests.

This dissertation describes the development and prototype implementation of a new high-fidelity inductive loop sensor and a ground-breaking commercial vehicle classification system based on the vehicle inductive signatures obtained from this sensor technology. This new sensor technology is relatively easy to install and has the potential to yield reliable and highly detailed vehicle inductive signatures for advanced traffic surveillance applications.

The Speed PProfile INterpolation Temporal-Spatial (SPRINTS) transformation model developed in this dissertation improves vehicle signature data quality under adverse traffic conditions where acceleration and deceleration effects can distort inductive vehicle signatures. The axle classification model enables commercial vehicles to be classified accurately by their axle configuration. The body classification models reveal the function and unique impacts of the drive and trailer units of each commercial vehicle.

Together, the results reveal the significant potential of this inductive sensor technology in providing a more comprehensive commercial vehicle data profile based on a unique ability to extract both axle configuration information as well as high fidelity undercarriage profiles within a single sensor technology to provide richer insight on commercial vehicle travel statistics.

# **CHAPTER 1 INTRODUCTION**

## **1.1 INFLUENCE OF COMMERCIAL VEHICLES**

Commercial vehicles represent a small fraction of vehicular traffic on most roadways. However, their influence on the economy, environment, traffic performance, infrastructure, and safety are much more significant than their diminutive numerical presence suggests.

### **1.1.1 Economic**

Commercial vehicles are the mode of choice for freight transportation in California: 65.9 percent by weight, and 73.5 percent by value representing \$6,200.5 million (USDOT, 2003), and their traffic volume is expected to grow throughout the state over the next 20 years (FHWA, 2002). Hence, the performance of the commercial vehicle transportation system has direct implications on the economy.

### **1.1.2 Air Quality**

Freight movements increasing contribute to air pollution (USDOT, 2003). There has been increased concern about health and environmental impacts due to emissions of nitrogen oxides (NO<sub>x</sub>) and particulate matter (PM) from commercial vehicles, which are

predominantly powered by diesel engines. In addition, freight transportation also contributes significantly to greenhouse gas emissions that lead to global climate change. Heavy commercial vehicles are by far the largest contributor to freight emissions in the United States, accounting for two-thirds of NO<sub>x</sub> and PM-10 from the freight sector (FHWA, 2006).

### **1.1.3 Traffic Performance**

Due to their large size and mass, medium and large commercial vehicles often travel slower, have slower acceleration rates and require much larger braking distances. These characteristics are more seriously amplified at steep grades, where their enormous masses place an even greater strain on their handling limits. Consequently, they may create slow moving bottlenecks and have an adverse impact on traffic performance of roadway sections, which warrants the need to better understand their travel characteristics (Newell, 1998). This concern has led several studies to investigate the traffic performance impacts of commercial vehicles as well as potential operational solutions (Benekohal et al., 1999, Crainic et al., 2004, Peeta et al., 2004, Yun et al., 2005, Laval, 2007).

### **1.1.4 Pavement**

According to the American Association of State Highway and Transportation Officials (AASHTO) Design Guide, commercial vehicles have a far more significant impact on pavement service life when compared to passenger vehicles, despite their smaller

proportion in vehicular traffic. Medium and large commercial vehicles rarely exceed fifteen percent of vehicular traffic volume. Still, the loading from a single 18,000 pound axle load of a typical heavy commercial vehicle is equivalent to about 4,000 times the axle loading of a large sport utility vehicle for a typical pavement. Hence, the impact on the pavement service life from a large commercial vehicle vastly exceeds its under-representation in vehicular traffic. Figure 1.1 shows a comparison of equivalent 18,000 pound axle loads (ESALs) for various vehicle types, contrasting the impacts of passenger vehicles from other commercial vehicles.

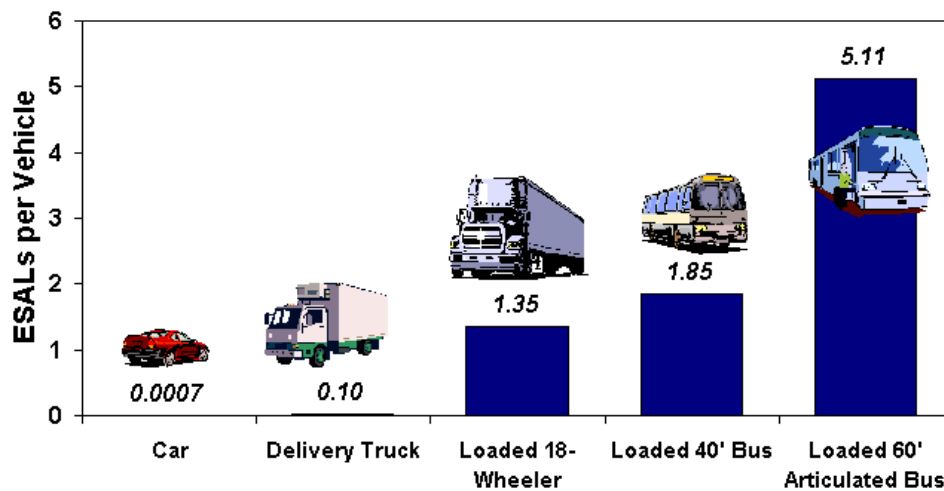


Figure 1.1. Typical Load Equivalency Factors (Source: WAPA, 2002)

### 1.1.5 Safety

Studies on commercial vehicle safety impacts have confirmed that accidents involving large commercial vehicular traffic are often severe with higher fatality rates, due to their

larger profile and mass compared with passenger vehicles (Braver et al., 1997, Lyman and Braver, 2003, FCMSA, 2007). However, there has been a lack of comprehensive and reliable measures of commercial vehicle exposure to facilitate an accurate appreciation of their adverse safety impacts (Brown et al., 2003).

## **1.2 SURVEILLANCE NEEDS**

For these abovementioned reasons, there has been a strong emphasis by the Federal Highway Administration to better understand commercial vehicle travel and its impacts.

In an attempt to achieve this objective, highway agencies have been encouraged to collect classification data in place of simple volume counts whenever possible. This is because directly measured classification data is needed to better understand truck travel on highways, while statistics obtained via adjustment factors estimates are frequently biased and hence discouraged (FHWA, 2001).

One compelling reason for discouraging the use of adjustment factors is that commercial vehicles have very different travel patterns compared with passenger vehicles at daily, weekly and seasonal levels (Hallenbeck and Kim, 1993). As a consequence, it is difficult to obtain factors that provide reliable results. Furthermore, seasonal adjustment factors are difficult to develop. For these reasons, few states use seasonal adjustment factors or have plans to develop them (Stamatiadis and Allen, 1997).

Hence, the use of adjustment factors to estimate the volume of commercial vehicles in vehicle traffic volume appears more as a stop-gap measure than an ideal long-term solution. The use of temporary vehicle classifiers do not provide adequate means to understand the patterns of travel behavior among commercial vehicles for obtaining the required adjustment factors to obtain unbiased and accurate commercial vehicle volume counts (FHWA, 2001).

### **1.3 CURRENT VEHICLE SURVEILLANCE DEPLOYMENT**

In California and the United States, the most prevalent type of classification method is the use of axle counts and configuration to determine vehicle classification. This is achieved through the use of piezo and weigh-in-motion (WIM) sensors at WIM stations and piezo sensors at Automatic Vehicle Classifier (AVC) stations. Piezo sensors provide axle counts and axle spacing configurations while WIM sensors provide axle loadings in addition to the information provided by piezo sensors. There are currently 106 active permanent WIM data stations located throughout California on major freeways (CALTRANS, 2008).

Although present WIM data stations are located on major transshipment routes along freeways, many other routes are still not equipped with WIM data stations. Without a thorough study of commercial travel behavior, it is questionable whether the present WIM data stations are adequate to measure the influence of truck travel on the expansive traffic network. A vast expansion of the current locations of WIM data sites is



prohibitive, due to their costly and labor-intensive pavement intrusive installations that require extensive lane-closures. In addition, WIM sensors are very sensitive to installation quality. For example, if the sensors are not installed flush with the pavement, they induce dynamic motion on axle loadings which adversely affects the accuracy of measurement. And unlike inductive loop sensors, WIM sensors require regular calibration to maintain their accuracy and are also especially vulnerable to large temperature variations (Hallenbeck and Weinblatt, 2004).

Because of the above-mentioned constraints of WIM data stations, AVCs are currently the preferred detector choice for collecting commercial vehicle volume data to obtain classification data. AVCs are generally set up to collect vehicle counts and classify them into 13 categories based on their axle configuration according to the FHWA Scheme F (See Table 1.1) as defined in the Traffic Monitoring Guide (FHWA, 2001).

Table 1.1. FHWA Scheme F Classification

<b>Class</b>	<b>Description</b>
1	Motorcycles
2	Passenger Vehicles
3	Other Two-Axle, Four-Tire, Single-Unit Vehicles
4	Buses
5	Two-Axle Six-Tire Single Units
6	Three-Axle Single Units
7	Four-or-More Axle, Single Units
8	Four-or-Fewer Axle Single Trailers
9	Five-Axle Single Trailers
10	Six-or-More Axle Single Trailers
11	Five-or-Less Axle Multi Trailers
12	Six-Axle Multi Trailers
13	Seven-or-More Axle Multi Trailers

### 1.3.1 Limitations and Implications

The above-mentioned FHWA scheme F provides quite a comprehensive distinction of axle configuration categories in the vehicle population, with 11 out of 13 categories assigned to commercial vehicle types. However, this may not be sufficient to provide adequate understanding of commercial vehicle travel behavior. This is because commercial vehicles that share similar axle configurations may perform very different functions, have different trip origins and destinations, have different axle loads, and may pose different types of environmental hazards depending on the types of freight they carry. Hence, the heterogeneity of commercial vehicles within the same axle-based

configuration limits the understanding of commercial vehicle travel and their impacts based on the current classification scheme. Figure 1.2 shows examples of vehicles serving different functions sharing similar axle configuration. According to the FHWA (refer to Table 1.1) and the modified California classification schemes (refer to Table 2.1), these vehicles would receive identical classification despite their inherent functional differences.



(a) Single Unit 3-axle Trucks

(b) 5-axle Single Trailers

Figure 1.2. Examples of different commercial vehicles with same axle configuration

Because of the inability to differentiate commercial vehicles by function in the present system, there is a need to classify commercial vehicles in a scheme that results in more meaningful data which allows better understanding of their travel patterns.

In addition, there is currently no publicly available comprehensive commercial vehicle travel data. While such information may be available within private carriers, they are not generally obtainable by public agencies. Without the knowledge of their specific travel patterns, it is difficult to measure supply and demand influences on commercial vehicle travel and provide forecasts of commercial vehicle travel and impacts.

Furthermore, piezo sensor-based AVCs used to generate the FHWA Scheme F classifications require vehicles to traverse the sensors at a constant speed to obtain accurate axle spacing measures. These systems also require a large sensor configuration footprint because they use inductive loop presence detectors as shown in Figure 1.3. Hence, they may not perform accurately under congested traffic conditions where significant vehicle acceleration and deceleration over sensors exist, and where reduced vehicle headways may allow a tail-gating vehicle to enter the sensor's field of detection before the previous vehicle leaves. This can cause multiple vehicles to be detected as single vehicles – resulting in both under-counting of traffic volume and erroneous axle classifications.

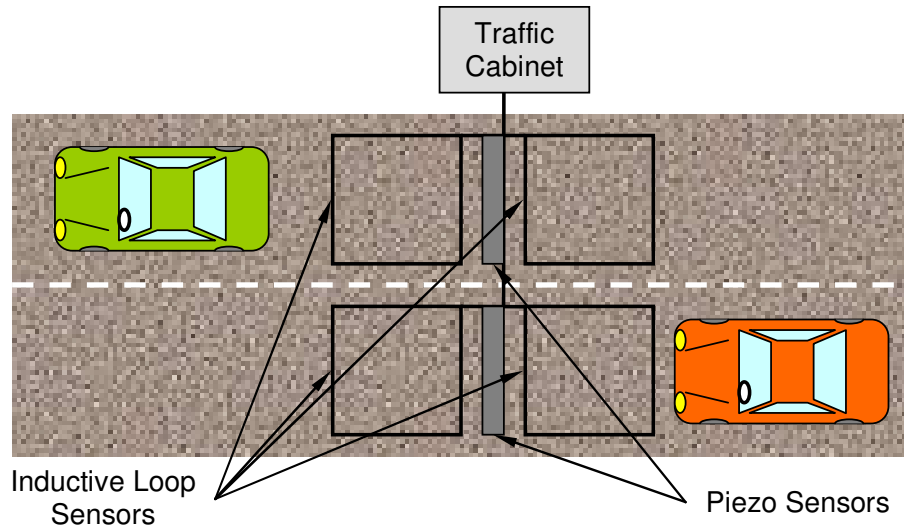


Figure 1.3. Typical configuration of Automatic Vehicle Classifiers (AVCs)

#### 1.4 PROPOSED SOLUTION

This dissertation describes the development of a ground-breaking modular commercial vehicle classification system based on a prototype implementation of a new high-fidelity inductive loop sensor called the Blade™ (IST, 2006). This new sensor technology is relatively easy to install and has the potential to yield highly detailed vehicle inductive signatures for advanced traffic surveillance applications. The system comprises four main models: the Speed PProfile INterpolation Temporal-Spatial (SPRINTS) transformation model, the General Vehicle Classification (G-VeC) model, the Commercial Vehicle Axle Classification model and the Commercial Vehicle Drive and Trailer Body Classification model.

The SPRINTS transformation model developed in this dissertation will improve vehicle signature data quality under adverse traffic conditions where acceleration and deceleration effects can distort inductive vehicle signatures. This will enable reliable extraction of input features from Blade™ inductive vehicle signatures for accurate traffic measures regardless of traffic conditions.

The G-VeC model will provide preliminary classification to distinguish between passenger vehicles, buses, light commercial vehicles, and medium and heavy commercial vehicles. The axle classification model will enable medium and heavy commercial vehicles to be classified accurately by their axle configuration. The body classification models will reveal the function and unique impacts of the drive and trailer units of each commercial vehicle. Together, these models exploit the potential of this inductive sensor technology to provide a more comprehensive commercial vehicle data profile based on its unique ability to simultaneously extract both axle configuration information as well as high fidelity undercarriage profiles within a single sensor technology to provide richer insight on commercial vehicle travel statistics.

## **1.5 ORGANIZATION**

The organization and description of the following chapters of this dissertation is explained in the following paragraphs:

Chapter 2 provides the background and the motivation of this study, which expounds on the multi-faceted impacts of commercial vehicles as well as a comprehensive review of previous research studies related to vehicle classification models. This is followed by a description of the sensor and detector technologies chosen for development of the models in this dissertation.

Chapter 3 presents an overview of the site locations used to collect the data used in the development of models in this dissertation. It also describes the overall design of data collection exercises performed and presents a summary of the data characteristics.

Chapters 4 through 7 describe the major model developments in this dissertation. The relationship between the models is illustrated in Figure 1.4.

Chapter 4 describes the SPRINTS transformation model that is used to correct Blade™ inductive vehicle signatures that have been distorted by vehicle acceleration and deceleration effects. This enables accurate classification of vehicles even under congested freeway conditions and in arterial sections where the assumption of constant speed over sensors does not prevail. The corrected signature from this model can then be used as inputs to models described in the subsequent chapters.

Chapter 5 describes the G-VeC model used to distinguish between passenger vehicles, small commercial vehicles, and medium and large commercial vehicles from the model outputs of the SPRINTS transformation model described in Chapter 4. Vehicles

classified as medium and large commercial vehicles are subsequently analyzed in further detail in Chapter 6 and Chapter 7.

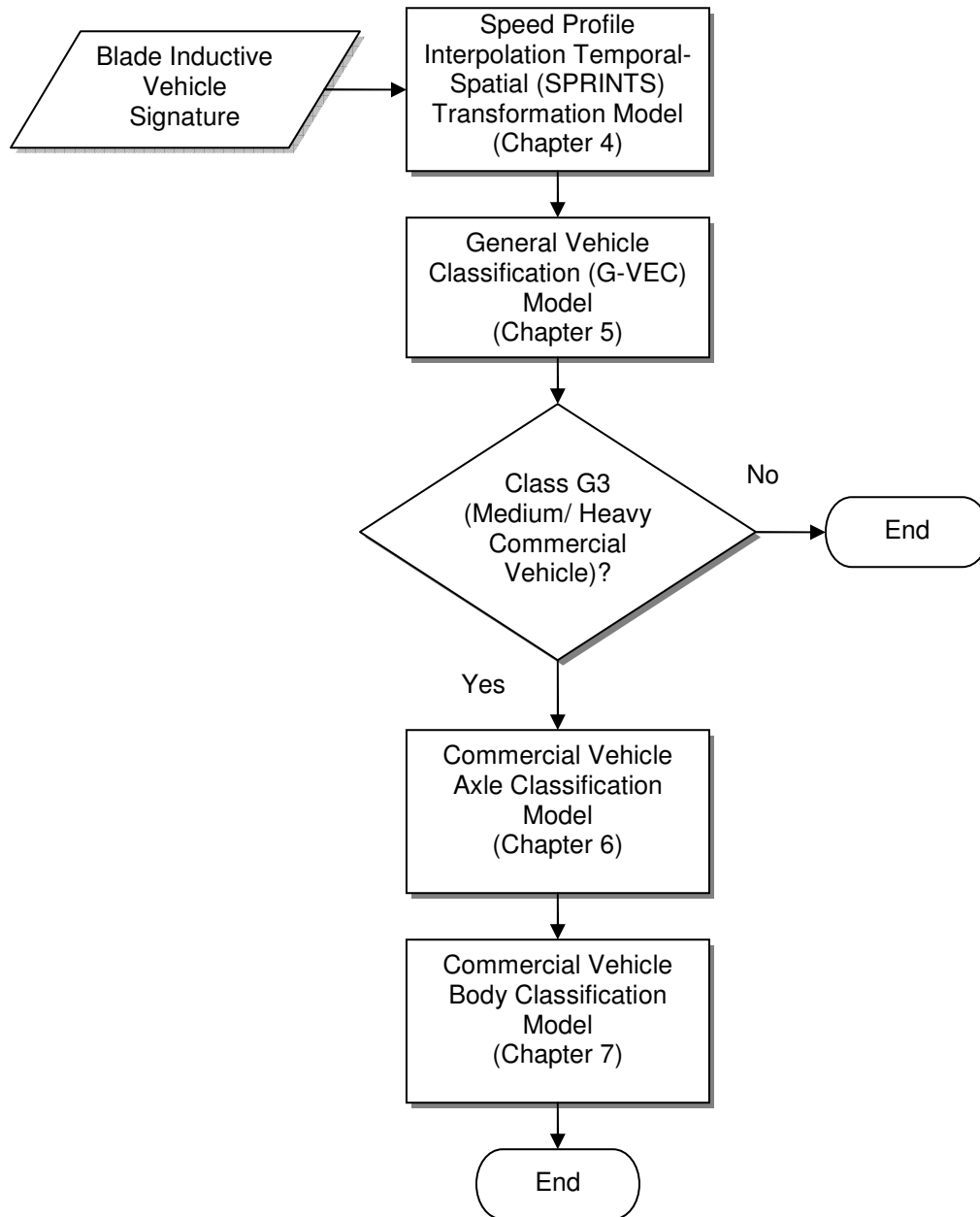


Figure 1.4. Relationship between major models in dissertation framework



Chapter 6 describes the development of a new and more detailed medium and heavy commercial vehicle axle configuration classification model through the detection of axle groupings and in-group configuration within the Blade™ inductive signature. The detailed axle classification information is used to provide better axle configuration information of commercial vehicles as well as for inputs to the commercial vehicle body classification model described in Chapter 7.

Chapter 7 presents the drive and trailer unit body classification models. These classification models provide more detailed profile that can yield further insight into the multi-faceted impacts of commercial vehicles.

Chapter 8 describes the further applications of the models developed in this dissertation. Sample case studies are also presented to enable the reader to appreciate the impacts of implementing the system described in this dissertation.

Chapter 9 presents the concluding remarks of this study, including contributions of this research to the field of transportation engineering and policy implications as a result of implementing the system developed in this dissertation. It also provides an overview of potential research areas that should be investigated as part of a continuing effort to this study.

## **CHAPTER 2 BACKGROUND**

### **2.1 THE VEHICLE CLASSIFICATION PROBLEM**

Vehicle classification involves the mapping of high dimensional feature data into groups based on predefined vehicle characteristics. The mapping algorithm can take the form of pattern recognition techniques such as artificial neural networks where all features are analyzed simultaneously, or heuristics such as decision trees where features are examined according to a pre-determined hierarchical order.

### **2.2 REVIEW OF VEHICLE CLASSIFICATION STUDIES**

#### **2.2.1 State of the Practice**

The current state of the practice in the United States uses the FHWA Scheme F classification for identifying different types of vehicles on the roadway (FHWA, 2001). This vehicle classification scheme is based on axle configuration, and uses a decision tree approach using axle spacings as input features to identify thirteen different vehicle classes of which eleven are commercial vehicle types as shown in Table 1.1. The state of California adopts a slightly modified scheme from the FHWA Scheme F as shown in Table 2.1. It adds an additional class to distinguish three-axle trucks pulling two-axle full trailers from three-axle semi-tractors pulling two-axle semi-trailers – both of which are

classified as class 9 five-axle single trailer vehicles under the FHWA scheme F classification. A fifteenth class is designated for vehicles that do not belong to any of the first fourteen categories. Vehicle axle configurations for both schemes are collected via Automatic Vehicle Classifiers (AVCs), which are primarily piezo sensors straddled fore and aft by inductive loop sensors as shown previously in Figure 1.3. The loop sensors indicate the presence of a vehicle as it traverses the sensors while the piezo sensors determine the axle configuration of the detected vehicle (FHWA, 2001).

Table 2.1. California-Modified FHWA Vehicle Classification Scheme

<b>Class</b>	<b>Description</b>
1	Motorcycles
2	Passenger Cars
3	Other Two-Axle, Four-Tire, Single-Unit Vehicles
4	Buses
5	Two-Axle, Six-Tire, Single-Unit Trucks
6	Three-Axle, Single-Unit Trucks
7	Four-or-More Axle, Single-Unit Trucks
8	Four-or-Less Axle, Single-Trailer Trucks
9	Five-Axle, Single-Semi Trailer Trucks
10	Six-or-More Axle, Single-Trailer Trucks
11	Five-or-Less Axle, Multi-Trailer Trucks
12	Six-Axle, Multi-Trailer Trucks
13	Seven-or-More Axle, Multi-Trailer Trucks
14	5 axle , 3 axle tractor pulling a full 2 axle trailer
15	Unclassified

One common misclassification error experienced by axle-based classification schemes is caused by the overlap of axle counts and spacing configuration of different categories, such as between buses and trucks (Lyles and Wyman, 1983). In addition, many passenger vehicles share common axle configuration with light commercial vehicles, and contribute to significant misclassification errors. A study by Kwigizile et al. (2005) reported an overall classification error of 9.5 percent using the decision tree approach for the FHWA Scheme F classification shown in Table 1.1. However, there was significant misclassification observed between vehicle classes 3 and 5.

Kwigizile et al. (2005) proposed an approach using probabilistic neural networks to obtain optimal axle spacing thresholds for the various vehicle classes in the FHWA Scheme F and obtained 6.2 percent errors when vehicle weight was not an input. The remaining errors are still due to axle configuration overlap between classes and indicate that vehicle classification is not a separable problem using vehicle axle configuration as the sole discerning criteria. An implication of using such a model may be performance deterioration if the developed models are tested under different traffic conditions or locations where vehicle type distributions are significantly different.

### **2.2.2 Review of other technologies and algorithms**

There have been several other vehicle classification studies using other detector technologies. These include conventional inductive loop sensors, image-based sensors, acoustic sensors, magnetic sensors and advanced inductive loop detector systems.

A simple approach developed by Kwon et al. (2003) applied lane-to-lane speed correlation using estimated speeds obtained from single inductive loop detectors. It assumed a known constant speed difference between truck and truck-free lanes and provided estimated truck volumes with a 5.7 percent error. It should be noted however, that this is not strictly a classification model—it does not identify the individual truck, but provides an aggregate estimate of truck volumes in traffic. Still, it possesses the advantage of using existing loop detector infrastructure without requiring installation of new detector hardware.

Studies by Lu et al. (1992), Harlow and Peng (2001), and Gupte et al. (2002) used image-based sensors to classify vehicles. Lu et al. developed a classification model using infrared image analysis that distinguished four vehicle classes including three commercial vehicle classes with an accuracy of 95 percent. Harlow and Peng's model was based on a laser range imaging system that identified six classes including three commercial vehicle classes with an accuracy of 92 percent, while Gupte et al. used video imaging to distinguish between cars and non-cars with 70 percent accuracy.

Nooralahiyan et al. (1997) performed acoustic signature analysis on vehicles and developed a model that was able to distinguish between four different vehicle types, including two commercial vehicle classes with 82.4 percent accuracy.

A recent study by Cheung et al. (2004) investigated the feasibility of wireless magnetic sensors in vehicle classification. The model obtained between 63 to 75 percent accuracy

for 6 vehicle classes depending on configuration, but was based on only a small sample of 37 vehicles.

Shin et al. (2007) developed a classification model from axle information and vehicle weight using strain gauge sensors. They investigated the Naïve Bayesian, back-propagation Neural Network and Support Vector Machines (SVMs) and found that the best results were obtained using the SVM approach. Their model distinguished between five vehicle types and achieved an overall classification accuracy of 94.8 percent on a test dataset with 100 vehicles in each class. However, this technology does not detect continuous vehicle presence. Hence, there could be potential issues of detecting tail-gating vehicles as a single vehicle or splitting a single long vehicle with large axle spacing into two separate vehicle detections, especially under unstable traffic conditions.

There has also been growing interest in vehicle classification using inductive signature systems. Pursula and Pikkarainen (1994) first used the self organizing map architecture to classify vehicles using feature vectors obtained from the vehicle inductive signatures.

Later, Oh et al. (2002) investigated several models and concluded that the backpropagation neural network architecture was superior to probabilistic neural networks and self organizing maps using vehicle features developed in their study as input to the models. The model distinguished between seven vehicle classes including four commercial vehicle classes and obtained 82 percent classification accuracy.

A more recent study by Sun et al. (2003) revisited the use of self organizing maps. They used typical vehicle signatures for each defined vehicle category as a template for the self-organizing map and was able to obtain also obtain 82 percent accuracy using the same vehicle classification scheme as Oh et al. (2002).

Ritchie et al. (2005) used a decision tree approach to classify vehicles using a scheme that follows closely to the FHWA scheme F classification. They proposed three different sub-models. A total of 17 vehicle classes were defined for the first model. However due to a lack of vehicle data for four of the classes, the resulting model yielded classification performance for 13 of the classes, including the distinction of pickup trucks, vans and SUVs into separate classes, and obtained 81.53 percent correct classification rate (CCR) using a single loop configuration. The second model combined pickup trucks, vans and SUVs into one vehicle class and obtained 85.43 percent CCR, while the third model further condensed passenger cars together with pickup trucks, vans and SUVs and achieved 97.72 percent CCR.

Most recently, Jeng and Ritchie (2008) used a heuristic method using a combination of decision tree and K-means clustering approaches to develop a classification model using inductive signature data from single loops. Three classification schemes were investigated, of which the most extensive scheme had fifteen vehicle classes including thirteen commercial vehicle classes yielded an overall CCR of 93.0 percent with clean data. However, the dataset comprised mainly passenger vehicles and light commercial

vehicles while only three of the remaining commercial vehicle classes had a sample size of at least ten in the test dataset.

### **2.2.3 Critique of studies and results**

Among the studies reviewed, the axle configuration based models using the FHWA classification scheme F presently provide the most comprehensive distinction of vehicle types, with the most number of vehicle classes, and provides the highest overall accuracy. This is followed closely by the results recently achieved using inductive signature systems to obtain vehicle classifications similar to the FHWA scheme F.

#### **Insufficient commercial vehicles in dataset**

A common weakness in vehicle classification studies is the lack of sufficient commercial vehicles in the model development dataset. This is not surprising, since commercial vehicles do not typically represent a significant proportion of general traffic. Hence, an immense data collection effort is required to obtain a comprehensive representation of commercial vehicles, requiring an effort that is prohibitive in most research studies. As a consequence, many classification models developed in these studies are unable to discriminate the heterogeneous composition of commercial vehicle types.



### **Over-representation of passenger vehicles**

Caution must be taken when making a direct comparison between the performances of the models developed in the studies reviewed, as few of them were focused on a dataset with extensive representation of commercial vehicles. Since passenger vehicles – which is a distinct vehicle class in most of the mentioned models – often comprise the major proportion of general traffic, the accuracy of the models presented can be biased by the type and distribution of non-passenger vehicles found in the test datasets used, as this is where models are called to make the distinction. A case in point would be a dataset where 80 percent of the vehicles are passenger vehicles and the rest made up of various other vehicle types. A trivial vehicle detection model performing volume counts that assumes all vehicles as passenger cars would still achieve an arguably acceptable 80 percent overall classification accuracy in such a dataset!

### **Diminished performance in adverse traffic conditions**

Accurate vehicle classification is dependent on reliable traffic measurement data, even under adverse traffic conditions. Presently, classification models based on in-pavement sensors such as piezo sensors, strain gauge sensors, inductive loop sensors as well as magnetic sensors require the assumption that vehicles traverse the sensors at constant speeds. This allows direct measurements of axle spacings, vehicle length or equally spaced interpolation information.

However, the constant speed assumption is violated under congested freeway conditions and on many arterial streets where vehicles often undergo significant acceleration and deceleration due to the influence of traffic intersections. This results in erroneous spatial-information measurements in axle-based classifiers. In addition, vehicle signatures obtained under such adverse traffic conditions are subjected to distortion due to the acceleration and deceleration effects. These errors diminish the accuracy and reliability of the information obtained from these vehicles resulting in diminished classification performance for the affected vehicles.

#### **2.2.4 Critique summary**

From the above studies, it can be concluded there is presently an insufficient emphasis on distinguishing between different commercial vehicle types. Apart from the current method used based on the FHWA scheme F and the modified California scheme which identify eleven and twelve distinct commercial vehicle classes, respectively, none of the other studies have been able to classify more than four different commercial vehicle types. Even then, the classes defined by the FHWA scheme F are based on axle configuration, which have little or no bearing to the body configuration and function of the commercial vehicle. This inherent limitation prevents further insight to be drawn from understanding the travel behavior and impacts of the wide array of commercial vehicles traveling on the roadways today. There is also concern of how well the reviewed studies would perform under unstable traffic conditions.

## **2.3 HIGH FIDELITY INDUCTIVE SENSORS**

### **2.3.1 Advanced Inductive Loop Detectors**

Inductive loop detectors are the most widely deployed traffic detector technology in the world. In contrast to conventional inductive loop detectors that produce bivalent outputs to indicate vehicle presence, advanced inductive loop detectors measure the inductance change in an inductive loop sensor at speeds of up to 1200 samples per second (IST, 2006). This series of inductance changes caused by a traversing vehicle produce an analog waveform output and is referred to as the inductive vehicle signature. Samples of inductive signatures of various vehicle types are presented in Figure 2.1.

An advantage of advanced inductive loop detectors is its compatibility with existing conventional bivalent inductive loop detectors. This allows existing conventional inductive loop detectors to be swapped with advanced inductive loop detectors without suffering any loss in system functionality. Figure 2.2 shows two advanced inductive loop detectors installed in a traffic cabinet. A Universal Serial Bus (USB) interface on the front of the detector card allows connectivity to a field computer for collection of inductive signature data.

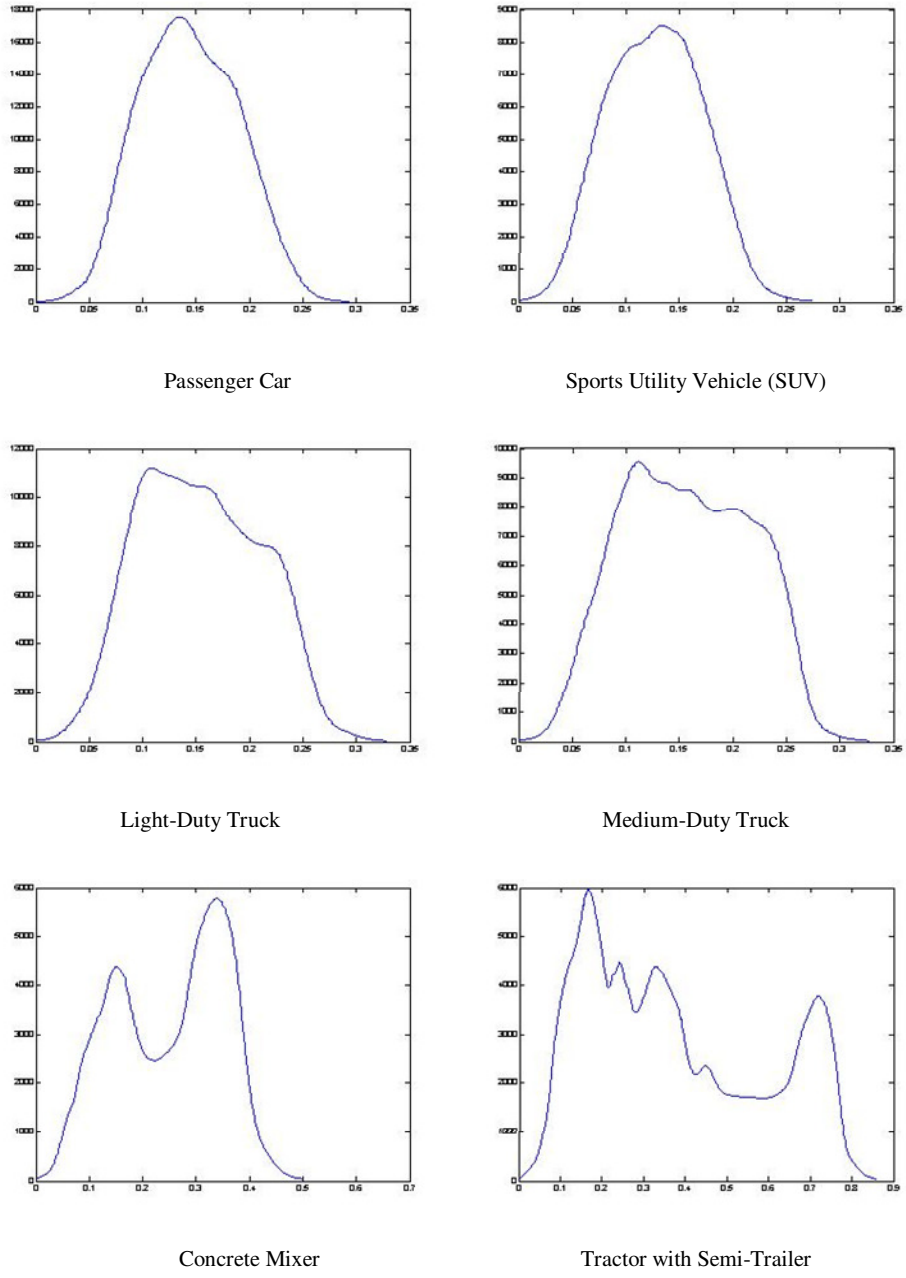


Figure 2.1. Samples of Inductive Vehicle Signatures obtained from a 1.8m Round Inductive Loop Sensor

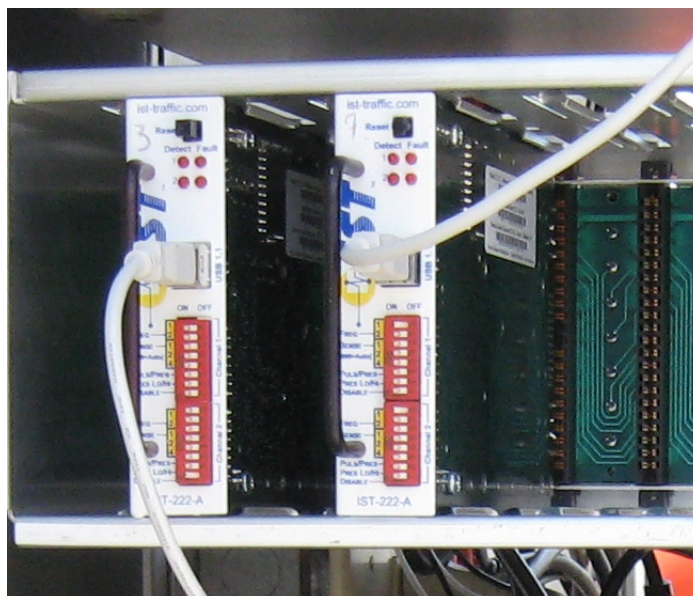


Figure 2.2. Advanced inductive loop detector cards installed in a traffic cabinet.

Unlike many other detector systems such as imaging or acoustic sensors, advanced inductive loop detectors have a low background noise, reporting a null signal in the absence of vehicular presence. Because of this, loop detectors are inherently accurate, achieving volume count accuracies typically between 98 and 99 percent even in conventional bivalent system applications, providing a good technology platform to develop the proposed system. Finally, loop detector systems are robust. Their performance and accuracy are not significantly affected by changes in temperature, lighting, visibility and humidity. This is because magnetic inductance is invariant to such effects. Such characteristics allow advanced systems based on inductive signature data to be very reliable highly transferable as well, provided that inductive loop geometries are preserved.

An often emphasized criticism of loop detector systems is the loss in sensitivity due to pavement wear which damages the inductance loops. However, studies have actually shown that loop detectors are more resilient than most other pavement intrusive sensors such as piezo or WIM sensors as they do not involve contact with vehicle axles and hence are not subject to the impact loading that causes sensor failure. Inductance loop sensor failure is more commonly attributed to freeze thaw conditions that result in pavement movements sufficient to cut the inductance loop coils (Hallenbeck and Weinblatt, 2004).

Because of these advantages over conventional bivalent inductive loop detectors, several studies have investigated this technology for Advanced Traveler Information Systems (ATIS) applications such as section-based freeway travel time measurement (Sun, 1998, Sun et al., 1999, Jeng et al., 2007), arterial travel time measurement (Oh and Ritchie, 2003), vehicle classification (Sun et al., 2003, Oh and Ritchie, 2007, Tok et al., 2007, Jeng and Ritchie, 2008), speed estimation (Oh et al., 2007) and real-time performance measurement systems (Oh et al., 2005, Tok et al., 2008).

In the above-mentioned studies, a required assumption is that vehicle speed remains constant while traversing the inductive loop sensor. This is because changing speeds distort the inductive signature waveform and may diminish its usability. While this assumption of constant speed is valid at free flow traffic conditions, it is violated in unstable traffic conditions often observed at peak congestion periods, where speeds are low and significant acceleration and deceleration can occur while a vehicle remains present over an inductive loop sensor. This is especially significant in conventional

double inductive loop sensor configurations where the overall sensor length is typically 7.5 m (26 feet). The extensive length of the conventional double inductive loop sensor also increases the occurrences of tail-gating vehicles – an event where a following vehicle enters the field of detection before the previous vehicle leaves resulting in vehicle inductive signatures containing two or more vehicles.

Figure 2.3 shows examples of inductive signatures obtained from conventional inductive loop sensors belonging to different passenger vehicles at constant speed, undergoing acceleration and deceleration, and stopping over a conventional inductive loop sensor, respectively. Under constant speeds, vehicles typically generate inductive signatures with similar leading and trailing slope gradients. However, inductive vehicle signatures are typically skewed left in accelerating vehicles with a steeper trailing slope gradient indicating a higher exit speed compared with the entry speed. Conversely, decelerating vehicles produce signatures that are typically skewed right with a steeper leading slope gradient. In stopped vehicles, inductive signatures show a flat segment corresponding to the period when the vehicle is stopped over the sensor.

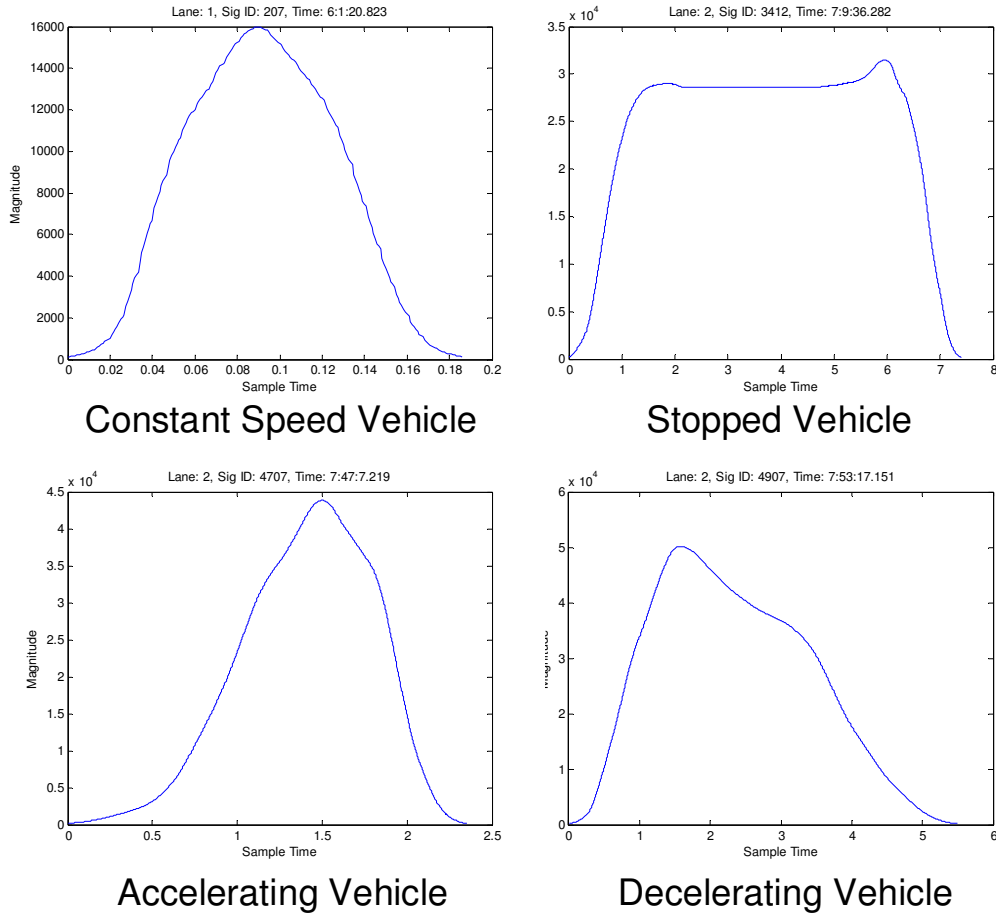


Figure 2.3. Normal vs. distorted round inductive loop signatures

### 2.3.2 Blade™ Inductive Sensors

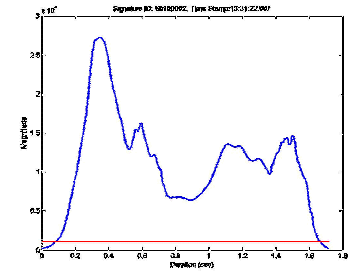
The Blade™ inductive sensor is a new remote vehicle sensor technology. The physical embodiment of this concept uses two matched harmonic oscillating circuits whose induction coils are oriented and contained within a single, solid ‘sensor blade’ that is then embedded in a 3/16 inch wide pavement slot (for a permanent installation). The sensing coil is oriented toward the surface of the pavement and the reference coil is oriented



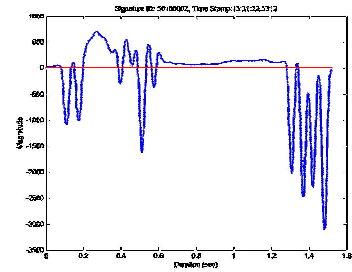
toward the base of slot. Because the sensing coil is positioned nearer passing vehicles, it responds more strongly to this stimulus than the reference coil. Data collection is initiated by simultaneously charging both circuits to a threshold voltage using an impulse function and then allowing them to rapidly decay to a base line asymptote. This differential signal is amplified and digitized using an A/D converter.

A continuous stream of signed integers is generated by the Blade™ inductive sensor, which can be monitored by a dedicated on-board microprocessor. The resulting measurement data produce the vehicle's inductive signature.

The use of Blade™ inductive sensors combines the advantages of axle-based systems as well as inductive signature-based conventional loop sensors. In addition, its short traverse length addresses the integration issues found in conventional loop sensors and its full lane coverage ensures uniform data over entire lane width of traffic. Figure 2.4 shows an example of signatures obtained via a conventional preformed round inductive loop sensor and a Blade™ inductive sensor obtained from a single tractor trailer. This new sensor technology combines the ability of obtaining high fidelity inductance signatures of the vehicle undercarriage as well as axle configuration information, as shown in Figure 2.5. This fusion of information within a single sensor technology provides the potential for further improvement in vehicle classification and other surveillance related studies.



Round Loop Signature



Blade™ Signature

Figure 2.4. Example of Round and Blade™ inductive loop sensor signatures from a tractor with semi-trailer

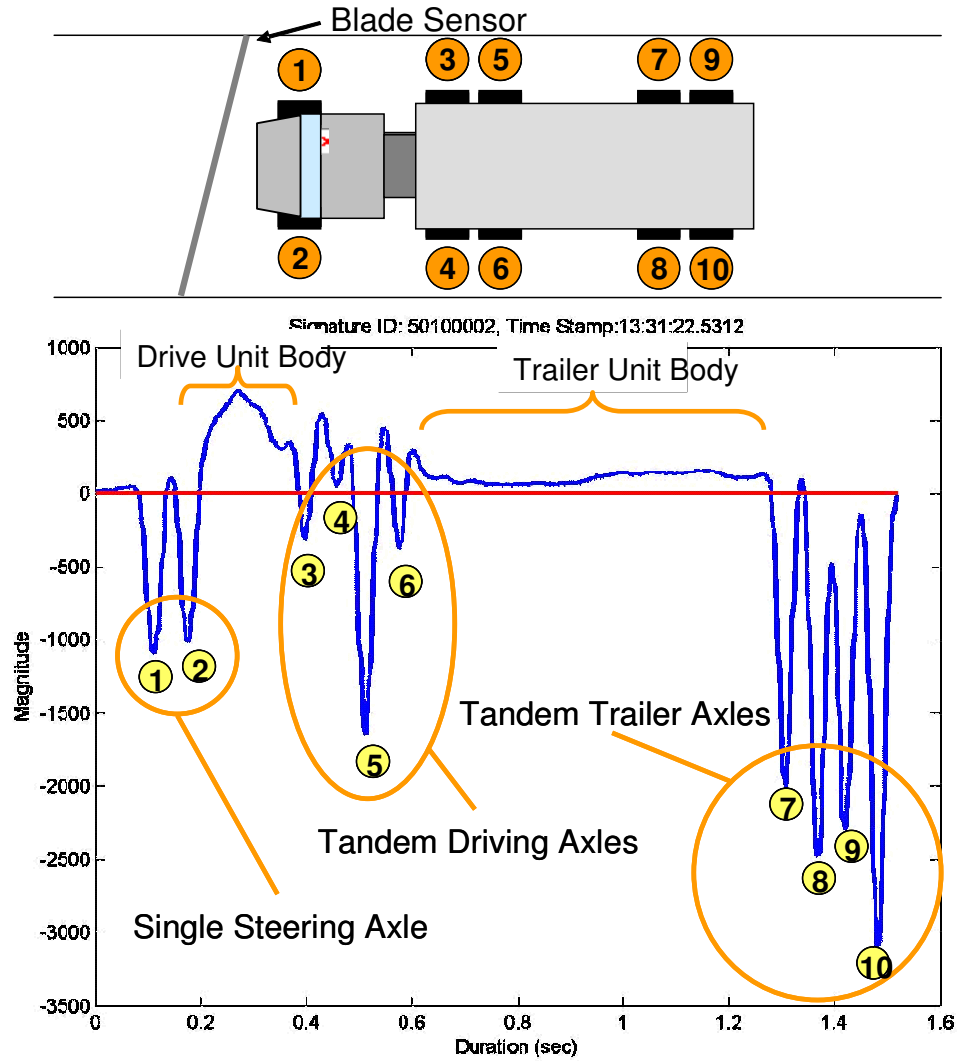


Figure 2.5. Characteristics of a Blade™ inductive signature

### 2.3.3 Previous studies on Blade™ Inductive Sensors

The first investigation into this sensor technology was made by Oh et al. (2004) on developing a re-identification system based on heterogeneous inductive loop sensors installed on a major multi-lane arterial facility.

Later, Park et al. (2006) obtained wheel base information from Blade™ inductive sensors to develop a two-way and three-way vehicle classification model under slow or varying speed conditions. The two-way model distinguished between trucks and non-trucks, while the three-way model added the distinction of sport-utility vehicles. They tested their model on two different sites and were able to obtain between 81 and 85 percent correct classification rate for the two-way vehicle classification model and between 57 and 70 percent for the three-way model.

Oh and Ritchie (2007) also explored the potential of Blade™ inductive sensors in vehicle classification using vehicle signature data obtained in the study by Oh et al. (2004). The study distinguished between four passenger and light duty commercial vehicle types with combined classification accuracy of 70.8 percent. No medium or large commercial vehicle classes were investigated as they were insufficient samples in the dataset for analysis.

These studies indicate that Blade inductive sensors show potential in obtain vehicle classification information. However, the datasets used to develop the models described were small, and may not have explored the full potential of this technology.

## **CHAPTER 3 STUDY SITES AND DATA DESCRIPTION**

This chapter presents the study locations and provides a description of the surveillance setup at each site as well as how real traffic data was collected to develop the models presented in this dissertation.

Two study sites were investigated in this dissertation. The first site is located within the campus of the University of California at Irvine. The second is located at the southbound San Onofre Truck Weigh and Inspection Facility along the I-5 freeway in north San Diego County, California.

### **3.1 UNIVERSITY OF CALIFORNIA, IRVINE AT BISON AVE**

#### **3.1.1 Site Description**

This study site is located within the University of California, Irvine on westbound Bison Ave towards the SR-73 freeway as shown in Figure 3.1, upstream of the intersection with California Ave. Bison Ave serves as one of the main arterials for traffic entering and egressing the University of California, Irvine and provides access to the closest freeway – the SR-73. Hence, it is an ideal location for obtaining a large dataset with heterogeneous vehicle types.

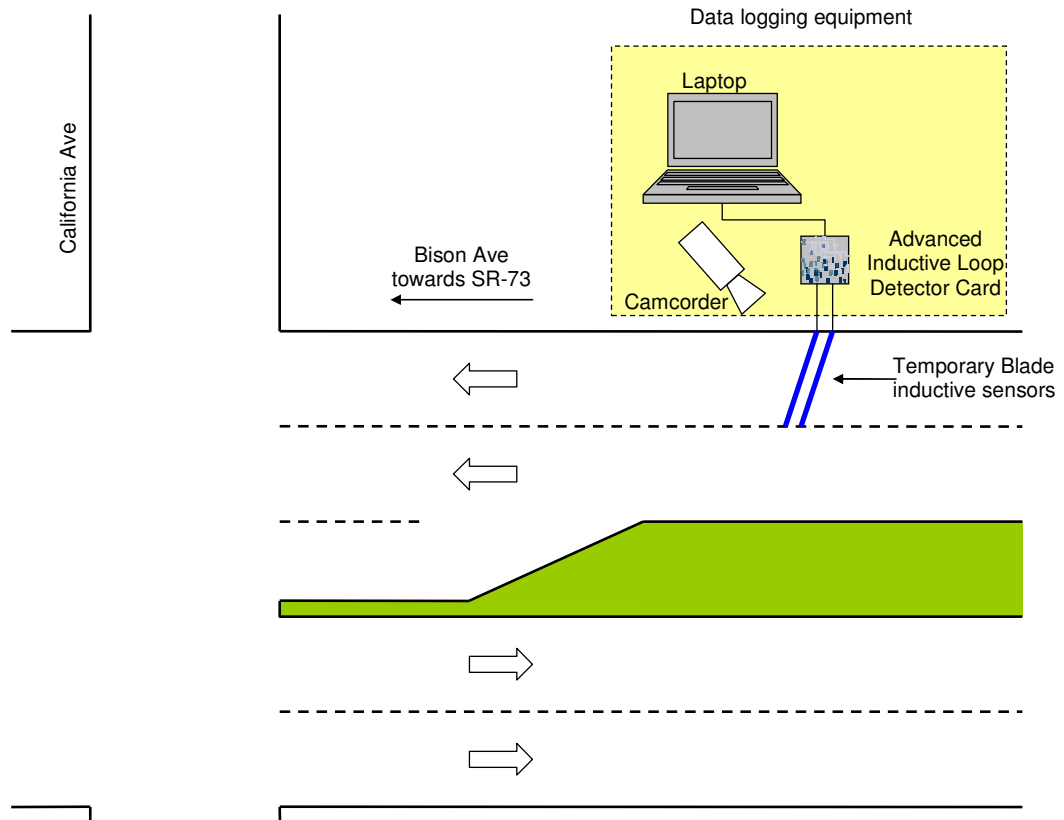


Figure 3.1. Study site location in University of California, Irvine

### 3.1.2 Surveillance System Set-up

The data used in this study was collected from double surface-mounted Blade™ inductive sensors via advanced inductive loop detector cards sampling inductive loop data at 1200 samples per second. The surface-mounted Blade™ inductive sensors were installed at an angle of 20 degrees from perpendicular to the direction of travel on the rightmost lane. This alignment was chosen as it is similar to the ones used in previous studies conducted in the City of Irvine and at San Onofre, California (Oh et al, 2004, Oh and Ritchie, 2007,

Tok et al, 2007). Hence, the data obtained and models developed can be compared with the above-mentioned studies. The Blade™ inductive sensors were spaced at 30 cm (1 foot), measured between the leading edge of each sensor. This close spacing ensures that changes in vehicle speeds across the sensors are negligible even under severe stop and go conditions. The sensors were located about 75 m (250 ft) upstream of the signalized traffic intersection with California. The influence of the intersection enables the collection of Blade™ inductive signatures to simulate heavy arterial traffic and congested freeway congestions where significant acceleration and deceleration over inductive sensors regularly occur.

The advanced inductive loop detector cards were connected to a laptop for inductive signature data logging via the universal serial bus (USB) interface. Inductive signature data was collected in a continuous stream via proprietary software provided by Inductive Signature Technologies – the manufacturers of the advanced inductive loop detector cards. Video data was collected simultaneously using a side-fire camcorder to provide ground truth of the vehicles traversing the Blade™ inductive sensors (as shown in Figure 3.1). The clocks of the laptop and camcorder were matched with a handheld GPS unit. This ensures synchronization between the signature and video data as well as timestamps obtained from control vehicles equipped with in-vehicle GPS units.

### **3.1.3 Data Description**

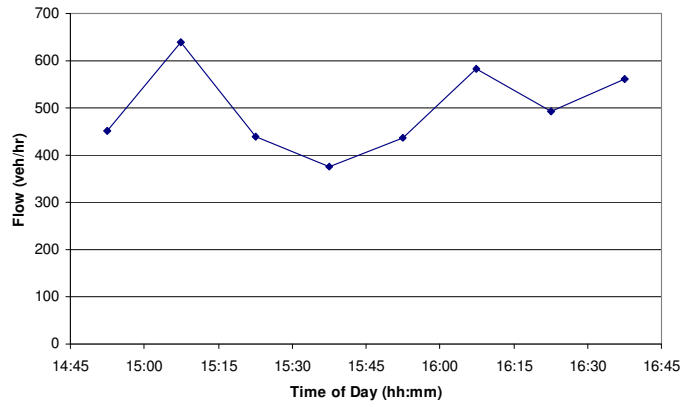
Data was collected on March 7 2008 between 2:45 pm and 4:50 pm, March 10 2008 between 9:15 am and 11:00 am and on April 15 2008 between 2:20pm and 4:40 pm, yielding a total of about 2600 vehicle signatures. Two control vehicles were used in the March 7 2008 dataset while five were used in the April 15 2008 dataset. Figure 3.2 shows the variation in traffic flow during the data collection periods. Traffic flows are aggregated at 15 minute intervals and represent hourly rates.

## **3.2 SOUTHBOUND SAN ONOFRE TRUCK WEIGH AND INSPECTION FACILITY**

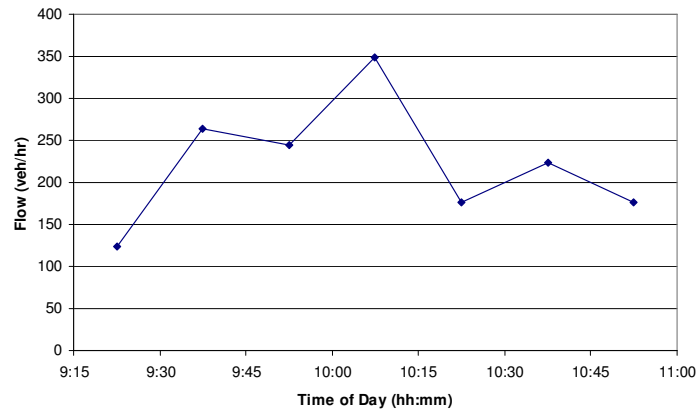
### **3.2.1 Site Description**

The San Onofre study site is located at the California Highway Patrol (CHP) I-5S Truck Weigh and Inspection Station in San Onofre, between Los Angeles and San Diego. This site was chosen due to the high volume and variety of commercial vehicles that enter the site daily. It has a single lane entrance ramp from the I-5S, which expands into three lanes approaching the weighing scales followed by a single lane exit ramp back to the mainline freeway.

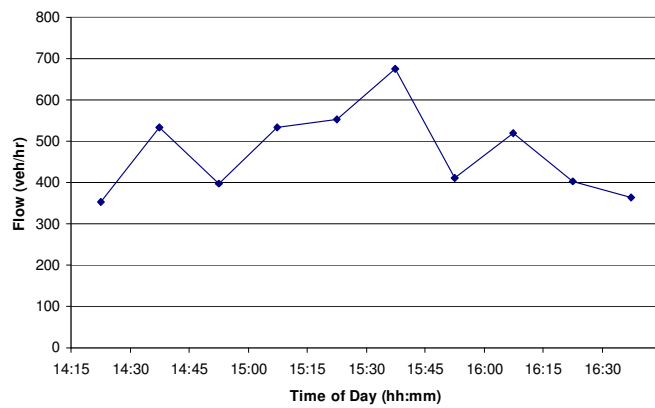




(a) March 7 2008 dataset



(b) March 10 dataset



(c) April 15 dataset

Figure 3.2. Traffic flow at Bison Ave during data collection

### 3.2.2 Surveillance System Set-up

A temporary detector station was setup at the entrance ramp as shown in Figure 3.4. It was instrumented with single preformed conventional surface-mounted round inductive loop sensor as well as double surface-mounted Blade™ inductive sensors installed at an angle of 20 degrees from perpendicular to the direction of travel. Figure 3.3 shows the installation of the double surface-mounted Blade™ inductive sensors. Each sensor was connected to advanced inductive loop detector cards. These detector cards were in turn connected via the USB interface to an industrial PC running the Windows 2000 operating system. The equipment was housed in an existing traffic cabinet. These advanced detector cards process inductance signals induced by vehicles passing over the loops at 1200 samples per second, while a client program logs these signals in binary format to the PC hard drive, to be later retrieved for analysis after the data collection.



Figure 3.3. Installation of double surface-mounted Blade™ inductive sensors at the San Onofre study site

The clocks of the camcorder and PC were synchronized to ensure accurate data ground truth of inductance signature records with video information. The synchronization was performed manually, with an expected accuracy within fractions of a second. It was found that the drifting of the clocks in each device was generally negligible, and did not significantly affect the accuracy of data ground truth. A detailed layout of the sensor configuration is shown in Figure 3.5. Figure 3.6 shows the wiring diagram of equipment used during the data collection exercise.

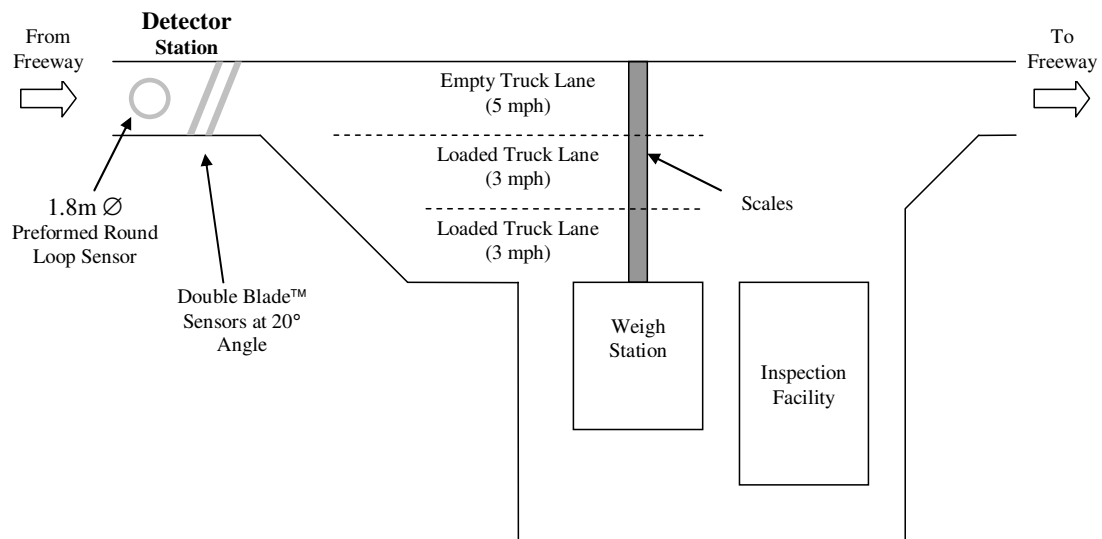


Figure 3.4. Southbound San Onofre data collection study site

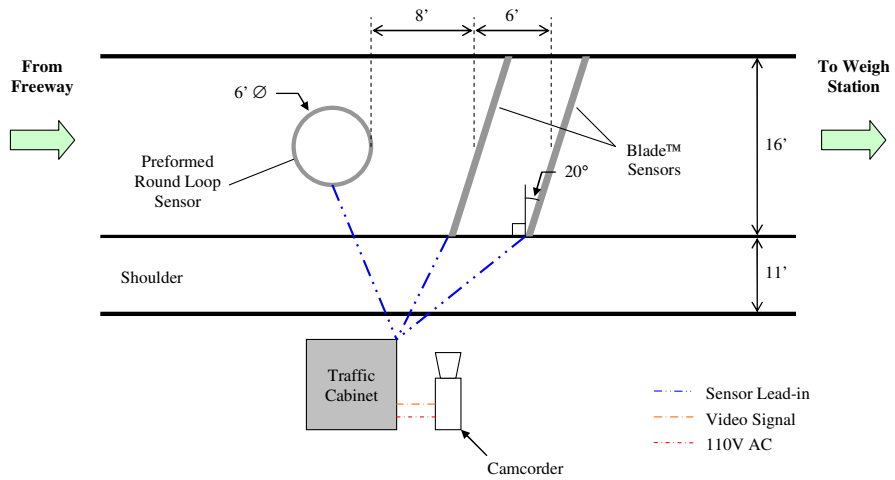


Figure 3.5. Sensor and equipment layout at San Onofre detector station

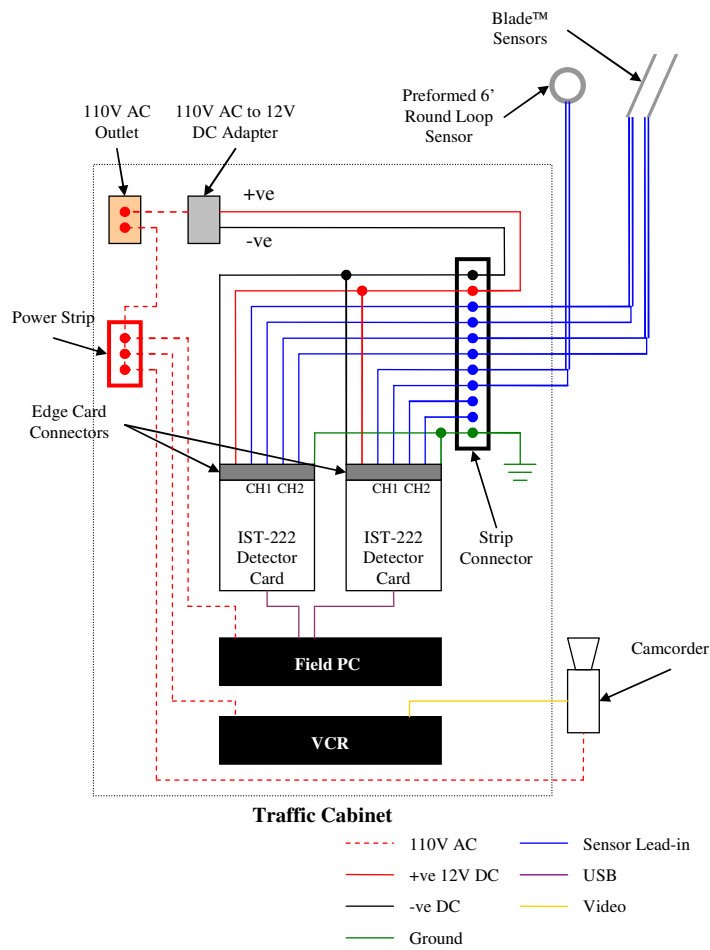


Figure 3.6. Wiring diagram of equipment setup at San Onofre

### 3.2.3 Data Description

Data was collected on May 3 2006 from 1:40 pm to 6:30 pm for developing and testing the models presented in this study. A total of 1029 commercial vehicle samples were obtained during this period. The variation of traffic flow at the study site during the data collection period is presented in Figure 3.7. Traffic flows are aggregated at 15 minute intervals and represent hourly rates. The speed of vehicles during the data collection period ranged from 14.2 km/h (8.8 mph) to 108.8 km/h (67.6 mph). From Figure 3.8, it is observed that most vehicles traversed the study site between 32 km/h (20 mph) and 64 km/h (40 mph). The average and median speeds during the data collection period were 48.6 km/h (30.2 mph) and 47.6 km/h (29.6 mph) respectively. The standard deviation of the vehicle speeds was 12.7 km/h (7.9 mph). Individual vehicle speeds were obtained by dividing the distance between the Blade™ inductive sensors (1.82 m or 6 ft) by the time stamp difference between inductive signatures obtained by each Blade™ inductive sensor.

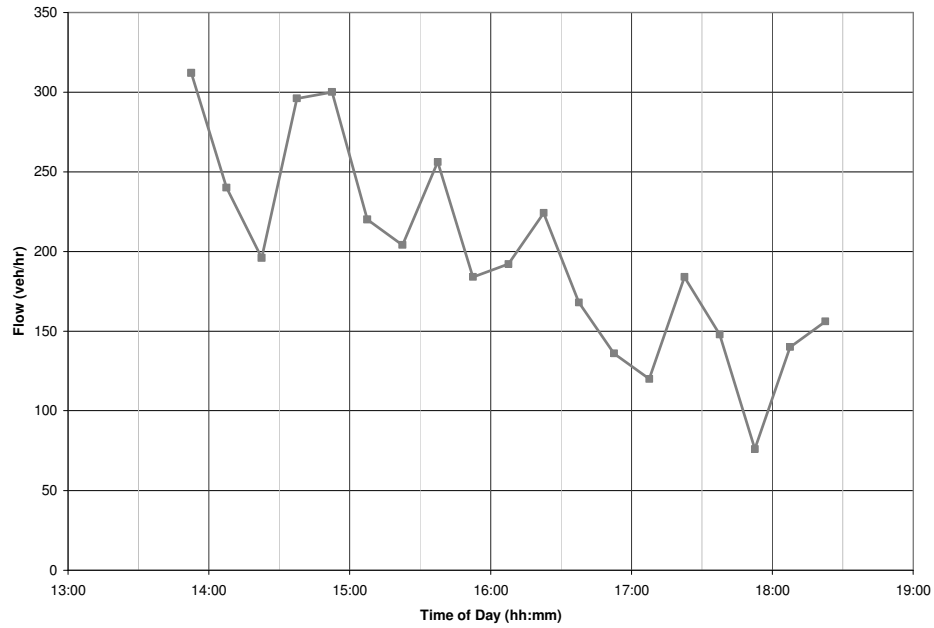


Figure 3.7. Traffic flow in San Onofre dataset

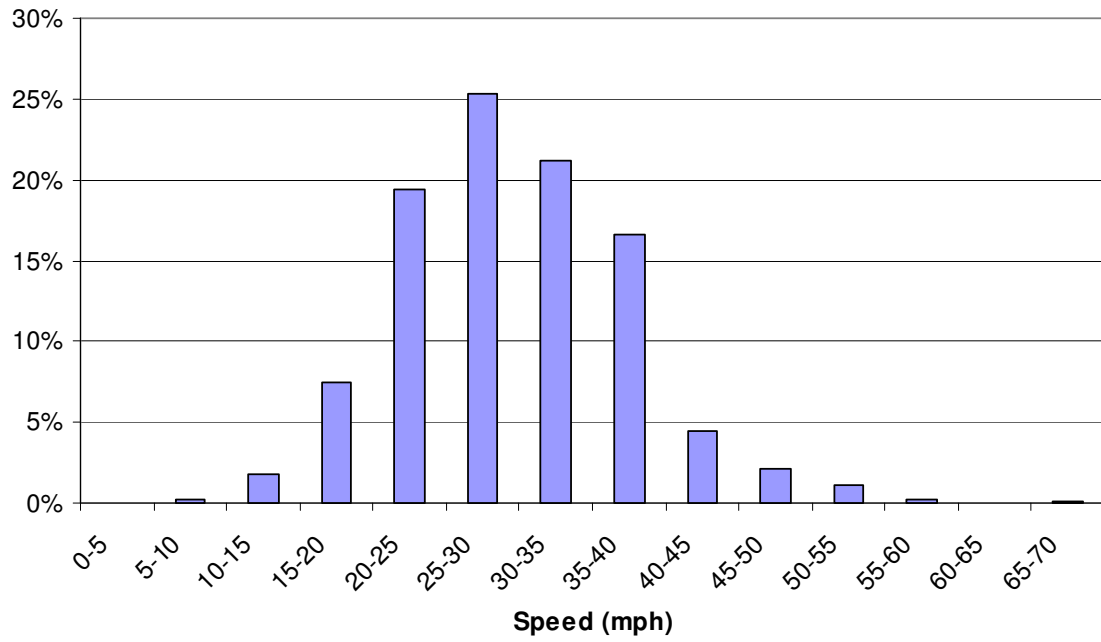


Figure 3.8. Speed distribution of vehicles in San Onofre dataset

### **3.2.4 Data ground truth system design**

Due to the large variety of commercial vehicles observed at the site, a new data ground truth system was developed to enable accurate and efficient description of the vehicle data collected. This system was designed with the Microsoft Access 2000 database platform integrated with a user interface developed in Microsoft Visual Basic 6.0.

The ground truth data entry system possesses a quick query system shown in Figure 3.9 coupled with an intuitive graphical user interface with an array of pull-down classification selection menus. This design enables efficient classification data entry and visual validation of vehicle signatures corresponding to each vehicle record. A screenshot of the commercial vehicle ground truth data entry system is shown in Figure 3.10. For each vehicle record, descriptions entries are available to comprehensively describe the vehicle by its drive unit axle configuration, trailer unit axle configuration, drive unit body type and trailer unit body type. The inductive signature figures are displayed with each vehicle record to provide further validation with video data obtained from side-fire camcorders.

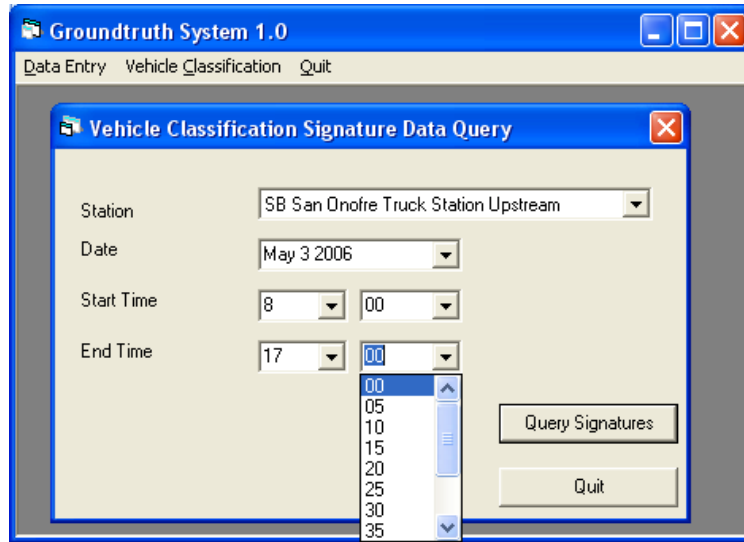


Figure 3.9. Vehicle Classification Signature Data Query input



Groundtruth System 1.0 - [Vehicle Classification Groundtruth]

Data Entry Vehicle Classification Quit

Time	Truck Body Config	Truck Type	Truck Axle Config	Trailer Body Config	Trailer Type	Trailer Axle Config
1:40:34 p	Semi Tractor	Extended Cab	Single - Tandem	Van	Enclosed Van	Tandem on Semi-Trailer
1:40:39 p	Semi Tractor	Extended Cab	Single - Tandem	Van	Enclosed Van	Tandem on Semi-Trailer
1:40:44 p	Semi Tractor	Extended Cab	Single - Tandem	Platform	Basic Platform	Split Tandem on Semi-Trailer
1:41:01 p	Van Type	Enclosed Van	Single - Single 6 Tire	No Trailer	No Trailer	No Trailer
1:41:10 p	Platform Type	Basic Platform	Single - Single 4 Tire	No Trailer	No Trailer	No Trailer
1:41:47 p	Van Type	Enclosed Van	Single - Single 6 Tire	No Trailer	No Trailer	No Trailer
1:41:58 p	Van Type	Enclosed Van	Single - Single 6 Tire	No Trailer	No Trailer	No Trailer
1:42:06 p	Semi Tractor	Extended Cab	Single - Tandem	Van	Enclosed Van	Tandem on Semi-Trailer
1:42:11 p	Platform Type	Basic Platform	Single - Tandem	Platform	Basic Platform	Single-Single on Single Trailer
1:42:17 p	Semi Tractor	Extended Cab	Single - Tandem	Van	40' Box Container	Tandem on Semi-Trailer

**SB San Onofre Truck Station Upstream**  
May 3 2006  
1:40:44.47 pm  
1057 Vehicle Records

**Vehicle Classification**

Drive Unit Information: Semi Tractor  
Trailer Unit Information: Platform

Extended Cab  
Basic Platform

Single - Tandem  
Split Tandem on Semi-Trailer

**Reference Time**

Round  
Blade (Front)  
Blade (Rear)

**Alerts**

Time difference > 2 sec

Quick Add Exit

**Edit Vehicle Record**

Round Blade (Front) Blade (Rear)

Add to New Vehicle Record Delete Current Vehicle Record

Add to Current Vehicle Record Remove From Vehicle Record

**Aggregate Signature Operations**

Previous Record(s) 1 Following Record(s)

Set All Signature Qualities to Good

First Record Last Record

**Attached Signatures**

Round				Blade (Front)				Blade (Rear)			
Time	Lane	ShortSigID		Time	Lane	ShortSigID		Time	Lane	ShortSigID	
1:40:44 p	1	41		1:40:44 p	1	45		1:40:45 p	1	46	

**Round Signatures**

1:40:43.97 pm 50100041 Good Signature

Record 41 of 1000

**Blade (Front) Signatures**

1:40:44.47 pm 50100045 Good Signature

Record 45 of 1105

**Blade (Rear) Signatures**

1:40:44.61 pm 50100046 Good Signature

Record 46 of 1107

Figure 3.10. Commercial vehicle classification ground truth data entry system

## **CHAPTER 4 SPEED PROFILE INTERPOLATION TEMPORAL- SPATIAL TRANSFORMATION**

### **4.1 BACKGROUND**

Accurate vehicle classification is dependent on reliable traffic measurement data. Presently, classification models based on in-pavement sensors such as piezo sensors (Kwigizile et al., 2005), inductive loop sensors (Sun et al., 2003, Zhang et al., 2006, Coifman and Kim, 2007, Oh and Ritchie, 2007, Jeng and Ritchie, 2008), magnetic sensors (Cheung et al., 2004) and strain gauge sensors (Shin et al., 2007) require the assumption that vehicles traverse the sensors at constant speeds. This allows direct temporal-spatial transformation techniques to obtain spatial measures such as axle spacings, vehicle length and extracted signature feature information.

However, the constant speed assumption is violated under unstable traffic conditions found along congested freeways and on arterial streets where vehicles often undergo significant acceleration and deceleration due to the influence of traffic intersections. This results in erroneous spatial-information measurements in the aforementioned sensor technologies. Similarly, vehicle signatures obtained under such adverse traffic conditions are also subjected to distortion errors due to the acceleration and deceleration effects. These errors diminish the accuracy and reliability of the information obtained from affected vehicles, and may result in poor classification accuracy.

This chapter presents the theoretical framework for obtaining the speed profile from a vehicle signatures and subsequently performing a temporal-spatial transformation to yield a distortion-corrected signature—free from acceleration and deceleration effects. This method can be applied to any sensor technology that has a short traversal length and can generate reliable, locally unique high-fidelity signatures.

The Speed PRofile INterpolation Temporal-Spatial (SPRINTS) transformation model is developed from this theoretical framework and applies specifically to the Blade inductive signature system. The advanced high-speed detector cards to which Blade™ inductive sensors are connected to, coupled with the ability to install double Blade inductive sensors with much smaller sensor headways due to their shorter sensor footprint make Blade™ inductive sensors the ideal candidate technology for the development of the SPRINTS transformation model. Results from control vehicles indicate a significant decrease in variance of length estimates within vehicle classes.

## **4.2 THE SPEED PROFILE SIGNATURE TRANSFORMATION PROBLEM**

### **4.2.1 Theoretical Framework**

Two measures are required from an in-pavement sensor for vehicle length to be accurately estimated under acceleration and deceleration conditions: the duration of time

which the vehicle remains over the sensor and the change in vehicle speed within that time duration.

If the speed trajectory  $v(t)$  of a vehicle is known along the duration  $t_v$  which the vehicle remains over a sensor, the vehicle length can be obtained by integrating  $v(t)$  w.r.t.  $t$  as shown:

$$L_v = \int_0^{t_v} v(t) dt$$

$$= \int_0^{t_v} \frac{dx}{dt}(t) dt$$

Where:

- $L_v$  - True vehicle length
- $t_v$  - Total duration of vehicle over sensor

Assume that speed  $v$  is estimated from the sensor by measuring the time  $t$  taken to traverse the sensor length  $L_s$  (typically the distance between the leading edges of double sensor speed traps),  $v$  can be obtained by dividing  $L_s$  with  $t$ . Next, consider that  $n+1$  points equally spaced at  $\Delta t$  intervals are obtained, spanning the duration  $t_v$  of the vehicle traversing the sensor. Each point  $i$  corresponds to a longitudinal location on the vehicle and  $t_i$  represents the time taken by point  $i$  to traverse the sensor as shown in the context of vehicle signatures in Figure 4.1. Hence, the speed  $v_i$  at each point  $i$  can be subsequently obtained as follows:

$$v_i = \frac{L_s}{t_i}$$

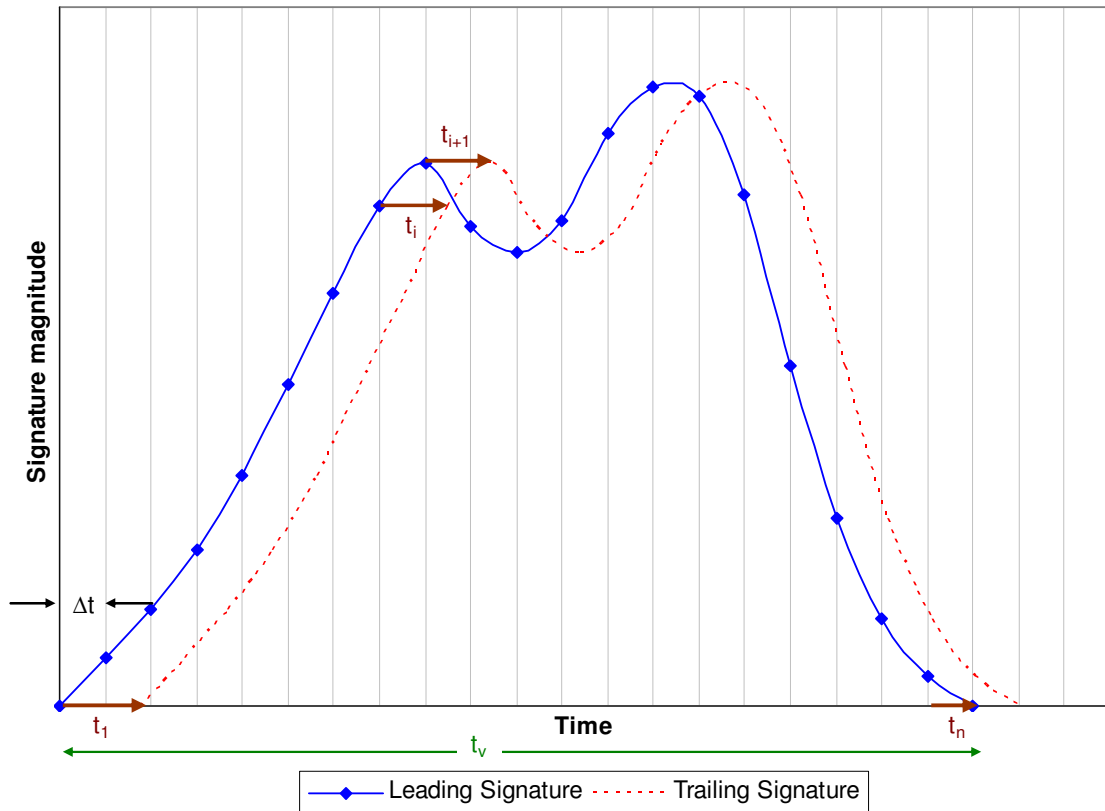


Figure 4.1. Extracting time measures at equal intervals along a vehicle signature

The plot of  $v_i$ 's spanning the vehicle yields the speed profile as shown in Figure 4.2.

The longitudinal distance  $\Delta x_i$  between adjacent points  $i$  and  $i+1$  can be obtained by multiplying  $v_i$  with  $\Delta t$ :

$$\begin{aligned}\Delta x_i &= v_i \Delta t \\ &= \left( \frac{L_s}{t_i} \right) \Delta t\end{aligned}$$

Where

- $L_s$  - Sensor length (the distance between leading edges of double Blade™ inductive sensors in the case of this study)
- $t_i$  - Time taken for point  $i$  of vehicle to traverse  $L_s$
- $\Delta t$  - Time step



Figure 4.2. Obtaining the speed profile from sampled speeds spanning a vehicle signature

Hence, the speed profile transformed vehicle length  $L_v^{sp}$  can be estimated as follows:

$$\begin{aligned}
\int_0^{t_v} \frac{dx}{dt}(t)dt &\approx \sum_{i=1}^n \left( \frac{L_s}{t_i} \right) \Delta t \\
&= \sum_{i=1}^n \Delta x_i \\
&= L_v^{spt}
\end{aligned}$$

The above formulation assumes that the sensor length  $L_s$  is sufficiently small such that the change in speed of a vehicle while traversing the sensor is negligible.

The transformed signature shows the variation of the inductance magnitude along the longitudinal length of the vehicle (shown in Figure 4.3), and is invariant with speed and acceleration of the vehicle. Hence, the repeatability and reliability of the vehicle signature and vehicle length is improved to provide more accurate results for advanced inductive signature applications such as vehicle classification and vehicle re-identification.

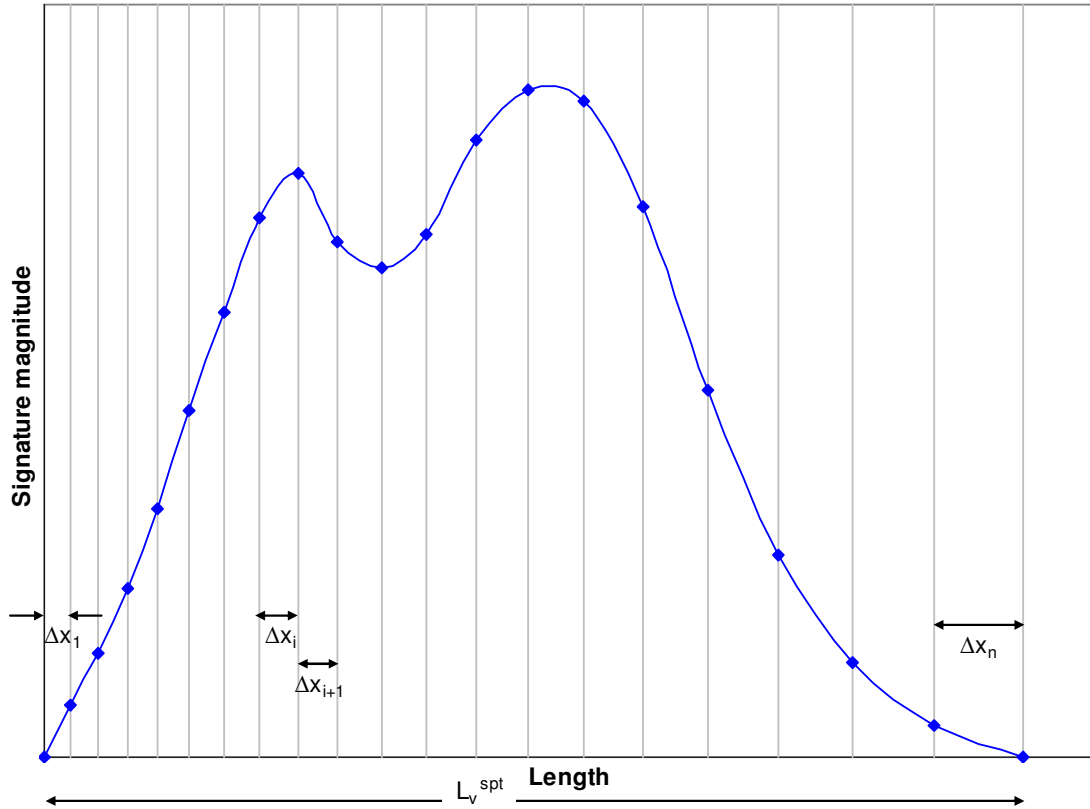


Figure 4.3. Speed profile transformation of vehicle signature

#### 4.2.2 Proposed Sensor Technology

The Blade™ inductive sensor’s short traversal length permits a short installation distance between adjacent sensors in a speed-trap configuration as shown in Figure 4.4 at the UCI Bison study site. This yields double inductive signatures with a significantly smaller temporal headway between them compared with convention inductive loop sensors as illustrated in Figure 4.5. In addition, the high sampling rate of the advanced detector cards used with these sensors minimizes time measurement quantization errors across the



short traversal distance between the sensors, which allows accurate speed estimates to be obtained.

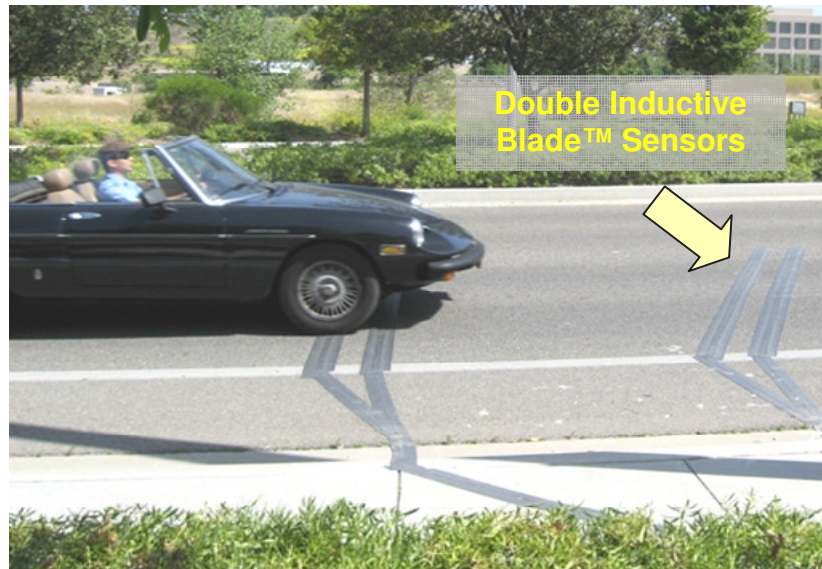
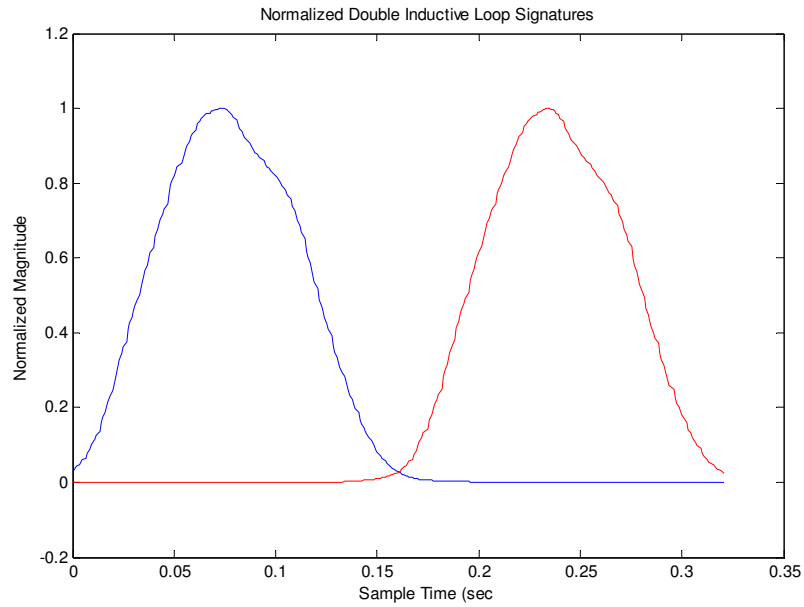
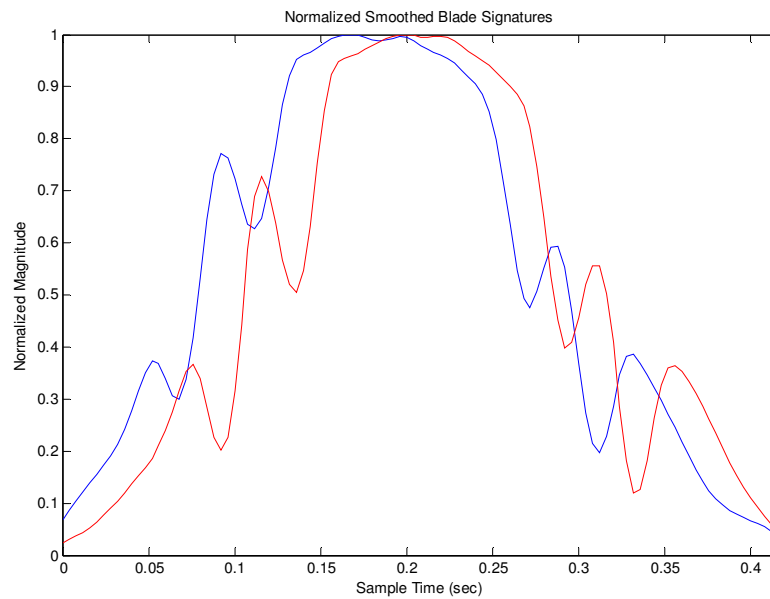


Figure 4.4. Double Blade™ Inductive Sensors on Bison Ave in the University of California, Irvine



a. Normalized double conventional round inductive loop signatures



b. Normalized double Blade™ inductive signatures

Figure 4.5. Comparison of double conventional round and Blade™ inductive signatures

### **4.3 DATA ORGANIZATION**

The data used to develop the speed profile transformation model was obtained from the UCI Bison Ave study site as described in Section 3.1. The March 7 2008 dataset was used as the calibration dataset, while the April 15 2008 was assigned as the test dataset for model evaluation.

### **4.4 SIGNATURE PRE-PROCESSING**

#### **4.4.1 Signature Interpolation and Noise Filtering**

The first step in signature preprocessing involves interpolation to achieve a consistent rate of sampling for all vehicle signatures. This helps to address the issue of inconsistent sampling due to random dropped data found in the Blade™ inductive signatures.

A non-causal averaging filter is then applied to the raw signatures to subdue white noise effects. This procedure helps to improve measurement of headways along the Blade™ inductive signatures described in the following steps. Each filtered data point  $FiltMag_{ji}^k$  is obtained as the average of neighboring data points from the normalized signature as shown in the following equation:

$$FiltMag_{ji}^k = \frac{1}{n} \left( \sum_{m=i-(n-1)/2}^{i+(n-1)/2} Mag_{ji}^k \right), \quad \forall 1 \leq i \leq I$$

Where

- $FiltMag_{ji}^k$  -  $i^{\text{th}}$  filtered magnitude sample of  $k^{\text{th}}$  vehicle obtained from sensor position  $j$
- $Mag_{ji}^k$  -  $i^{\text{th}}$  raw magnitude sample of  $k^{\text{th}}$  vehicle obtained from sensor position  $j$
- $n$  - size of averaging filter ( $n = 3$  is used in this study)

Figure 4.6 shows the double Blade™ inductive signatures of a vehicle before and after applying signature interpolation and noise filtering, where it is observed that noise observed in the raw signatures is suppressed after the noise filtering process.

#### 4.4.2 Magnitude Normalization

The signatures from both sensors are then normalized in the magnitude axis to address differences in sensitivity between the two sensors. Unlike conventional inductive round loop vehicle signatures, Blade™ inductive signatures occasionally have less consistent peak magnitudes due to the influence of wheel spikes. As a consequence, normalizing both signatures of a double loop sensor setup by their corresponding peak magnitudes – a common method used in previous inductive signature studies (Jeng and Ritchie 2006, Tok et al. 2007, Jeng et al. 2007, Jeng and Ritchie 2008) – may not yield inductive signatures with equal sensitivity.

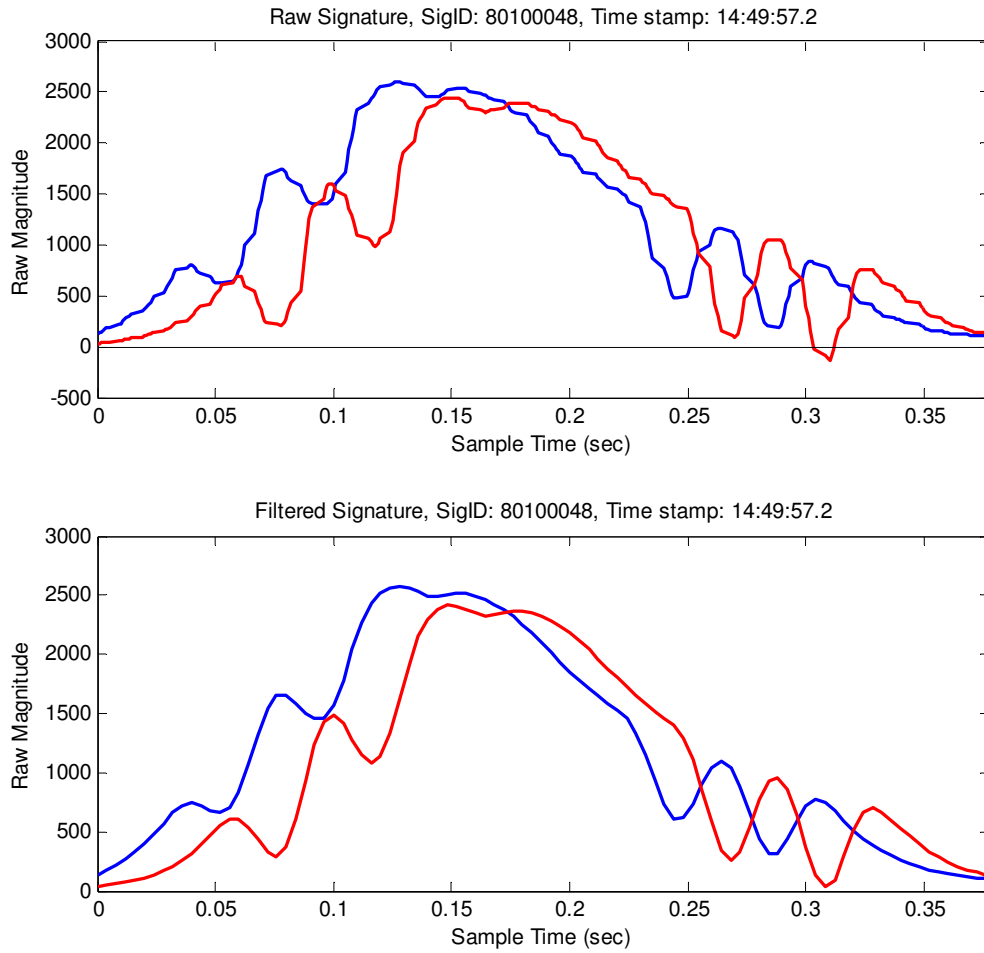


Figure 4.6. Comparison of raw vs. interpolated and filtered Blade™ inductive signatures

The approach used in this study assumes that the sensitivity of the Blade™ inductive sensors remain constant. A statistically significant sample of vehicles is first analyzed to determine the sensitivity ratio between the sensors. This is achieved by taking signature samples of the initial 30 vehicles in each dataset. The ratio of the peak magnitudes between the leading and trailing Blade™ inductive sensors is obtained for each of the 30 sampled vehicles. The median peak magnitude ratio of this sample is assigned as the

Magnitude Normalization Ratio (MNR). To obtain the normalized inductive signatures, the signature from the leading sensor is divided by its peak magnitude. Next, the signature from the trailing (second) sensor is divided by the peak magnitude of the first signature and subsequently multiplied by the MNR to obtain a signature of equal sensitivity to the first.

$$\begin{aligned}
 PeakMag_j^k &= \max\{FiltMag_{ji}^k\}, \quad \forall 1 \leq i \leq I_j^k \\
 MNR &= \text{median}\{PeakMag_2^k / PeakMag_1^k\}, \quad \forall k = 1, \dots, 30 \\
 NormMag_{ji}^k &= \begin{cases} FiltMag_{ji}^k / PeakMag_1^k, & \forall 1 \leq i \leq I_j^k, j = 1, k > 30 \\ (FiltMag_{ji}^k / PeakMag_1^k) \times MNR, & \forall 1 \leq i \leq I_j^k, j = 2, k > 30 \end{cases}
 \end{aligned}$$

Where

- $i$  - interpolated magnitude sample number within a vehicle signature
- $j$  - sensor position (1 – leading sensor, 2 – trailing sensor)
- $k$  - vehicle sample number
- $I_j^k$  - total number of interpolated magnitude samples in  $k^{\text{th}}$  vehicle obtained from sensor position  $j$
- $PeakMag_j^k$  - peak signature magnitude of  $k^{\text{th}}$  vehicle obtained from sensor position  $j$
- $NormMag_{ji}^k$  -  $i^{\text{th}}$  normalized magnitude sample of  $k^{\text{th}}$  vehicle obtained from sensor position  $j$

Figure 4.7 shows a comparison of double Blade™ inductive signatures normalized using the conventional method used in previous inductive signature studies and the new MNR-based method. In the conventional method, the body of the leading signature (blue) is noticeably lower than the trailing signature (red) after normalization. In contrast, there is

no observable difference in the body of the leading and trailing signatures using the new MNR-based signature normalization technique.

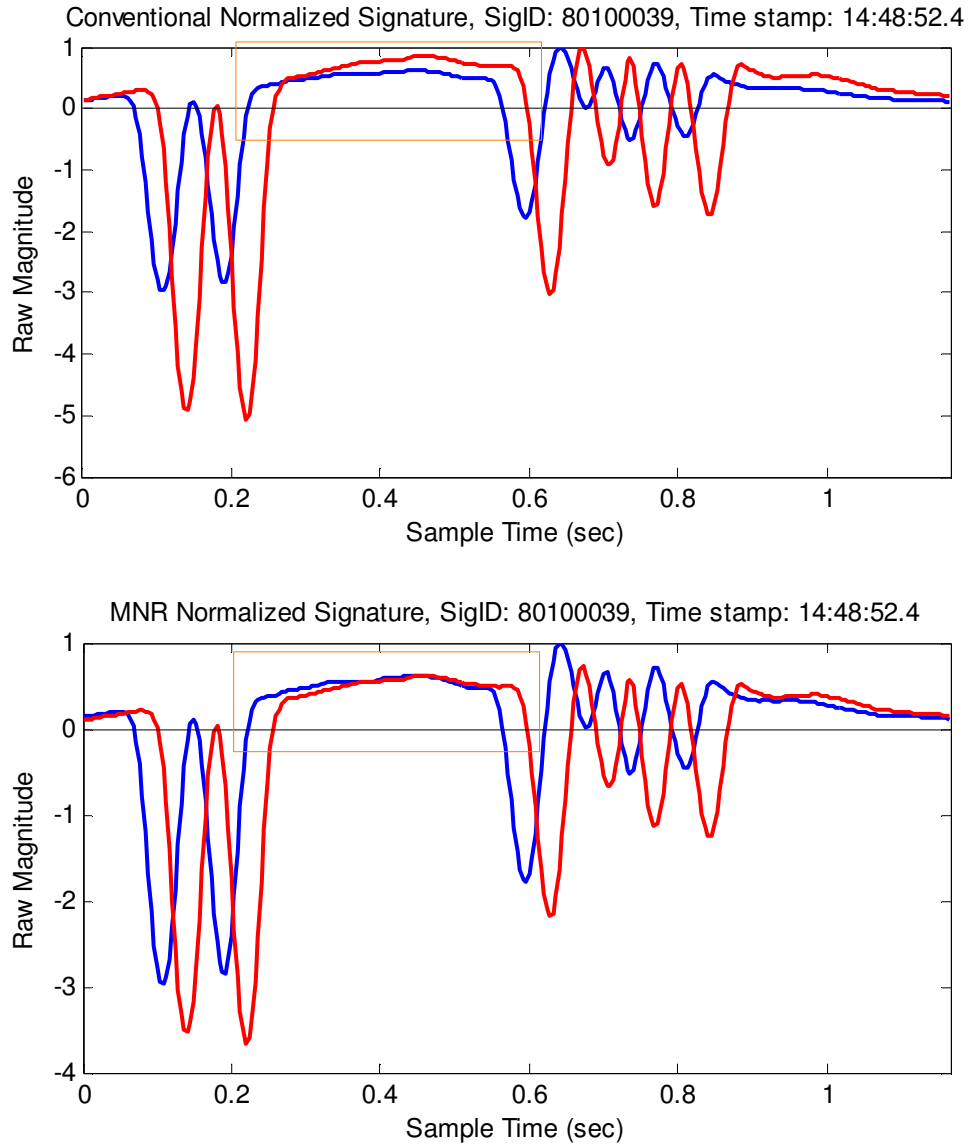


Figure 4.7. Comparison between conventional magnitude normalization and MNR magnitude normalization

## 4.5 METHODOLOGY

### 4.5.1 Speed Profile Estimation

#### Point Sampling

The first step in speed profile estimation involves measuring headways between the leading and trailing Blade™ inductive signatures at uniform intervals. The interval needs to be small enough such that it can provide aggregated estimates of the vehicle speed, yet large enough to minimize computational burden. In this study, the headways are measured at intervals of 0.02 seconds along each Blade™ inductive signature.

#### Slope Analysis

Blade™ inductive signatures are obtained from an analog signal which is subject to external noise interference. Because of this, there exists some level of data uncertainty which may lead to errors in measuring the each signature headway sample. Figure 4.8 illustrates that the margin of error of the signature headway measurement varies along the signature, and is dependent on the slope of the signature. Assuming a consistent range of magnitude uncertainty  $\delta$  across the signature, it can be observed that the margin of headway measurement error  $\epsilon_2$  corresponding to a point on the signature with a gentle gradient is significantly larger than  $\epsilon_1$ , which is obtained from a point with steeper gradient. Hence the selected points along the signature need to be subjected to a slope



threshold test prior to headway measurement. This test rejects points where the slope gradients are too gentle and are likely to yield significant headway measurement errors.

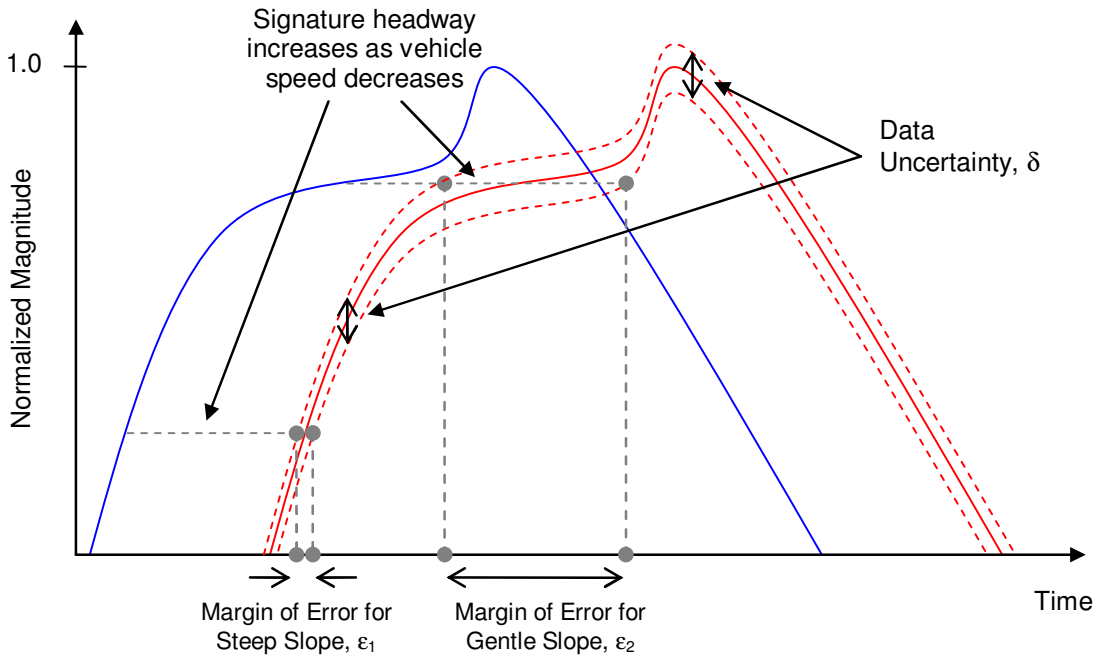


Figure 4.8. Error Sensitivity with respect to Signature Gradients

However, slope gradients of slow moving vehicle signatures also yield gentler slope gradients than fast moving ones. Thus, a fixed gradient threshold would likely reject most headway measures sampled from slow vehicles. Since slow vehicles yield a corresponding larger headway nonetheless, the percentage error of the headways measured from slow vehicles would be smaller than on fast ones. Hence, the slope threshold should be relaxed for slow vehicles. This is addressed by using a threshold that varies with the signature duration. Consequently, the slope threshold used in this study is 0.003 divided by the signature duration for each vehicle signature. Figure 4.9 shows a

sample signature with corresponding slope values at 0.02 second intervals. Accepted points are shown as blue circles and rejected points are shown as red crosses.

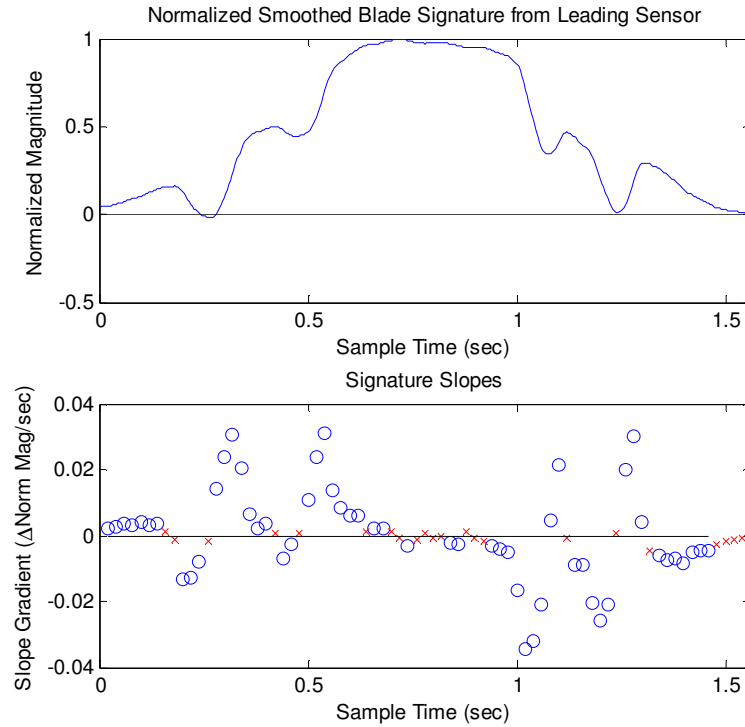


Figure 4.9. Analysis of slopes computed from normalized and smoothed Blade™ inductive signature

### **Representative Segment Speed Estimation**

To obtain the speed corresponding to each accepted point, a forward search is performed to find a data point on the second Blade™ inductive signature with equal magnitude and possessing the same gradient direction as the reference data point from the first Blade™ inductive signature. The preliminary speed estimates along the signature are

subsequently calculated by dividing the distance  $L_s$  between the leading edges of the double Blade™ inductive sensors by each headway measurement.

Ideally, the preliminary speed estimates should provide an accurate speed profile of the vehicle if both Blade™ inductive sensors provide clean and equally sensitive signatures. However, this cannot be achieved in the field due to external influences and hardware limitations. Hence, the vehicle speed profile needs to be approximated from the preliminary speed estimates obtained. First, the vehicle signature is divided into equal time segments from which a Representative Segment Speed (RSS) is obtained. The RSS is defined as the median of the preliminary speed estimate samples within the segment as the median statistic is not biased by outliers. The optimal segment size should be sufficiently large such that there are adequate preliminary speed estimate samples to obtain an accurate RSS, yet small enough that speed remains relative constant within. The Maximum Time Segment (MaTS) parameter specifies the largest segment size constraint with the objective minimizing the total number of equal segment partitions within the vehicle signature. MaTS values ranging from 0.5 to 1.5 seconds were analyzed in this study.

### **Speed Profile Estimation**

After the RSSs are obtained for each time segment, the RSSs are subsequently interpolated to yield the estimated speed profile of the vehicle. The shape-preserving Piecewise Cubic Hermite Interpolating Polynomial (PCHIP) interpolation method was used as it preserves monotonicity and the shape of the data (Fritsch and Carlson, 1980).

In addition, it has no bumps and shows less oscillation compared with the more commonly used cubic spline interpolation method, making it an ideal method for estimating the vehicle speed profile.

Figure 4.10 shows an example of double Blade™ inductive signatures followed by the preliminary speed estimates (shown as blue circle plots) that subsequently yield the RSSs (shown as red crosses) and finally the speed profile using the PCHIP interpolation method. Figure 4.11 shows samples of vehicles with their speed profiles accelerating, decelerating and stopped over the Blade™ inductive sensors. The blue lines represent the leading signature, the red represent the trailing signatures and the speed profiles are represented by each green curve.

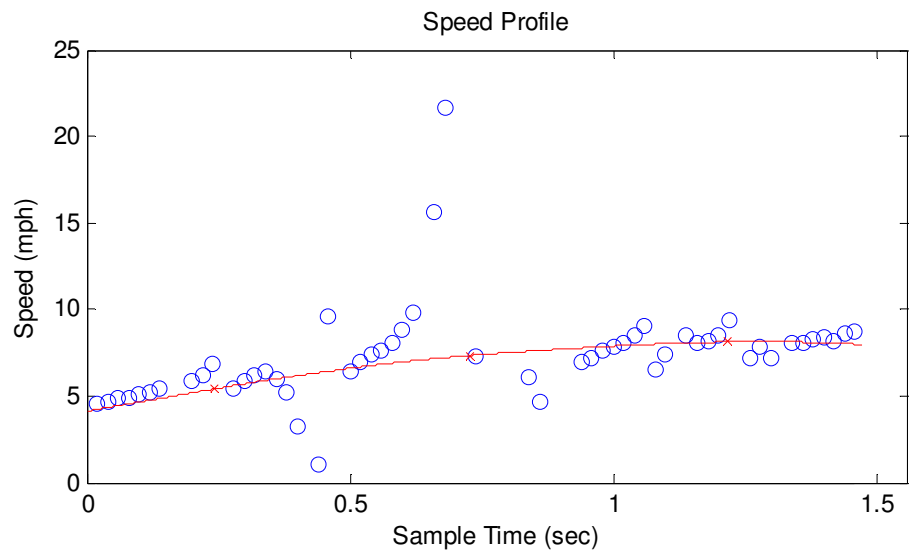
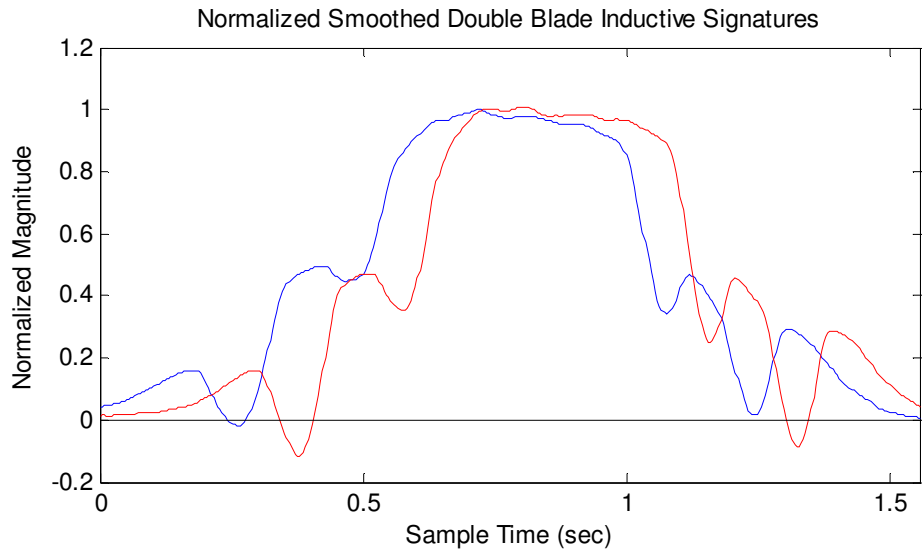
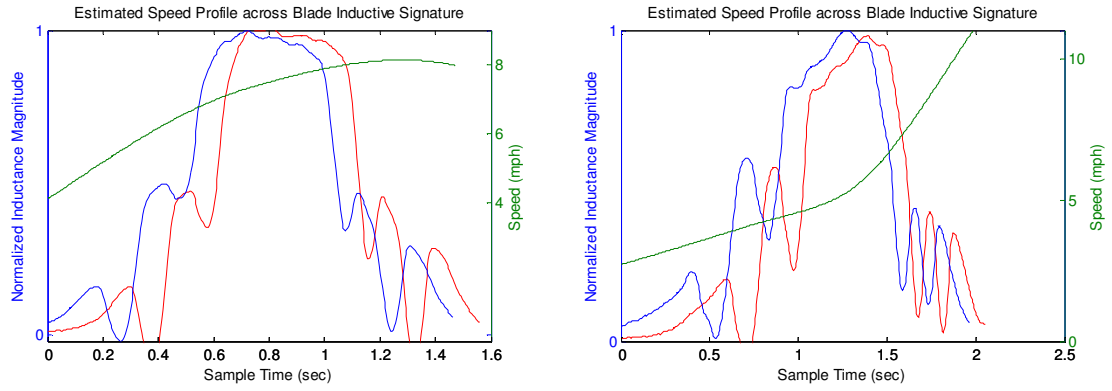
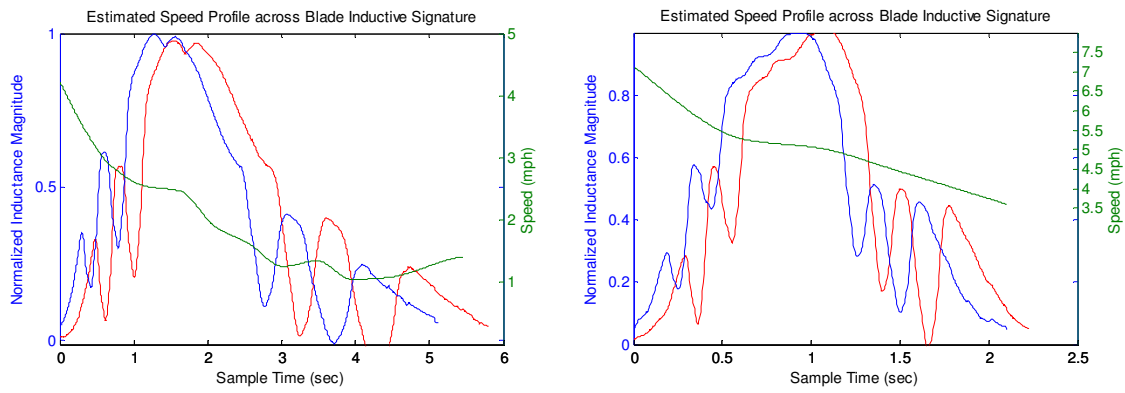


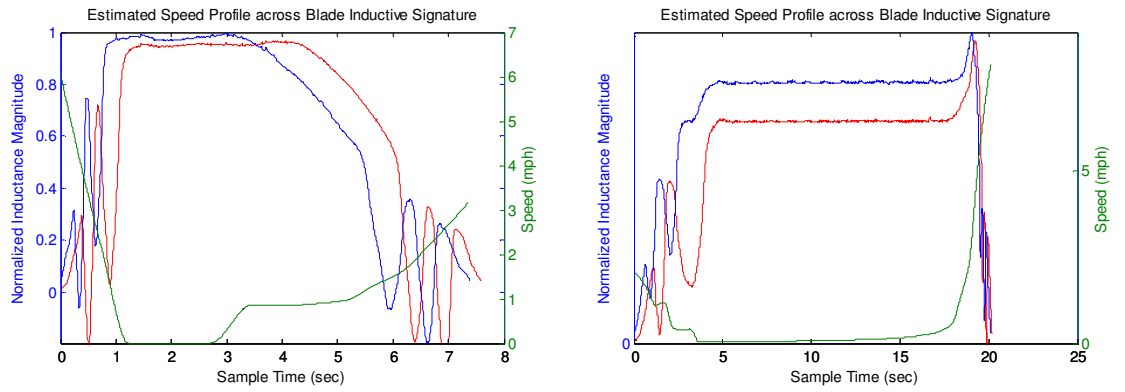
Figure 4.10. Estimation of vehicle speed profile



a. Accelerating Vehicles



b. Decelerating Vehicles



c. Stopped Vehicles

Figure 4.11. Sample of Blade™ Inductive Signatures with Corresponding Speed Profiles

## 4.5.2 Temporal-Spatial Transformation

### **Speed Profile Interpolation Temporal-Spatial Transformation**

After the speed profile is obtained, the Speed PRofile INterpolation Temporal-Spatial (SPRINTS) transformation is performed on the normalized Blade™ inductive signature to obtain the SPRINTS transformed signature. This is achieved by multiplying the estimated speed at every interpolated data point by the interpolated time step between inductance samples,  $\Delta t$ . Each resulting product represents the physical longitudinal distance between adjacent interpolated signature data points. The sum of these points yields the SPRINTS transformed vehicle length.

### **Conventional Speed-trap Temporal-Spatial Transformation**

The Conventional Speed-trap Temporal-Spatial (COSTS) transformation is used as a baseline performance comparison with the SPRINTS transformation. In the COSTS transformation method, the first reference point is identified as the first point on the leading signature that crosses the normalized magnitude value of 0.5 subjected to the constraint such that the slope at the first reference point is positive. The second reference point is identified as the first point on the trailing signature that crosses the normalized magnitude value of 0.5 subject to the constraints such that the signature slope at the second reference point is positive and the timestamp of the second reference point is greater than the first as shown in Figure 4.12. The temporal difference between these reference points yields the headway between the leading and trailing signatures,  $\Delta \tilde{t}$ .

Since, constant speed is assumed in the COSTS transformation, dividing the sensor length  $L_s$  by  $\Delta \tilde{t}$  gives the representative speed of the vehicle  $\tilde{v}$ .

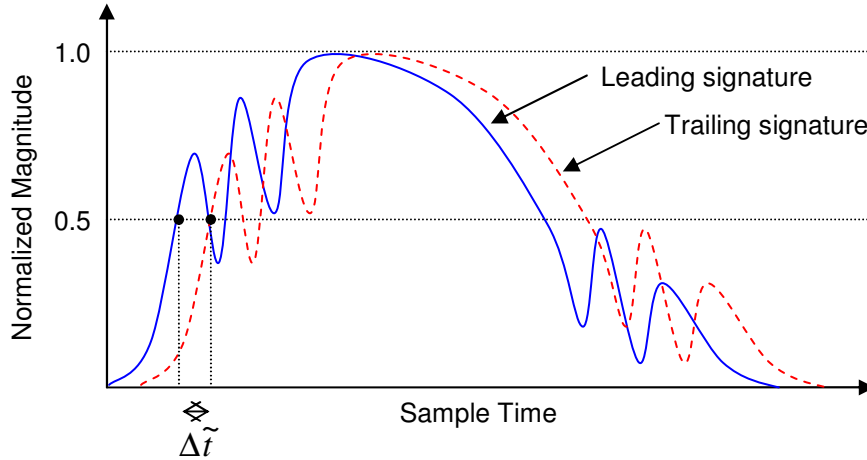


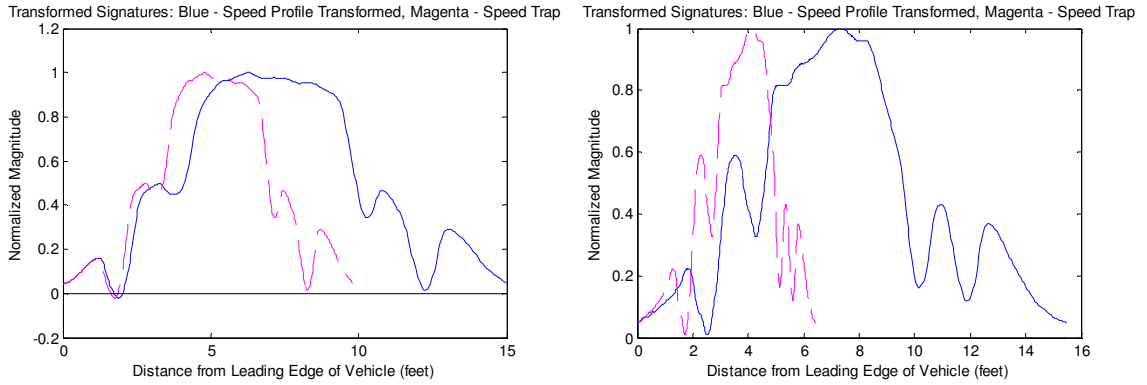
Figure 4.12. Obtaining signature headway for Conventional Speed-trap Temporal-Spatial (COSTS) transformation

### **Comparison of SPRINTS and COSTS Transformation Methods**

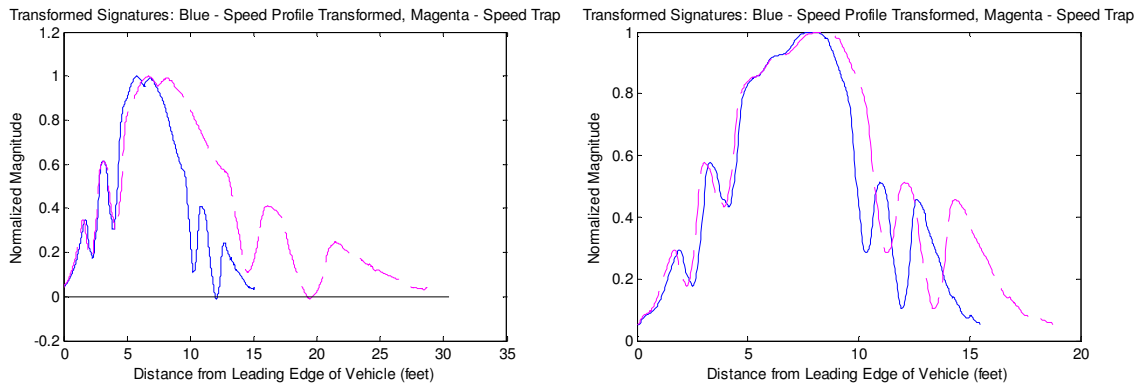
Figure 4.13 shows a comparison of the temporal-spatial transformed Blade™ inductive signatures from passenger vehicles estimated using the SPRINTS transformation (shown in solid blue) and the COSTS transformation method (shown in dashed magenta). Each plot shown in Figure 4.13 corresponds to the same vehicle in Figure 4.11 in their respective positions. In Figure 4.13a, it is observed that inductive signatures subjected to the COSTS transformation yield shorter vehicle length estimates for vehicles undergoing acceleration compared with the SPRINTS transformation. On the other hand, inductive signatures undergoing deceleration yield longer length estimates with the COSTS transformation than with the SPRINTS transformation as shown in Figure 4.13b.



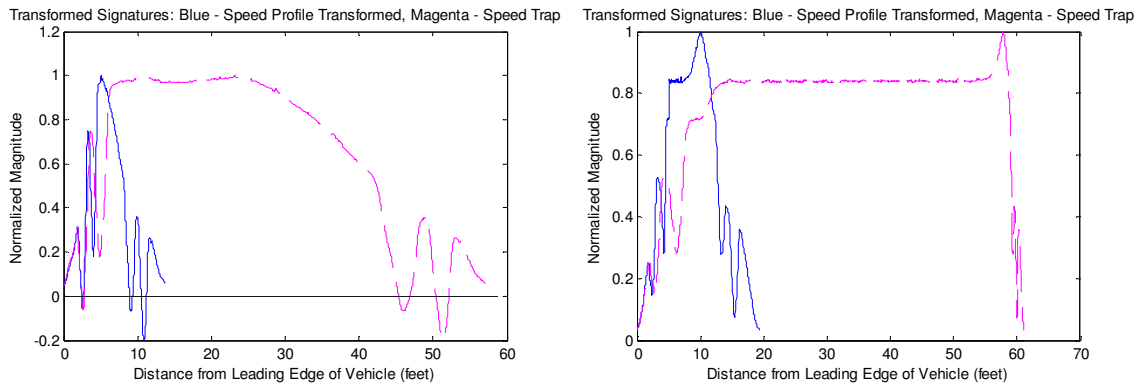
Stopped vehicles result in the most extreme length estimates by the COSTS transformation method as shown in Figure 4.13c.



a. Accelerating Vehicles



b. Decelerating Vehicles



c. Stopped Vehicles

Figure 4.13. Comparison of vehicle signatures and estimated vehicle lengths obtained via SPRINTS vs. COSTS Transformation

**Sensitivity Analysis of Maximum Time Segment (MaTS)**

Table 4.1 presents the comparison of estimated lengths of the control vehicles used in the test data set using the conventional speed trap method and the speed profile transformation method with MaTS values ranging from 0.50 to 1.50. The duration analysis shows the variability of duration measures across all sampled runs from each control vehicle. This provides an indicator for the variation in driving patterns across the sensors.

Table 4.1. Comparison of Estimated Control Vehicles Lengths in Calibration Dataset (March 7 2008)

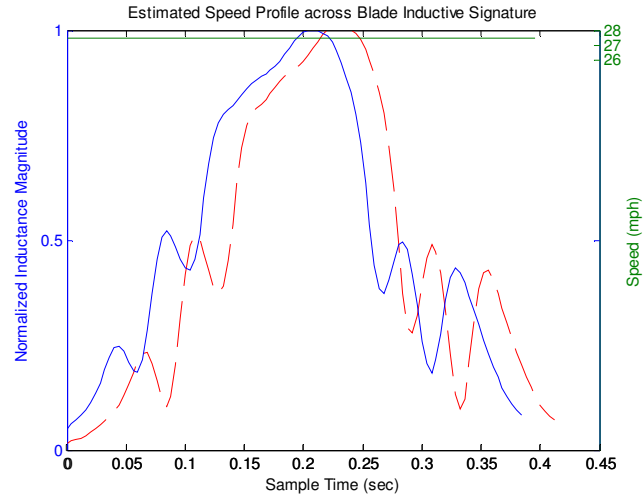
Control Vehicle No.	Description	No. Runs	Duration (sec)				Transformation Method	Max Time Segment (MaTS)	Length Estimation		
			Max	Min	Mean	Std Dev			Mean (feet)	Std Dev (feet)	Δ Std Dev (%)
1	Honda Civic	14	1.12	0.29	0.55	0.29	COSTS	-	15.38	1.08	-
							SPRINTS	0.50	16.12	0.93	-13.5%
								0.75	16.14	0.96	-10.9%
								1.00	16.12	0.98	-8.9%
								1.25	16.20	1.13	4.8%
								1.50	16.20	1.13	4.8%
2	BMW 325is	19	5.31	0.27	1.25	1.24	COSTS	-	16.02	6.32	-
							SPRINTS	0.50	15.85	0.82	-87.1%
								0.75	16.02	1.26	-80.0%
								1.00	15.81	0.76	-88.0%
								1.25	15.78	0.80	-87.3%
								1.50	15.65	0.61	-90.4%

The first control vehicle had relatively consistent speed runs, exhibiting a standard deviation of only 0.29 seconds across all 14 runs. Furthermore, the average duration of 0.55 seconds from the first control vehicle also indicate that most of the signature samples were obtained at relatively high and constant speeds. The duration analysis results for second control vehicle showed an average duration of 1.25 seconds with a standard deviation of 1.24 seconds. The maximum duration obtained was 5.31 seconds. Figure 4.14 shows a comparison of Blade™ inductive signatures obtained from control

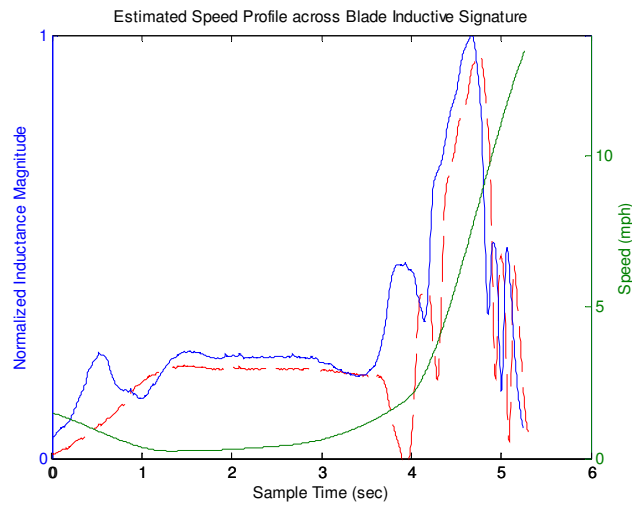
vehicle 2 with low duration (Figure 4.14a) at constant speed and maximum duration (Figure 4.14b) where effects of acceleration and deceleration are evident.

According to the results on the control vehicles from the calibration dataset shown in Table 4.1, the SPRINTS transformation reduces the standard deviation of length estimates for control vehicle 1 with MaTS values ranging from 0.5 to 1.0 and for control vehicle 2 across all MaTS values tested. In particular, the SPRINTS transformation shows exceptional improvement for control vehicle 2 with standard deviation reductions of at least 80 percent across the range of MaTS values. This indicates that the SPRINTS transformation shows the most significant improvements in length estimates corresponding to Blade™ inductive signatures with high durations—a proxy for significant acceleration and deceleration effects—that would result in erroneous length measures using the COSTS transformation method. Overall, the results also show that standard deviations of estimated vehicle speeds are relatively insensitive to MaTS values.

There are however some observable trend differences in estimated vehicle length standard deviations of the two control vehicles as shown in Figure 4.15. Control vehicle 1 shows increase of estimated vehicle length standard deviation with larger MaTS values. However, there is a general decreasing trend of estimated vehicle length standard deviation with increase in MaTS values for control vehicle 2. The ideal MaTS value was chosen to be 1.0 based on these observations.



(a) Control vehicle 2 at constant speed over double Blade™ inductive sensors



(b) Control vehicle 2 decelerating and accelerating over double Blade™ inductive sensors

Figure 4.14. Control vehicle inductive signatures under different driving conditions

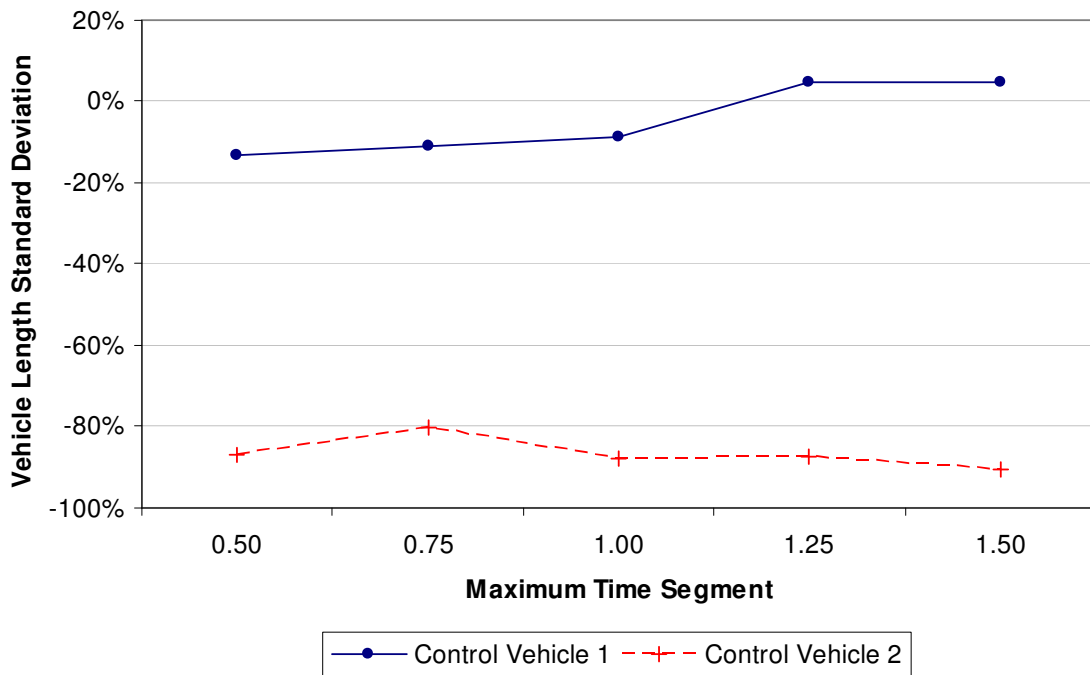


Figure 4.15. Comparison of standard deviation changes with Maximum Time Segment values

## 4.6 RESULTS ANALYSIS

### 4.6.1 Evaluation of Control Vehicles in Test Dataset

Table 4.2 shows the comparison of length estimations using the COSTS and SPRINTS transformation model using a MaTS value of 1.0. Control vehicles 2 and 3 had relatively consistent speed samples, while control vehicles 1, 4 and 5 performed acceleration and deceleration over the sensors at low speeds on some runs to generate distorted vehicle signatures, as evidenced by the larger standard deviation of vehicle durations. Overall, the SPRINTS transformation method consistently yielded more reliable vehicle length

estimations than the COSTS transformation method, shown by the reduction of estimated vehicle length standard deviations obtained. In fact, estimated vehicle length standard deviations across all control vehicles were less than one foot using the SPRINTS transformation method.

Table 4.2. Length statistics from control vehicles in test dataset (April 15 2008)

Control Vehicle No.	Description	No. Runs	Duration (sec)				Transformation Method	Length Estimation		
			Max	Min	Mean	Std Dev		Mean (feet)	Std Dev (feet)	Δ Std Dev (%)
1	Alfa Romeo Spider	20	1.50	0.29	0.69	0.38	COSTS	15.68	1.476	-
							SPRINTS	15.13	0.450	-69.5%
2	Toyota Camry V6	18	0.96	0.32	0.50	0.17	COSTS	18.01	2.260	-
							SPRINTS	17.07	0.590	-73.9%
3	Toyota Camry	18	0.76	0.30	0.46	0.12	COSTS	17.11	1.260	-
							SPRINTS	17.29	0.997	-20.9%
4	Acura Integra	24	2.54	0.33	0.69	0.53	COSTS	13.23	3.561	-
							SPRINTS	15.40	0.606	-83.0%
5	Hyundai Santa Fe	19	1.54	0.28	0.53	0.37	COSTS	14.73	2.235	-
							SPRINTS	15.23	0.726	-67.50%

#### 4.6.2 Length Statistics within Vehicle Classes

In this analysis, vehicles in each dataset are classified into one of three vehicle classes: passenger vehicles, small commercial vehicles and medium/ large commercial vehicles. Passenger vehicles consist of sedans, coupes, station wagons, cross-overs, sport utility vehicles and minivans. Small commercial vehicles include light duty four-tire commercial vehicles such as vans and pick-up trucks. Single and multiple unit

commercial vehicles with two or more axles with a total of six or more tires are classified as medium/ large commercial vehicles.

Table 4.3 and Table 4.4 show the comparison of length statistics for the three vehicle classes on the calibration dataset obtained from March 7 2008 and test dataset from April 15 2008, respectively. The mean and standard deviation of vehicle lengths for each vehicle class are reported using the COSTS and SPRINTS transformation methods. The SPRINTS transformation resulted in significant reductions of estimated vehicle length standard deviations across all three vehicle classes for both the calibration as well as the test datasets.

These results indicate that the SPRINTS transformation method yields better length estimates than the COSTS transformation method, since they corroborate the assumption that vehicle lengths within passenger vehicles and small commercial vehicles should be similar given the homogeneity of vehicle lengths observed in these vehicle classes. Medium/ large commercial vehicles obtained a higher standard deviation of estimated vehicle lengths than the passenger vehicle and small commercial vehicle classes using the SPRINTS transformation method. This is expected, as there is higher heterogeneity of vehicle lengths amongst medium and large commercial vehicles, which vary from two-axle six-tire single unit to multiple-unit trucks. Still the standard deviation of vehicle length for this class obtained using the SPRINTS transformation is 28.0 percent lower compared with the COSTS transformation method as reported by the results on the test

dataset in Table 4.3. This indicates that length estimation accuracy is still significantly improved for vehicles in the medium/ large commercial vehicle class.

The reduction in standard deviation of estimated vehicle lengths using the SPRINTS transformation method compared with the COSTS transformation method in the test dataset as shown in Table 4.4 confirms that the SPRINTS transformation model shows good temporal transferability.

Table 4.3. Comparison of Estimated Lengths by Vehicle Types from Mar 7 2008 Calibration Dataset

Vehicle Type	Count	Conventional Speed-Trap (CSTS)		Speed Profile (SPTS)		$\Delta$ Std Dev (%)
		Mean (feet)	Std Dev (feet)	Mean (feet)	Std Dev (feet)	
Passenger Vehicle	873	16.02	7.55	16.15	1.79	-76.3%
Small Commercial Vehicle	99	14.67	7.39	18.25	2.53	-65.8%
Medium / Large Commercial Vehicle	23	24.96	11.31	25.68	8.14	-28.0%

Table 4.4. Comparison of Estimated Lengths by Vehicle Types from Apr 15 2008 Test Dataset

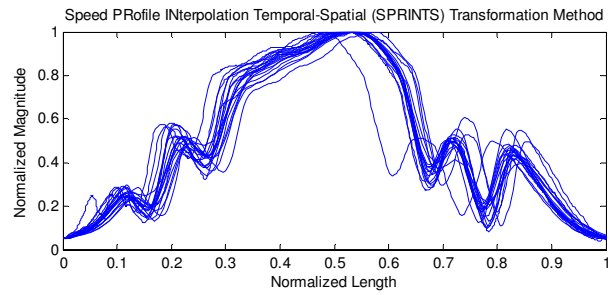
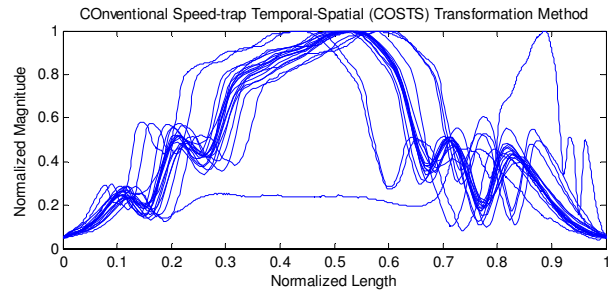
Vehicle Type	Count	COSTS		SPRINTS		$\Delta$ Std Dev (%)
		Mean (feet)	Std Dev (feet)	Mean (feet)	Std Dev (feet)	
Passenger Vehicle	966	16.19	11.41	16.08	1.26	-88.9%
Small Commercial Vehicle	144	17.61	2.90	17.53	1.88	-35.1%
Medium / Large Commercial Vehicle	19	29.95	10.98	27.44	7.09	-35.4%



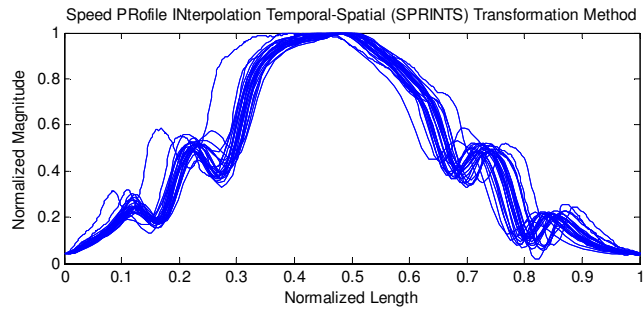
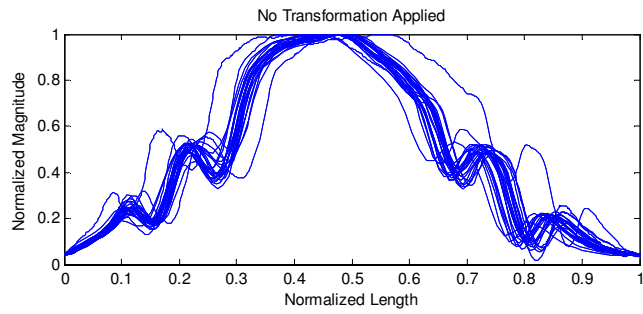
Results from Table 4.3 and Table 4.4 confirm that significant vehicle signature distortion errors can be found in arterial traffic. Such distortion errors may not only affect the consistency and reliability of features extracted from these signatures but also result in erroneous individual vehicle length measures as shown in Figure 4.13. They have the potential to affect the reliability of advanced transportation surveillance systems based on vehicle signatures if the distortions within the vehicle signatures are not corrected.

### **4.6.3 Consistency of Signatures**

The purpose of this analysis is to evaluate the consistency of Blade™ inductive signatures from a control vehicle before and after application of the SPRINTS transformation model. Figure 4.16 shows overlays of Blade™ inductive signature samples from two control vehicles. For each vehicle, the top plot shows signatures where no distortion correction was applied. The bottom plot shows signatures obtained using the SPRINTS transformation method. Signatures in both plots were normalized in the length axis for a clearer presentation of signature distortion. It is evident that the bottom plots for each vehicle show more consistent Blade™ inductive signature samples than the top, indicating significantly improved repeatability of Blade™ inductive signatures from a vehicle through the SPRINTS transformation method.



(a) Calibration dataset control vehicle 2



(b) Test dataset control vehicle 4

Figure 4.16. Comparison of signature distortion before and after SPRINTS transformation

## 4.7 DISCUSSIONS

The SPRINTS transformation model described in this chapter provides the solution to obtain distortion-corrected vehicle inductive signatures from vehicles traversing Blade™ inductive sensors in unstable traffic conditions. This is especially useful for advanced traffic surveillance systems based on inductive signatures to provide accurate traffic performance measures under peak congestion periods, where reliable information is of the essence.

The analysis of signature consistency further illustrates that the SPRINTS transformation method has the potential to improve the performance of inductive signature-based vehicle re-identification models by generating more repeatable inductive vehicle signatures even under adverse traffic circumstances.

## CHAPTER 5 GENERAL VEHICLE CLASSIFICATION

### 5.1 CLASSIFICATION SYSTEM FRAMEWORK

The General Vehicle Classification (G-VEC) model described in this chapter classifies vehicles into four distinctive categories as shown in Table 5.1. The corresponding FHWA scheme F assignments for each class are also shown. Class G1 consists of passenger-type vehicles such as motorcycles, sedans, coupes, sport utility vehicles, cross-overs and minivans. Class G2 includes small commercial vehicles such as four-tire vans and pick-up trucks and class G3 consists of all medium and large commercial vehicles.

Table 5.1 General Vehicle Classification (G-VEC) Scheme

<b>Class</b>	<b>Description</b>	<b>FHWA Scheme F Equivalent</b>
G1	Passenger Vehicles	1,2
G2	Light Commercial Vehicles	3
G3	Medium/ Heavy Commercial Vehicles	4 through 13

The main purpose of this classification model is to provide an initial distinction of medium and heavy commercial vehicles (G3) from other vehicles types (G1 and G2) using a simple classification approach that uses minimal computational resources. This allows vehicles in class G3 to be analyzed in further detail using models described in Chapters 6 and 7.

## **5.2 DATA ORGANIZATION**

The G-VEC model was developed using data collected from the UCI Bison Ave and the southbound San Onofre Truck Weigh and Inspection Facility study sites as described in Sections 3.1 and 3.2, respectively. 300 randomly selected passenger vehicles together with all light, medium and heavy commercial vehicles were sampled from March 7 2008, March 10 2008 and April 15 2008 UCI Bison Ave datasets. As medium and heavy commercial vehicle samples were limited in the UCI Bison Ave datasets, an additional 363 medium and heavy commercial vehicles were sampled from the San Onofre dataset to improve the representation of commercial vehicles for model development, resulting in an overall dataset of 990 vehicles used for developing the G-VEC model.

Of this combined dataset described above, 50 percent was randomly selected for model training, a further 20 percent was set aside for model validation, with the remaining 30 percent used for model testing.

## **5.3 SIGNATURE PRE-PROCESSING**

Blade™ vehicle inductive signatures obtained from the UCI Bison Ave study site were pre-processed and transformed with the SPRINTS transformation method as described in sections 4.4, 4.5, respectively.

The double Blade™ inductive sensors at the San Onofre study site were spaced at 1.8 m (6 feet) between the leading edges of the sensors (refer to Figure 3.5). As a consequence, the Blade™ inductive signatures obtained at this site were not suitable for the SPRINTS transformation method. Hence, the COSTS transformation method described in Section 4.5.2 was applied instead.

## **5.4 MODEL DEVELOPMENT**

### **5.4.1 Feature Extraction**

Seven input features are extracted for development of the G-VEC model. The first input feature is the temporal-spatial transformed vehicle length as described in section 4.5.2. Next all negative magnitude regions of the Blade™ inductive signature are set to zero. The subsequent six features extracted are the interpolated NOrmalized MAgnitude Difference (NOMAD) values as shown in Figure 5.1.

#### **Normalized Magnitude Difference Feature Extraction**

In NOMAD feature extraction, the SPRINTS transformed Blade inductive signature is first length normalized by dividing the x-component of each sample data point by the signature length. The cubic spline interpolation method is subsequently applied to obtain the normalized magnitude values at six equally-spaced interval values along the length-normalized Blade™ inductive signature.

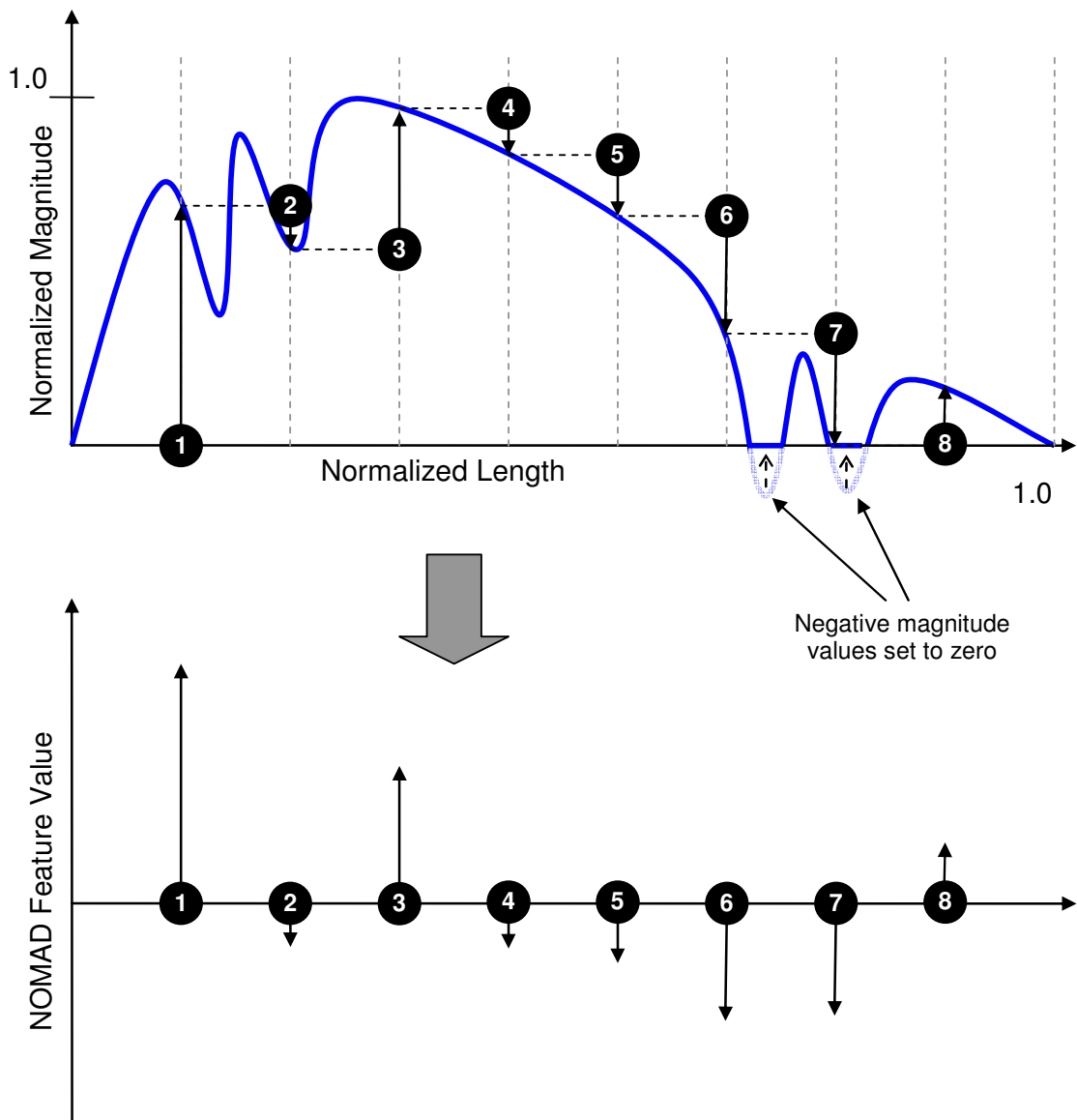


Figure 5.1. Extracting NOMAD features from a Blade inductive signature

## 5.4.2 Statistical Analysis of Input Features

Statistical analysis was performed to determine the suitability of features for model development. Ideally, input features should be independent and show good of potential for distinguishing vehicle types according to the G-VEC classification scheme presented in Table 5.1.

### Pearson's Bivariate Correlation Analysis

Table 5.2 shows results of the Pearson's bi-variate correlation analysis on the model input features extracted from Blade™ inductive signatures. The strongest absolute correlations are observed between Signature Length and features NOMAD1 and NOMAD3 with correlations of 0.662 and 0.624. Other features that showed correlation above 0.5 are between Signature Length and NOMAD6, NOMAD1 and NOMAD 2 as well as NOMAD 1 and NOMAD3. All other variables showed relatively low correlation.



Table 5.2. Pearson’s correlation analysis on extracted Blade™ inductive signature features

	Signature Length	NOMAD1	NOMAD2	NOMAD3	NOMAD4	NOMAD5	NOMAD6	NOMAD7	NOMAD8
Signature Length	1.000	0.662	-0.438	-0.624	0.149	0.133	0.588	0.105	0.024
NOMAD1	0.662	1.000	-0.586	-0.512	0.309	0.035	0.362	0.016	-0.107
NOMAD2	-0.438	-0.586	1.000	-0.229	-0.163	-0.026	-0.171	0.018	-0.031
NOMAD3	-0.624	-0.512	-0.229	1.000	-0.310	-0.180	-0.461	-0.112	0.126
NOMAD4	0.149	0.309	-0.163	-0.310	1.000	-0.105	0.001	-0.189	-0.165
NOMAD5	0.133	0.035	-0.026	-0.180	-0.105	1.000	-0.122	-0.020	0.065
NOMAD6	0.588	0.362	-0.171	-0.461	0.001	-0.122	1.000	-0.260	-0.298
NOMAD7	0.105	0.016	0.018	-0.112	-0.189	-0.020	-0.260	1.000	-0.147
NOMAD8	0.024	-0.107	-0.031	0.126	-0.165	0.065	-0.298	-0.147	1.000

**Levene’s Homogeneity-of-Variance Test**

Next, the Levene’s homogeneity-of-variance test was performed on the extracted input features, grouped by vehicle class. This test determines if the variance of input features with vehicle classes are equal – a necessary condition for applying the analysis of variance (Levene, 1960). Table 5.3 shows the analysis results obtained from Levene’s homogeneity-of-variance test. All input features show significance beyond the 1 percent level. Hence, it is concluded that significance differences in variance within G-VEC vehicle classes for all input features exist, and that the analysis of variance is not suitable for this data. For this reason, the Kruskal-Wallis one-way analysis of variance by ranks was performed instead to determine if there is significant difference in population medians among the vehicle classes for each input feature (Kruskal and Wallis, 1952).

Table 5.3. Levene’s homogeneity-of-variance test on extracted Blade™ inductive signature features

	<b>Levene Statistic</b>	<b>df1</b>	<b>df2</b>	<b>Sig.</b>
<b>Signature Length</b>	1272.59922	2	996	4.532E-275
<b>NOMAD1</b>	493.432994	2	996	1.205E-149
<b>NOMAD2</b>	275.430017	2	996	6.1171E-96
<b>NOMAD3</b>	131.076803	2	996	2.9227E-51
<b>NOMAD4</b>	99.1580959	2	996	5.3423E-40
<b>NOMAD5</b>	5.53771476	2	996	0.00405765
<b>NOMAD6</b>	46.947796	2	996	3.277E-20
<b>NOMAD7</b>	29.1572315	2	996	4.9432E-13
<b>NOMAD8</b>	72.6346486	2	996	3.5798E-30

**Kruskal-Wallis One-Way Analysis-of-Variance Test**

Table 5.4 shows the rank results by vehicle class obtained for each input feature. All input features show clear distinction of mean ranks between all vehicle classes with the exception of features NOMAD5 and NOMAD8, where mean ranks for G-VEC classes 1 and 2, and classes 2 and 3 are similar, respectively. The results from the Kruskal-Wallis one-way analysis of variance test shown in Table 5.5 confirm that all input features are significantly different among vehicle classes at the 1 percent level of significance. This indicates that the features chosen are good candidates for classification model development.

Table 5.4. Rank results by vehicle class for each input feature

	G-VeC Class	Mean Rank
<b>Signature Length</b>	1	248.5
	2	381.3
	3	751.1
<b>NOMAD1</b>	1	572.6
	2	273.4
	3	593.3
<b>NOMAD2</b>	1	647.5
	2	423.4
	3	445.6
<b>NOMAD3</b>	1	506.6
	2	781.8
	3	316.3
<b>NOMAD4</b>	1	683.2
	2	338.5
	3	474.6
<b>NOMAD5</b>	1	450.5
	2	441.5
	3	571.7
<b>NOMAD6</b>	1	332.1
	2	424.2
	3	665.5
<b>NOMAD7</b>	1	370.3
	2	453.3
	3	620.3
<b>NOMAD8</b>	1	385.2
	2	559.0
	3	542.7

Table 5.5. Kruskal-Wallis one-way analysis of variance test on extracted Blade™ inductive signature features

	Signature Length	NOMAD1	NOMAD2	NOMAD3	NOMAD4	NOMAD5	NOMAD6	NOMAD7	NOMAD8
<b>Chi-Square</b>	597.5	232.0	112.5	433.0	209.1	46.4	260.9	142.0	68.1
<b>df</b>	2	2	2	2	2	2	2	2	2
<b>Asymp. Sig.</b>	1.82E-130	4.10E-51	3.65E-25	9.62E-95	3.90E-46	8.27E-11	2.27E-57	1.48E-31	1.64E-15

### 5.4.3 Model Architecture

#### **The Multi-Layer Feedforward neural network**

The G-VEC model follows the Multi-Layer Feedforward (MLF) neural network architecture, consisting of artificial neurons designed to mimic the first-order characteristics of the biological neuron. In essence, a set of inputs is applied to the neuron. Each of these inputs is multiplied by a corresponding weight, similar to a synaptic strength, and all of the weights are then summed to determine the response of the neuron. The summation block cumulates all of the weighted inputs algebraically together with a bias value unique to the neuron, and produces an output NET as shown in Figure 5.2.

The NET signal is usually further processed by an activation function  $F$  to produce the neuron's response, OUT. Commonly, the  $F$  acts as a squashing function, which compresses the range of NET, such that OUT does not exceed some low limits regardless of the value of NET.

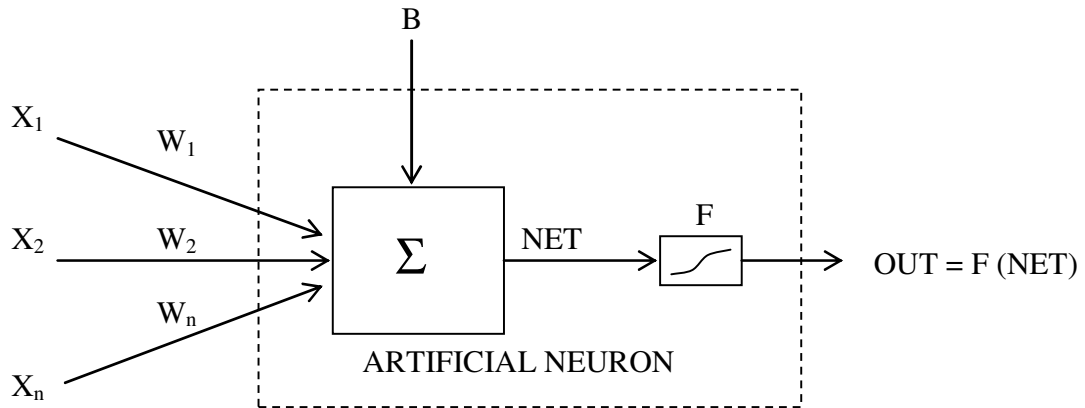


Figure 5.2. Artificial neuron with activation function

The artificial neuron has two modes of operation; the training mode and the simulation mode. The training mode conditions the neuron in a controlled environment. The neuron can be trained to fire (or not), depending on the characteristics of input patterns. Shown a set of inputs, the neurons self-adjust to produce desired responses consistently. Once trained, the network is able to give the desired response not only to patterns that are identical to the training data, but also minor variations in its input. This ability to see through noise and distortion to the pattern that lies within is vital to pattern recognition in the real-world environment (Wasserman, 1989).

The architecture of the G-VEC MLF neural network model is shown in Figure 5.3. It consists of three distinct sets of layers of neurons: the input layer, two hidden layers and the output layer. The connections of the neurons are unidirectional. However, there are no connections between neurons within the same layer.

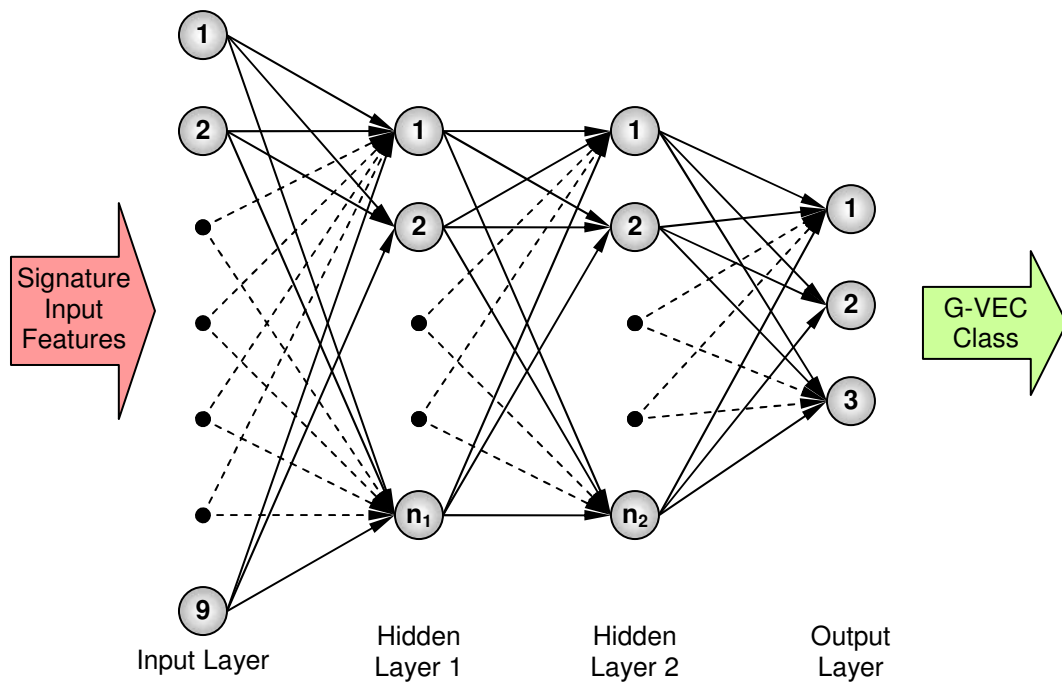


Figure 5.3. General Vehicle Classification (G-VeC) model Multi-Layer Feedforward (MLF) neural network architecture

The number of input neurons corresponds to the input features extracted from the Blade inductive signature while the number of output neurons corresponds to the number of G-VEC classes. The numbers of neurons in both hidden layers were varied between 5 and 15 to determine the optimized model configuration. Each configuration received 10 training repetitions.

### **Multi-Layer Feedforward Neural Network Training**

Backpropagation learning algorithms fall into two broad categories: ad hoc techniques and standard numerical optimization techniques. Ad hoc techniques include varying the

learning rate, using momentum and rescaling variables, while the most popular approaches in standard numerical optimization techniques have used conjugate gradient or quasi-Newton (secant) methods. Although quasi-Newton methods are considered more efficient, they require significant storage and computational requirements in larger networks. Nonlinear least squares is another area of numerical optimization that has been applied to neural networks. Most applications of nonlinear least squares to neural networks have been focused on sequential implementations where weights are updated after each presentation of an input/output pair. While useful when on-line adaptation is needed, several approximations are required to the standard algorithms where weights are only updated after the training data set is completely analyzed.

### **Levenberg-Marquardt Learning Algorithm**

The Levenberg-Marquardt backpropagation was chosen as the learning algorithm for training the G-VEC model. The Levenberg-Marquardt is an application of nonlinear least squares to batch training. It was found to be more efficient training algorithm, and had a higher convergence rate compared with the conjugate gradient and variable learning rate algorithm, and is very efficient when training networks with up to a several hundred weights (Hagan and Demuth, 1994).

## 5.5 RESULTS ANALYSIS

The trained G-VEC neural network model yielded an overall correct classification rate (CCR) of 93.4 and 93.0 percent on the training and test datasets, respectively. The cross classification results by vehicle class obtained on the training and test datasets are presented in Table 5.6, Table 5.7, respectively. Cross classification counts are presented in bold with cross classification rates shown below each count.

Table 5.6 Trained G-VEC model cross-classification results on training dataset

Training Data		Predicted Class			Actual Total
		G1	G2	G3	
Actual Class	Passenger Vehicles G1	<b>139</b> 95.2%	<b>7</b> 4.8%	<b>0</b> 0.0%	<b>146</b>
	Small Commercial Vehicles G2	<b>11</b> 8.2%	<b>118</b> 87.4%	<b>6</b> 4.4%	<b>135</b>
	Medium Large Commercial Vehicles G3	<b>3</b> 1.4%	<b>6</b> 2.7%	<b>210</b> 95.9%	<b>219</b>
<b>Predicted Total</b>		<b>153</b>	<b>131</b>	<b>216</b>	<b>500</b>
<b>% Error</b>		4.8%	-3.0%	-1.4%	

The results of the test dataset are very consistent, showing CCR performance of above 85% percent across all three vehicle classes using only nine model input parameters extracted from Blade™ inductive vehicle signatures. In addition, both datasets report fewer than 10 percent error in predicted vehicle counts for each class.



The trained G-VEC neural network architecture consists of only twenty-one nodes in the hidden layers: eleven in the first layer and ten in the second. Such a model would be computationally efficient and shows promise for practical implementation. Furthermore, the classification accuracy of class G3 is excellent with 98.4 percent of vehicles correctly classified in the test dataset. This ensures that few medium or large commercial vehicles will be missed in the more detailed commercial vehicle classification models presented in Chapters 6 and 7.

Table 5.7. Trained G-VEC model cross-classification results on test dataset

Test Data		Predicted Class			Actual Total
		G1	G2	G3	
Actual Class	Passenger Vehicles G1	87 91.6%	4 4.2%	4 4.2%	95
	Small Commercial Vehicles G2	5 6.2%	70 86.4%	6 7.4%	81
	Medium Large Commercial Vehicles G3	1 0.8%	1 0.8%	122 98.4%	124
Predicted Total		93	75	132	300
% Error		-2.1%	-7.4%	6.5%	

## **CHAPTER 6 COMMERCIAL VEHICLE AXLE CONFIGURATION CLASSIFICATION**

Axle location and configuration provides one of the most straightforward and reliable approaches to vehicle classification. This chapter describes the procedure used to extract axle-based information from Blade™ inductive signatures. This information is subsequently used to develop a detailed commercial vehicle axle classification model using the dataset obtained from the San Onofre Truck Weigh and Inspection Facility described in section 3.2. The intermediate and final outputs of this model are also used as inputs to the drive and trailer body unit classification model described in Chapter 7.

### **6.1 THE VEHICLE AXLE CONFIGURATION CLASSIFICATION PROBLEM**

Axle configuration classification involves the mapping of multi-dimensional axle-based information extracted from traffic sensors into distinct categories. However, vehicles possess different number of axles and axle groups. Hence, if the locations of axles or axle groups are used as input features, empty input features would exist in vehicles with fewer axles or axle groups. In addition, each axle group has its distinct significance in determining the vehicle classification. Since the input feature size varies with vehicle types, hierarchical models such as decision trees are best suited for such applications.

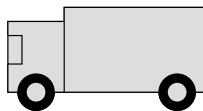
Furthermore, they can be used to analyze a subset of the input features at each decision level according to their significance in determining the vehicle class.

## **6.2 AXLE CONFIGURATION CLASSIFICATION SCHEME**

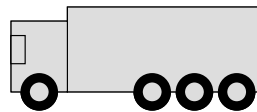
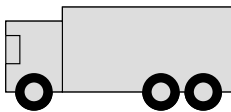
The proposed axle configuration classification scheme distinguishes between the axles from the drive and trailer units. Hence, each unit receives a separate classification subscheme as shown in Figure 6.1 and Figure 6.2. This scheme provides a more in depth vehicle distinction than the current FHWA Scheme F classification, as when fully expanded, consists of 27 distinct commercial vehicle axle classes as shown in Table 6.1.

## **6.3 DATA ORGANIZATION**

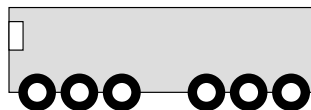
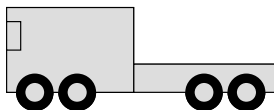
Two mutually exclusive samples are drawn from the commercial vehicle dataset obtained from the San Onofre study site for development of the axle configuration classification model. The first comprises of 720 randomly selected commercial vehicles, and is assigned as the calibration dataset, while the second independent set of 309 vehicles is designated as the test dataset for evaluating the performance of the calibrated model.



(A1-x) Single Steering, Single Drive Axles

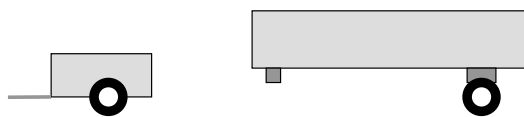


(A2-x) Single Steering, Tandem Drive Axles

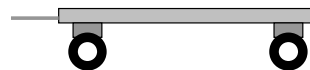


(A3-x) Tandem Steering, Tandem Drive Axles

Figure 6.1. Drive unit axle sub-classification



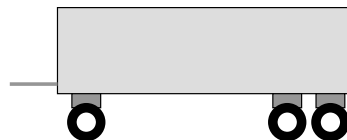
(Ax-1) Single Axle Trailer



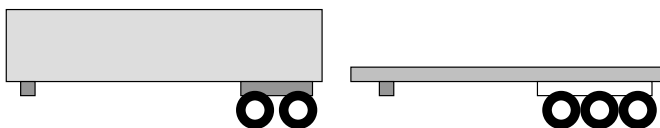
(Ax-5) Single - Single Axles Full Trailer



(Ax-2) Tandem Axles Small Trailer



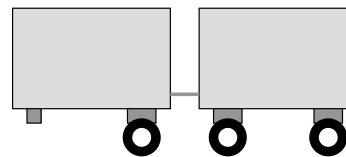
(Ax-6) Single - Tandem Axles Full Trailer



(Ax-3) Tandem Axles Semi-Trailer



(Ax-4) Split Tandem Axles Semi-Trailer



(Ax-7) Single - Single - Single Axles Multi-Trailers

Figure 6.2. Trailer unit axle sub-classification

Table 6.1. Expanded Axle Configuration Classification Scheme

Axle Class	Drive Unit	Trailer Unit	No. Trailers	Total Axles	FHWA F	California
A1-0	Single Steering, Single Drive Axle	No Trailer	0	2	5	5
A1-1		Single Axle Trailer	1	3	8	8
A1-2		Tandem Axle Small Trailer	1	4, 5	8, 9	8, 9
A1-3		Tandem Axle Semi Trailer	1	4, 5	8, 9	8, 9
A1-4		Split-Tandem Axle Semi Trailer	1	4	8	8
A1-5		Single-Single Full Trailer	1	4	8	8
A1-6		Single-Tandem Full Trailer	1	5	9	9
A1-7		Single-Single-Single Multi Trailer	2	5	11	11
A1-8		Other Multi-Trailer	2 or more	6 or more	12, 13	12, 13
A2-0	Single Steering, Tandem Drive Axle	No Trailer	0	3, 4	6, 7	6, 7
A2-1		Single Axle Trailer	1	4, 5	8, 9	8, 9
A2-2		Tandem Axle Small Trailer	1	5, 6	9, 10	9, 10
A2-3		Tandem Axle Semi Trailer	1	5, 6	9, 10	9, 10
A2-4		Split-Tandem Axle Semi Trailer	1	5	9	9
A2-5		Single-Single Full Trailer	1	5	9	14
A2-6		Single-Tandem Full Trailer	1	6	10	10
A2-7		Single-Single-Single Multi Trailer	2	6	12	12
A2-8		Other Multi-Trailer	2 or more	7 or more	13	13
A3-0	Tandem Steering, Tandem Drive Axle	No Trailer	0	4 - 6	7	7
A3-1		Single Axle Trailer	1	5 - 7	9, 10	9, 10
A3-2		Tandem Axle Small Trailer	1	6 - 9	10	10
A3-3		Tandem Axle Semi Trailer	1	6 - 9	10	10
A3-4		Split-Tandem Axle Semi Trailer	1	6 - 8	10	10
A3-5		Single-Single Full Trailer	1	6 - 8	10	10
A3-6		Single-Tandem Full Trailer	1	7 - 9	10	10
A3-7		Single-Single-Single Multi Trailer	2	7 - 9	13	13
A3-8		Other Multi-Trailer	2 or more	8 or more	13	13

Note: Tandem axle refers to two or three axles in an axle assembly

## **6.4 METHODOLOGY**

The axle configuration based classification model described in this chapter involves three steps: Wheel spike detection, axle grouping based on the k-means clustering technique and axle-configuration classification using decision trees.

### **6.4.1 Wheel spike location determination**

Wheel information in each signature record is typically represented by downward negative spikes in the signature. A recent study by Park et al. (2006) detected wheel wells in a Blade™ inductive signature by identifying regions in the Blade™ inductive signature where the inductance magnitude is negative. However, it was observed that many vehicles generate wheel spikes that did not have a downward peak inductance magnitude that entered the negative magnitude domain as shown in Figure 6.3. Hence, using such a method may cause wheel information in many signatures to be missed and lead to potential errors in axle classification.

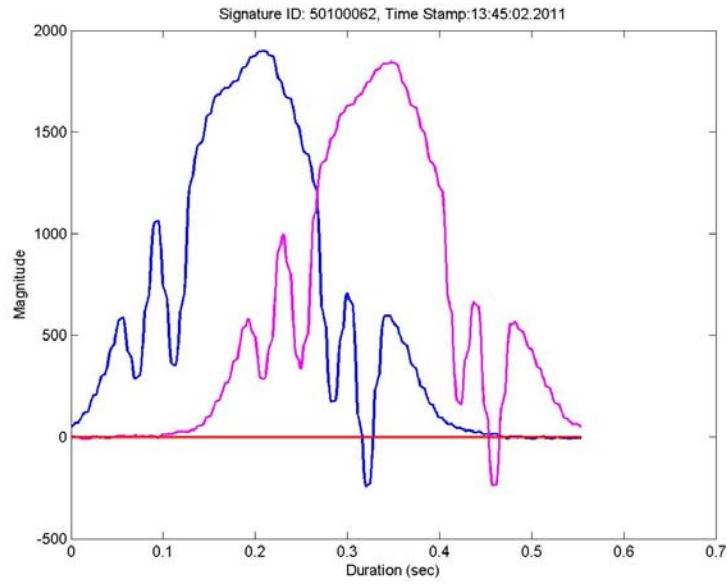


Figure 6.3. Sample double Blade™ inductive vehicle signatures with three non-negative domain wheel spikes

The approach used in this study detects wheel spikes using a combination of wheel spike characteristics in the Blade™ inductive signature. A discrete first-order derivative transformation of the inductive signature was initially performed to show the regions along of the signature where the gradients are consistently positive or negative.

When defining each region, small gradient discontinuities in the signature were addressed by introducing a continuity threshold (CT). This addresses possible fragmentation of each region caused by persisting noise in the inductive signature after the pre-processing stage. The CT value determines the number of continuous reverse gradient signature samples to ignore when determining a region of positive or negative gradient. Next, a Gradient Threshold (GT) was used to identify regions where positive and negative slopes contained slopes steep enough to be considered a characteristic wheel spike. A wheel

spike was then identified where a positive gradient region immediately followed an identified negative gradient region, where the first data point of the positive gradient region lay within a predetermined proximity threshold of the last data point of the negative gradient region, hence determining a downward spike, defined as the peak width threshold (PWT) value. The location and magnitude of the spike is determined as the average of the magnitude and location of the points of the positive and negative regions aforementioned.

However, the algorithm described above would still occasionally report false wheel spikes as shown in a signature example in Figure 6.4. In the figure, the small circles indicate a detected wheel spike in the Blade™ inductive signature. The spike indicated by the arrow is an erroneously detected wheel spike. These spikes in the vehicle signature are sometimes identified due to undercarriage characteristics found in low profile vehicles or trailers. The shape of these spikes is very similar to normal wheel spikes as they exhibit steep slopes and point in the negative direction. However, they do not have a negative-valued peak inductance magnitude and they do not usually occur in pairs or clusters. To address this observation, a simple heuristic was developed to detect false wheel spikes as downward spikes with a downward peak inductance magnitude in the positive magnitude domain that do not have a neighboring spike within a distance threshold (in feet) defined as the Spike Neighborhood Threshold (SNT) parameter.



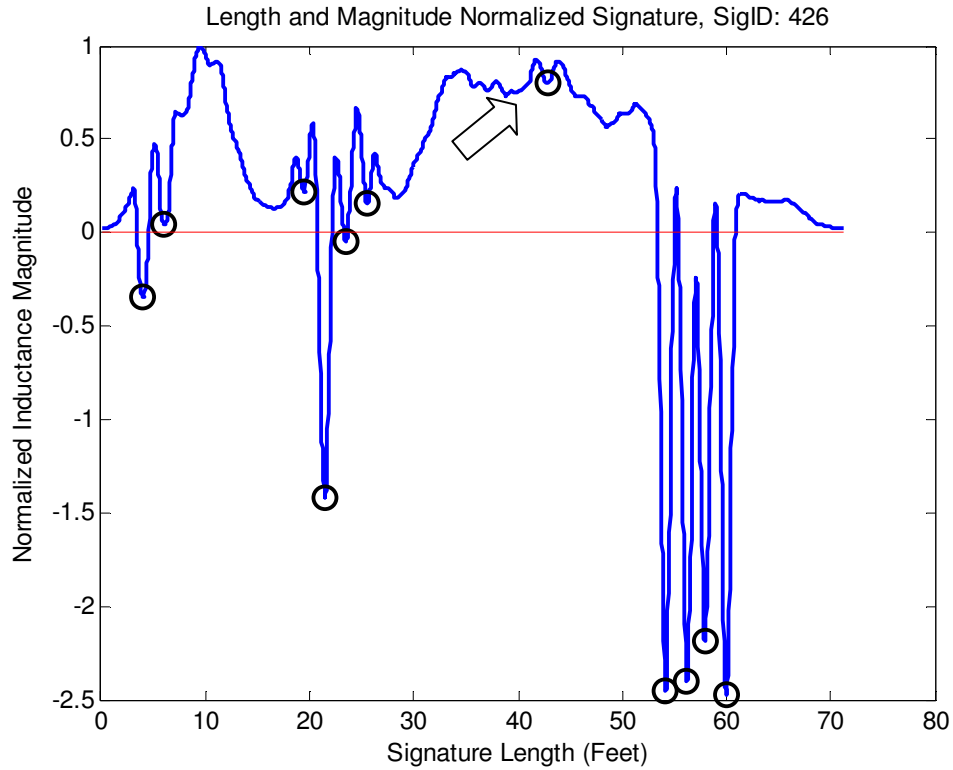


Figure 6.4. False wheel spike wrongly detected in Blade™ inductive signature

Figure 6.5 shows the sensitivity of the average axle error to the GT and PWT values. In this analysis, the number of axle counts for each vehicle is defined as half the number of spikes detected in the vehicle signature. It can be observed that the accuracy of axle counts is highest at GT values of 197 and 212, and has lower performance sensitivity in the proximity of 197. In general, lower performance sensitivity indicates better transferability with potentially less performance degradation, indicating that the GT value of 197 is preferred. A further analysis on axle count accuracy (ACA) defined by the percentage of vehicles with the correct number of axles identified shown in Figure 6.6 confirms that the GT value of 197 is optimal, as it achieves the highest ACA. The ACA

is less sensitive to the PWT as indicated by the vertical bands at GT values of 197 and 212, with the best performance obtained between the range of 0.140 and 0.260. For maximum transferability potential, the PWT is set as at the average value of 0.200. The result of the wheel detection processing stage reveals the location of wheel spikes along the Blade™ inductive signature.

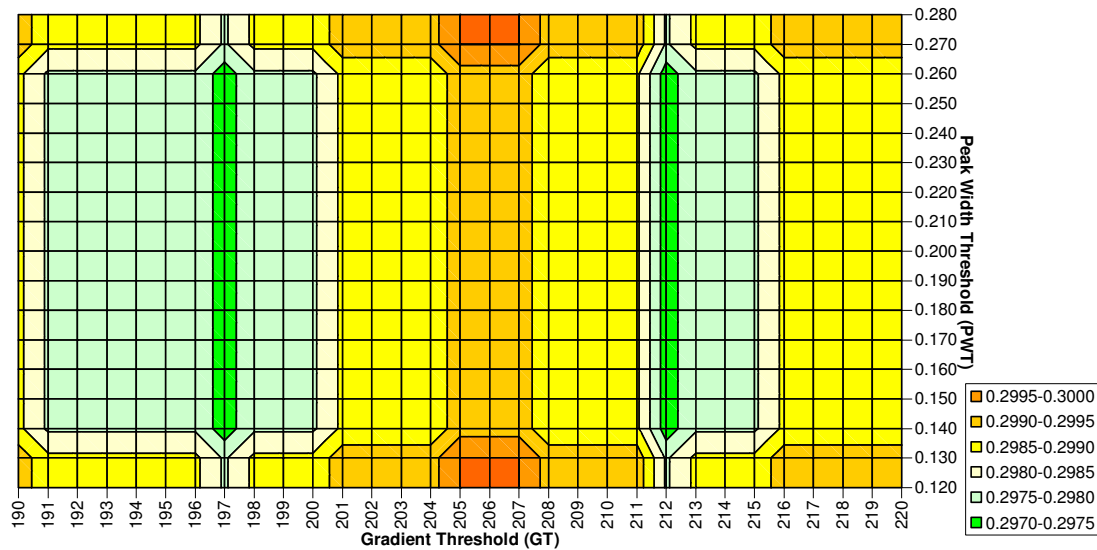


Figure 6.5. Sensitivity Analyses of Gradient Threshold (GT) and Peak Width Threshold (PWT) on Average Axle Count Errors

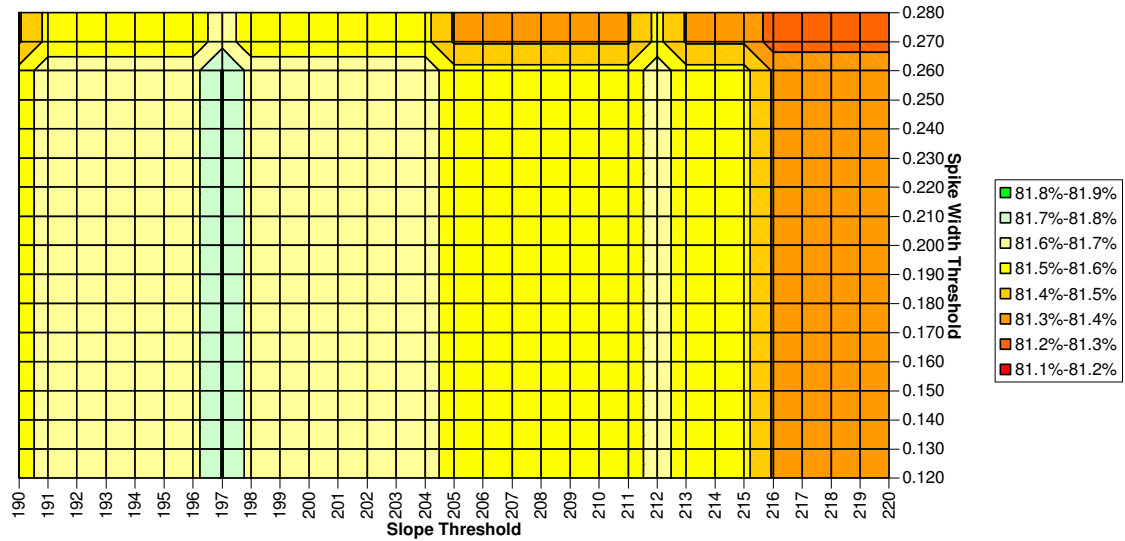


Figure 6.6. Sensitivity Analyses of Slope and Spike Width Threshold on Axle Count Accuracy (ACA)

#### 6.4.2 Axle assembly location and configuration determination

The purpose of axle clustering is to determine the membership of each wheel spike to corresponding axle groups in a vehicle. This facilitates the axle configuration classification procedure performed at the final stage of this vehicle classification model.

In this stage, the *k*-means clustering technique is used to identify axle groups and their corresponding locations within each vehicle. The *k*-means clustering technique (Kaufman and Rousseeuw, 1990) is a well-known method and is used to compute *k* representative axle cluster locations called centroids. The *k* clusters represent the number of axle groups in a vehicle. Each detected wheel spike time is then assigned to the cluster

corresponding to the nearest centroid. Hence, wheel spike  $i$  is placed into axle cluster  $v_i$  when it is closer to centroid  $c_{v_i}$  than any other centroid  $c_w$ :

$$d(i, c_{v_i}) \leq d(i, c_w) \quad \text{for all } w = 1, \dots, k$$

The  $k$  representative clusters should minimize the sum of the dissimilarities  $[d(i,m)]$  of all objects to their nearest centroid:

$$\text{Objective function} = \sum_{i=1}^n d(i, m_{v_i})$$

In determining the axle configuration, iterations of  $k$ -means clustering was applied with decreasing cluster sizes. At each cluster size, ten repetitions of  $k$ -means clustering were performed to ensure optimal axle clustering at each cluster level. The optimal cluster size was determined as the largest cluster size where the minimum distance between spikes of adjacent clusters, defined as the Adjacent Cluster Distance (ACD) is larger than the ACD threshold value. Figure 6.7 shows an inductive signature example where ten wheel spikes and three axle cluster locations have been determined using the algorithm described, denoted by circles at the tip of each wheel spike and crosses along the horizontal axis at the center of each axle cluster.

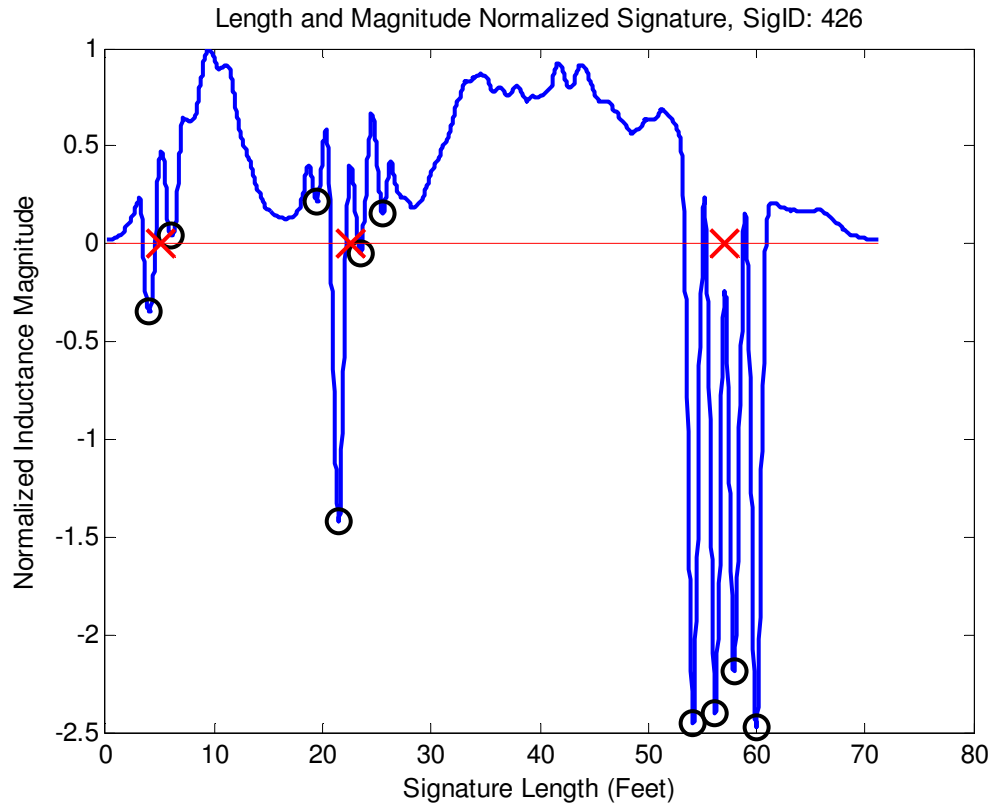


Figure 6.7. Detected Wheels Spikes and Axle Assemblies (Clusters) in a Blade™ signature

### 6.4.3 Axle Configuration Classification by Decision Trees

The axle configuration classification model based on the new scheme described in Table 6.1 was developed using the decision trees to determine the various classes. Vehicles were initially pre-classified into three preliminary classes. Class A was defined as single unit vehicles, class B as vehicles with single trailers and class C as vehicles with multi-trailers. The number of axle clusters was as the decision variable in this preliminary classification step. Vehicles with two detected axle clusters were classified as class A.

Vehicles with three or four detected axle clusters were classified as class B and vehicles with five or more detected axle clusters were classified as class C.

The model addresses some of the inherent characteristics of Blade™ inductive signatures observed in this study. First, it was found that some vehicle inductive signatures did not show distinct steering wheel spikes that could be picked up at the wheel detection stage as shown in Figure 6.8. To solve this problem, the model detects the location of the first axle cluster. If the location exceeds a distance threshold from the front of the vehicle, the first axle cluster is assigned as the driving axle and a dummy steering axle is added to the axle configuration to compensate for the missing steering axle. It was subsequently observed that almost all tractors with box container chassis trailers had tandem trailer axles which did not generate any wheel spikes. Hence, vehicles longer than a length threshold which had no detected trailer axles were assigned with a dummy tandem trailer axle configuration.

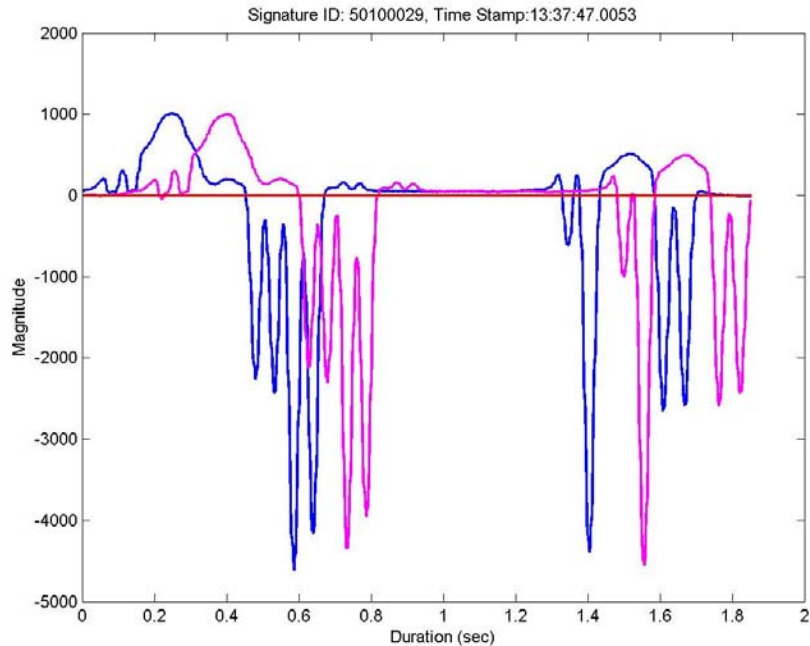


Figure 6.8. Sample double Blade™ inductive signatures with indistinct steering wheel spikes

Next, the number of axles in each axle cluster is determined by comparing the ACW of each axle cluster with a single axle width threshold parameter (SAW). If the ACW is lower than the SAW threshold, the axle cluster is assigned as a single axle. Otherwise, the axle cluster is assigned as a tandem axle.

Figure 6.9 shows the decision tree of the full axle configuration classification model with the following decision parameters defined as follows:

AC: Number of Axle Clusters

AN<sub>*i*</sub>: Number of axles at *i*th axle cluster from front of vehicle

CD<sub>*ij*</sub>: Distance between axle clusters *i* and *j*

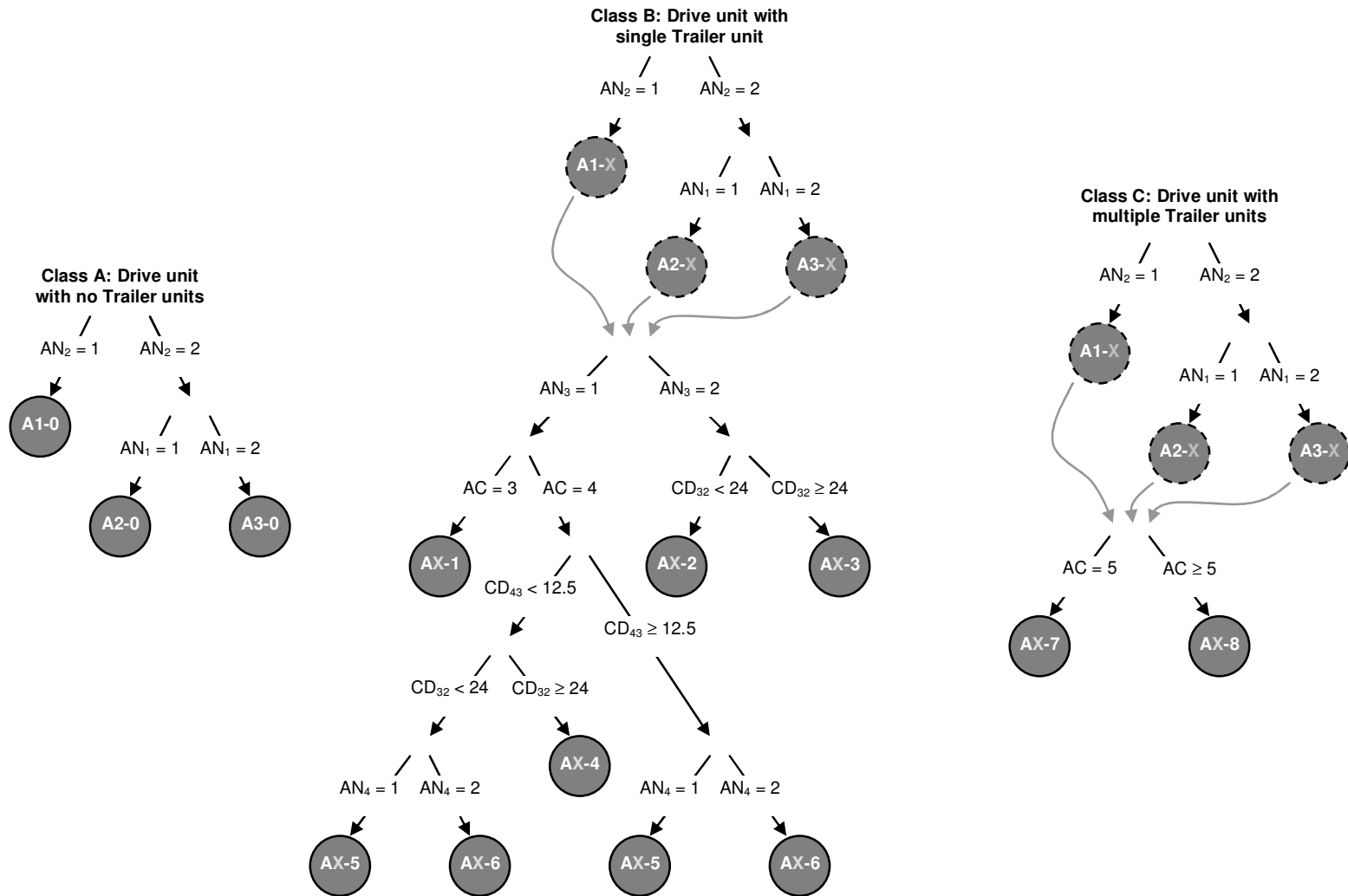


Figure 6.9. Axle Configuration Classification Model



## 6.5 RESULTS ANALYSIS

Table 6.2 summarizes the calibration and test dataset results for the axle configuration classification model. 12 out of 27 vehicle classes defined in the model were represented in the calibration dataset. The calibrated model achieved an overall classification accuracy of 99.0 percent correct matches on the calibration dataset. Seven out of 720 vehicles in the calibration dataset were misclassified. 10 vehicle classes were represented in the smaller independent test dataset. Performance of calibrated axle configuration classification model on the test dataset was also 99.0 percent. Only three out of 309 vehicles in the dataset were misclassified. This indicates that the axle configuration classification model has high potential for transferability and maintaining excellent classification accuracy.

Table 6.3 shows the cross classification results of the calibrated axle configuration classification model on the test dataset. It clearly indicates the cross-classification errors of the three misclassified vehicles in the test dataset. One vehicle had a missed small trailer (A1-1 → A1-0), one had a tandem axle semi trailer misclassified as a single-tandem full trailer unit (A2-3 → A2-6) and one had a misclassified drive unit (A2-3 → A3-3).

Table 6.2. Axle Configuration Classification Results

Axle Class	Drive Unit	Trailer Unit	No. Trailers	Total Axles	FHWA F	California	Calibration Data			Test Data		
							Count	Classified Correct	CCR	Count	Classified Correct	CCR
A1-0	Single Steering, Single Drive Axle	No Trailer	0	2	5	5	230	230	100.0%	110	110	100.0%
A1-1		Single Axle Trailer	1	3	8	8	14	13	92.9%	7	6	85.7%
A1-2		Tandem Axle Small Trailer	1	4, 5	8, 9	8, 9	1	1	100.0%	0	0	-
A1-3		Tandem Axle Semi Trailer	1	4, 5	8, 9	8, 9	9	9	100.0%	9	9	100.0%
A1-4		Split-Tandem Axle Semi Trailer	1	4	8	8	0	0	-	1	1	100.0%
A1-5		Single-Single Full Trailer	1	4	8	8	0	0	-	0	0	-
A1-6		Single-Tandem Full Trailer	1	5	9	9	1	1	100.0%	0	0	-
A1-7		Single-Single-Single Multi Trailer	2	5	11	11	11	10	90.9%	4	4	100.0%
A1-8		Other Multi-Trailer	2 or more	6 or more	12, 13	12, 13	0	0	-	0	0	-
A2-0	Single Steering, Tandem Drive Axle	No Trailer	0	3, 4	6, 7	6, 7	32	31	96.9%	12	12	100.0%
A2-1		Single Axle Trailer	1	4, 5	8, 9	8, 9	4	3	75.0%	1	1	100.0%
A2-2		Tandem Axle Small Trailer	1	5, 6	9, 10	9, 10	0	0	-	0	0	-
A2-3		Tandem Axle Semi Trailer	1	5, 6	9, 10	9, 10	390	388	99.5%	155	153	98.7%
A2-4		Split-Tandem Axle Semi Trailer	1	5	9	9	15	14	93.3%	6	6	100.0%
A2-5		Single-Single Full Trailer	1	5	9	14	12	12	100.0%	4	4	100.0%
A2-6		Single-Tandem Full Trailer	1	6	10	10	0	0	-	0	0	-
A2-7		Single-Single-Single Multi Trailer	2	6	12	12	0	0	-	0	0	-
A2-8		Other Multi-Trailer	2 or more	7 or more	13	13	0	0	-	0	0	-
A3-0	Tandem Steering, Tandem Drive Axle	No Trailer	0	4 - 6	7	7	1	1	100.0%	0	0	-
A3-1		Single Axle Trailer	1	5 - 7	9, 10	9, 10	0	0	-	0	0	-
A3-2		Tandem Axle Small Trailer	1	6 - 9	10	10	0	0	-	0	0	-
A3-3		Tandem Axle Semi Trailer	1	6 - 9	10	10	0	0	-	0	0	-
A3-4		Split-Tandem Axle Semi Trailer	1	6 - 8	10	10	0	0	-	0	0	-
A3-5		Single-Single Full Trailer	1	6 - 8	10	10	0	0	-	0	0	-
A3-6		Single-Tandem Full Trailer	1	7 - 9	10	10	0	0	-	0	0	-
A3-7		Single-Single-Single Multi Trailer	2	7 - 9	13	13	0	0	-	0	0	-
A3-8		Other Multi-Trailer	2 or more	8 or more	13	13	0	0	-	0	0	-
						<b>Overall</b>	<b>720</b>	<b>713</b>	<b>99.0%</b>	<b>309</b>	<b>306</b>	<b>99.0%</b>

Note: Tandem axles refers to two or three axles in an axle assembly

Table 6.3. Axle Configuration Test Data Cross-Classification Results

		Predicted Axle Class																											
		A1-0	A1-1	A1-2	A1-3	A1-4	A1-5	A1-6	A1-7	A1-8	A2-0	A2-1	A2-2	A2-3	A2-4	A2-5	A2-6	A2-7	A2-8	A3-0	A3-1	A3-2	A3-3	A3-4	A3-5	A3-6	A3-7	A3-8	
Actual Axle Class	A1-0	110	0	0	0	0	0	0	0	0	0	0	0	0	0	0	0	0	0	0	0	0	0	0	0	0	0	0	
	A1-1	1	6	0	0	0	0	0	0	0	0	0	0	0	0	0	0	0	0	0	0	0	0	0	0	0	0	0	
	A1-2	0	0	0	0	0	0	0	0	0	0	0	0	0	0	0	0	0	0	0	0	0	0	0	0	0	0	0	0
	A1-3	0	0	0	0	0	0	0	0	0	0	0	0	0	0	0	0	0	0	0	0	0	0	0	0	0	0	0	0
	A1-4	0	0	0	0	0	0	0	0	0	0	0	0	0	0	0	0	0	0	0	0	0	0	0	0	0	0	0	0
	A1-5	0	0	0	0	0	0	0	0	0	0	0	0	0	0	0	0	0	0	0	0	0	0	0	0	0	0	0	0
	A1-6	0	0	0	0	0	0	0	0	0	0	0	0	0	0	0	0	0	0	0	0	0	0	0	0	0	0	0	0
	A1-7	0	0	0	0	0	0	0	0	0	0	0	0	0	0	0	0	0	0	0	0	0	0	0	0	0	0	0	0
	A1-8	0	0	0	0	0	0	0	0	0	0	0	0	0	0	0	0	0	0	0	0	0	0	0	0	0	0	0	0
	A2-0	0	0	0	0	0	0	0	0	0	0	0	0	0	0	0	0	0	0	0	0	0	0	0	0	0	0	0	0
	A2-1	0	0	0	0	0	0	0	0	0	0	0	0	0	0	0	0	0	0	0	0	0	0	0	0	0	0	0	0
	A2-2	0	0	0	0	0	0	0	0	0	0	0	0	0	0	0	0	0	0	0	0	0	0	0	0	0	0	0	0
	A2-3	0	0	0	0	0	0	0	0	0	0	0	0	0	0	0	0	0	0	0	0	0	0	0	0	0	0	0	0
	A2-4	0	0	0	0	0	0	0	0	0	0	0	0	0	0	0	0	0	0	0	0	0	0	0	0	0	0	0	0
	A2-5	0	0	0	0	0	0	0	0	0	0	0	0	0	0	0	0	0	0	0	0	0	0	0	0	0	0	0	0
	A2-6	0	0	0	0	0	0	0	0	0	0	0	0	0	0	0	0	0	0	0	0	0	0	0	0	0	0	0	0
	A2-7	0	0	0	0	0	0	0	0	0	0	0	0	0	0	0	0	0	0	0	0	0	0	0	0	0	0	0	0
	A2-8	0	0	0	0	0	0	0	0	0	0	0	0	0	0	0	0	0	0	0	0	0	0	0	0	0	0	0	0
	A3-0	0	0	0	0	0	0	0	0	0	0	0	0	0	0	0	0	0	0	0	0	0	0	0	0	0	0	0	0
	A3-1	0	0	0	0	0	0	0	0	0	0	0	0	0	0	0	0	0	0	0	0	0	0	0	0	0	0	0	0
	A3-2	0	0	0	0	0	0	0	0	0	0	0	0	0	0	0	0	0	0	0	0	0	0	0	0	0	0	0	0
	A3-3	0	0	0	0	0	0	0	0	0	0	0	0	0	0	0	0	0	0	0	0	0	0	0	0	0	0	0	0
	A3-4	0	0	0	0	0	0	0	0	0	0	0	0	0	0	0	0	0	0	0	0	0	0	0	0	0	0	0	0
	A3-5	0	0	0	0	0	0	0	0	0	0	0	0	0	0	0	0	0	0	0	0	0	0	0	0	0	0	0	0
A3-6	0	0	0	0	0	0	0	0	0	0	0	0	0	0	0	0	0	0	0	0	0	0	0	0	0	0	0	0	
A3-7	0	0	0	0	0	0	0	0	0	0	0	0	0	0	0	0	0	0	0	0	0	0	0	0	0	0	0	0	
A3-8	0	0	0	0	0	0	0	0	0	0	0	0	0	0	0	0	0	0	0	0	0	0	0	0	0	0	0	0	

## **CHAPTER 7 COMMERCIAL VEHICLE BODY CLASSIFICATION**

Two body configuration-based signature classification models are described in this chapter: The drive unit and trailer unit body configuration classification models. In these models, the body signatures which correspond to the drive and trailer body sections of each signature are identified and extracted from the overall inductive Blade™ inductive signature for analysis.

### **7.1 CLASSIFICATION SCHEMES**

#### **7.1.1 Drive Unit Classification**

The drive unit classification scheme consists of nine distinct classes as shown in Figure 7.1. These classes can be broadly grouped into four categories. The first category consists of relatively common platform (D1) and van type (D2) drive units. These are typically the most commonly observed amongst single unit commercial vehicles. The second category includes three less common specialized use drive unit types: the concrete mixer (D3), gravel/dump (D4) and tank (D5) drive units. The third category encompasses semi-tractor type drive units: the conventional tractor (D6), extended cab tractor (D7), and the cab-over tractor (D8). This distinction is made due to potential differences in travel behavior between these tractor types. Extended cab tractors include a sleeper cabin, and are more suitable for long-haul trips such as inter-state travel compared with

conventional and cab-over tractors. The longer wheel-base of the extended cab tractor also improves ride quality for long distance travel. On the other hand, cab-over tractors have shorter wheel-bases than conventional and extended cab tractors. While this characteristic decreases ride quality, it permits a smaller turning radius which is essential for travel in dense urban cities with narrower streets. The final category consists of all other drive unit types (D9) that have not been previously defined in D1 through D8.

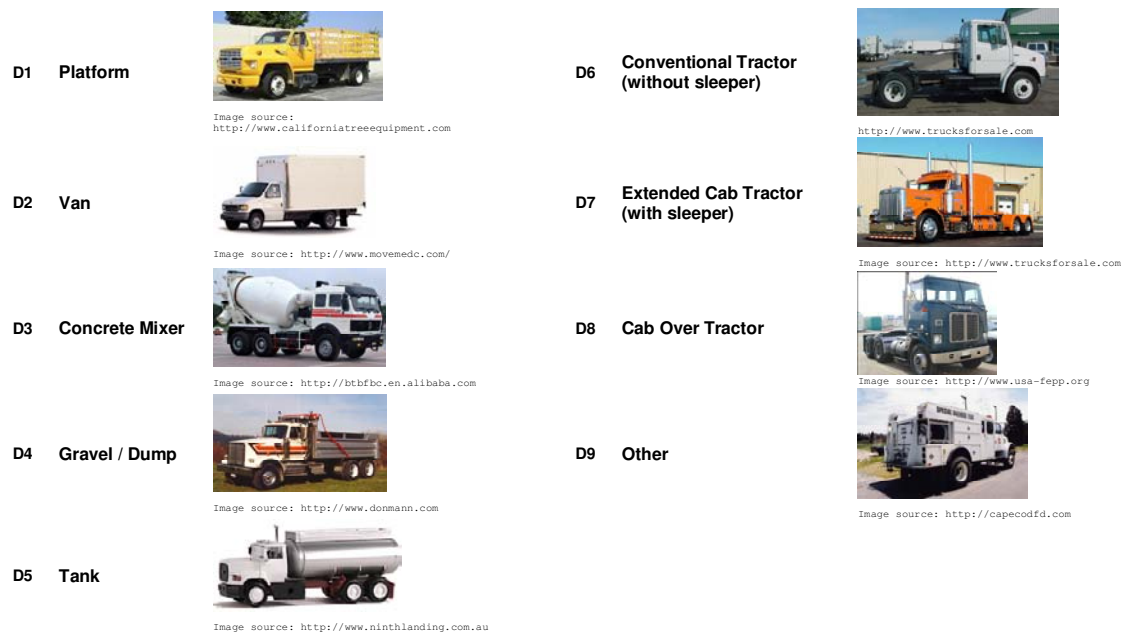


Figure 7.1. Drive unit body classification

### 7.1.2 Trailer Unit Classification

The trailer unit body classification scheme consists of ten trailer body types as shown in Figure 7.2. These ten classes can be divided in five more general categories. The first category consists of platform-type trailer bodies, and includes the basic platform (T1) and

low boy platform types (T2). Both these types of trailers are primary equipment movers. The second category consists of moving van trailer types: the enclosed van (T3) and dropped frame van (T4). The third category includes the 40-foot box container (T5) and 20-foot box container (T6) trailer types. Both these trailer body types are associated with port activities. Hence, statistics of these trailer body types are useful for determining transportation-related impacts from port facilities. The fourth category consists of three specialized-use trailer body types: the auto-transport (T7), chemical/dry bulk (T8) and gravel / dump (T9) trailer types. The last category consists of the towed vehicle or small trailer type (T10).

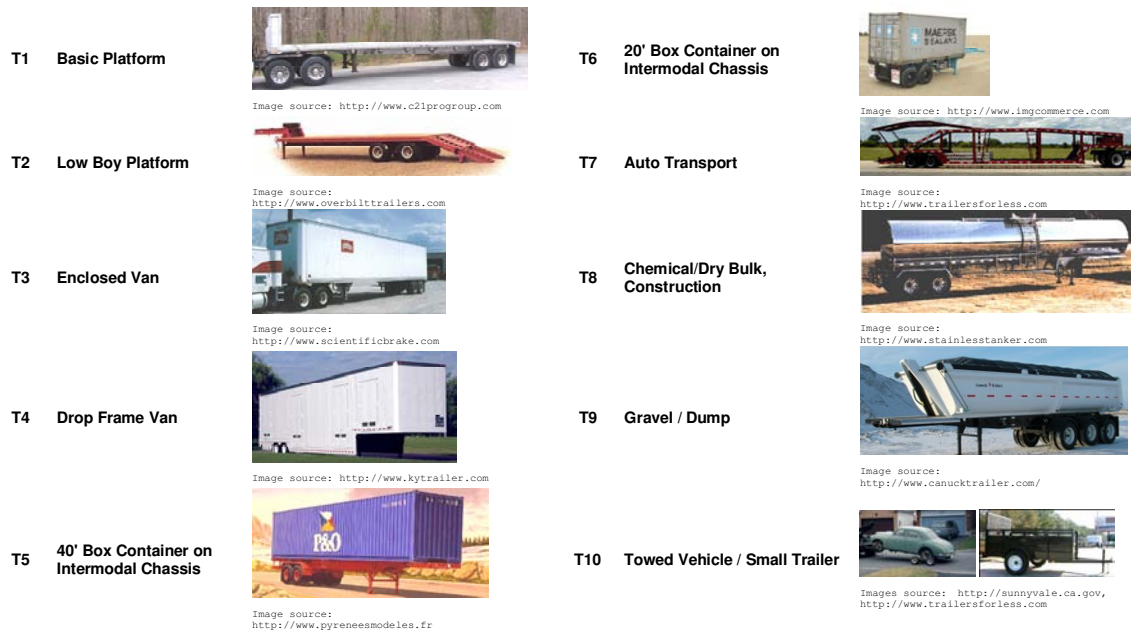


Figure 7.2. Trailer unit body classification

## 7.2 METHODOLOGY

### 7.2.1 Body Signature Extraction

The drive unit body signature is defined as the continuous positive inductive magnitude region of the vehicle signature between the last wheel spike of the steering axle cluster and the first wheel spike of the drive axle cluster as shown in Figure 7.3. This signature region is extracted from the overall length-normalized vehicle signature and analyzed for drive unit body classification.

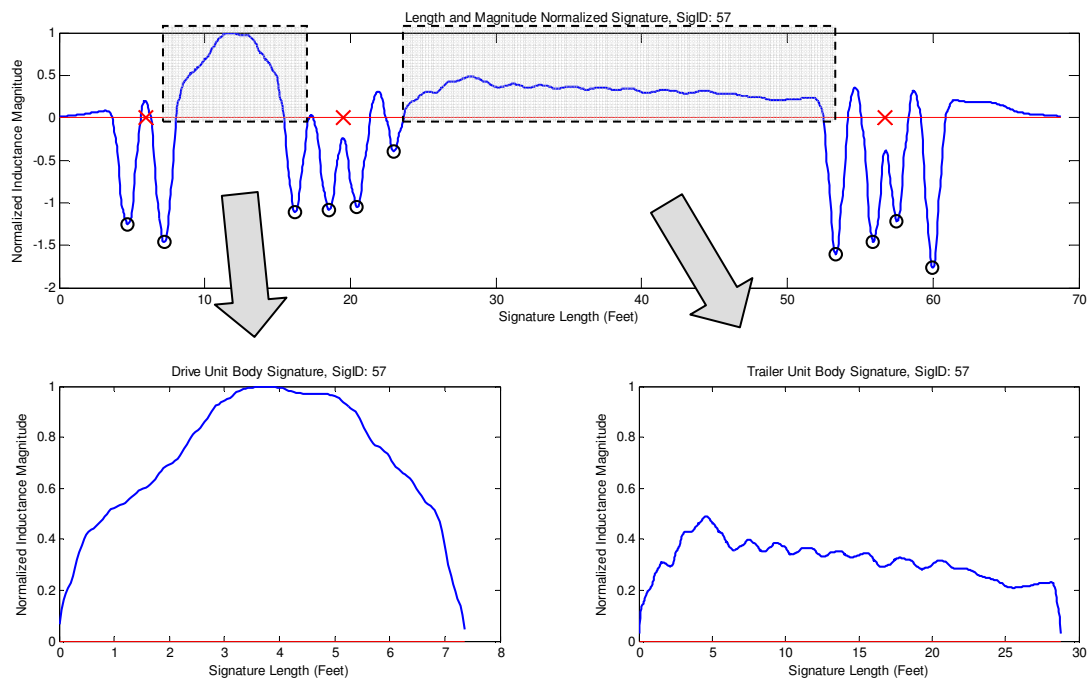


Figure 7.3. Sample of extracted of drive and trailer unit body signatures

The region where the trailer unit body signature is extracted from the overall Blade™ inductive signature depends on the trailer configuration determined by the axle configuration classification model. For vehicles with single or semi trailer units, the trailer unit body is obtained from the continuous positive magnitude region of the Blade™ inductive signature between the last wheel spike of the drive axle cluster and the first trailer axle cluster as shown in Figure 7.3. For other trailer types, the trailer unit body signature is extracted from the continuous positive inductive magnitude region of the vehicle signature between the last wheel spike of the first trailer axle and the first wheel spike of the last axle cluster.

Prior to feature extraction, the drive unit and trailer unit body signatures are normalized in the magnitude (vertical) axis. This normalization finds the peak positive magnitude in the inductive vehicle signature and subsequently divides all signature sample magnitudes in the drive unit and trailer unit body signatures by this peak positive magnitude.

## **7.2.2 Feature Extraction**

### **Description of Features**

Nine and fifteen features are extracted from the normalized drive unit body signature as inputs to the drive unit and trailer unit body classification models respectively. The features extracted for the drive unit body classification model is illustrated in Figure 7.4, where features are represented as an arrow with a corresponding ordinal label.



The first input feature represents the length of the drive unit body signature in feet. The subsequent nine input features are interpolated NOMAD values extracted along the length of the signature as described in Section 5.4.1.

Figure 7.5 shows the extraction of input features from the trailer unit body signature for input into the trailer unit body classification model. The first input feature for the trailer unit body classification model represents the length of the trailer unit body signature in feet. The following fourteen input features are NOMAD values extracted along the length of the signature.

### **7.2.3 Model Architecture**

Two distinct drive unit classification sub-models were developed for classifying drive units. The choice of sub-model was determined based on the presence of an attached trailer determined by the axle configuration classification model: The first Sub-model classifies drive units without attached trailers or attached to non-semi configured trailers, while the second classifies drive units with attached semi-trailers as illustrated in Figure 7.6. This was found to produce better results than a single universal drive unit classification model.

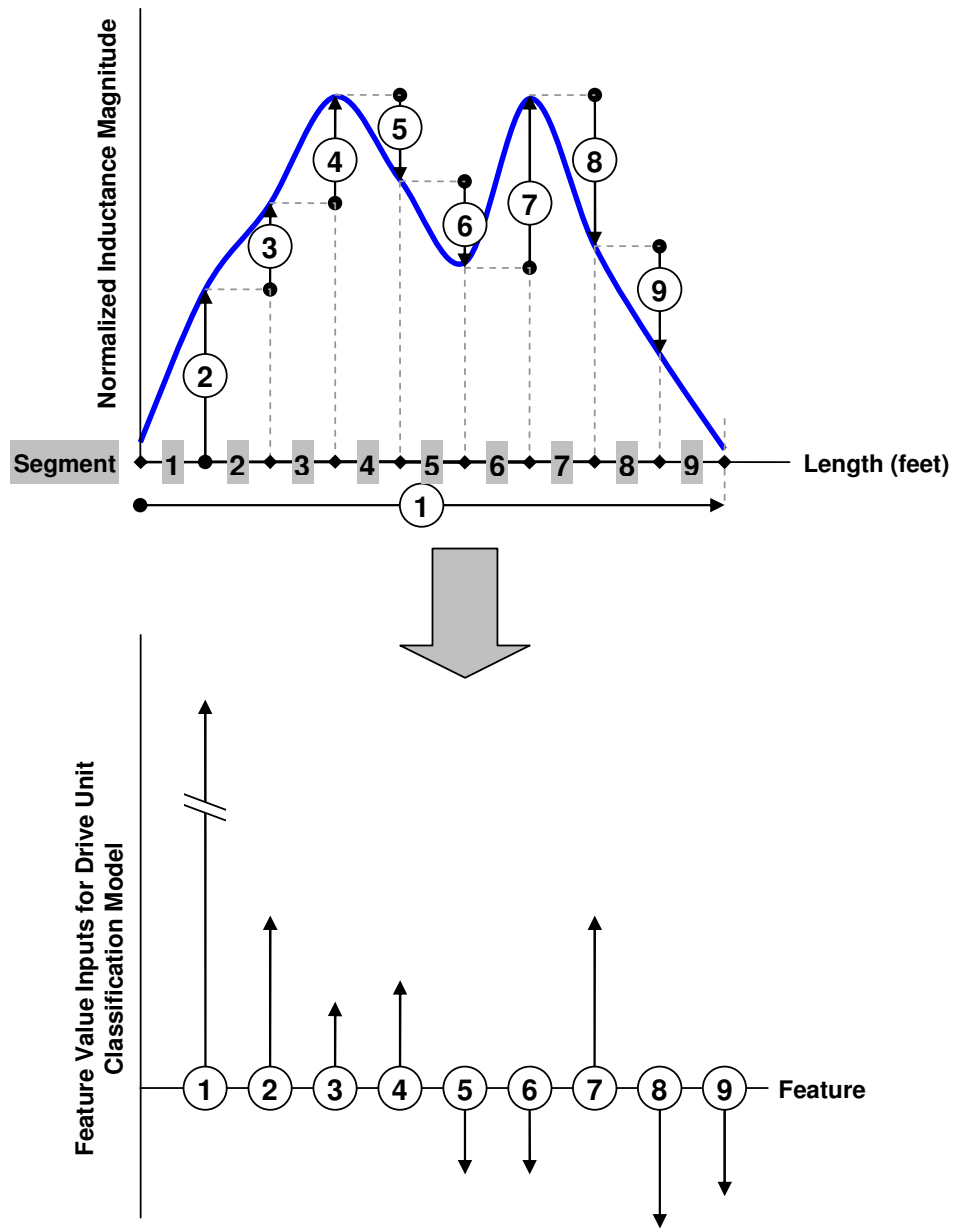


Figure 7.4. Extraction of drive unit body signature features

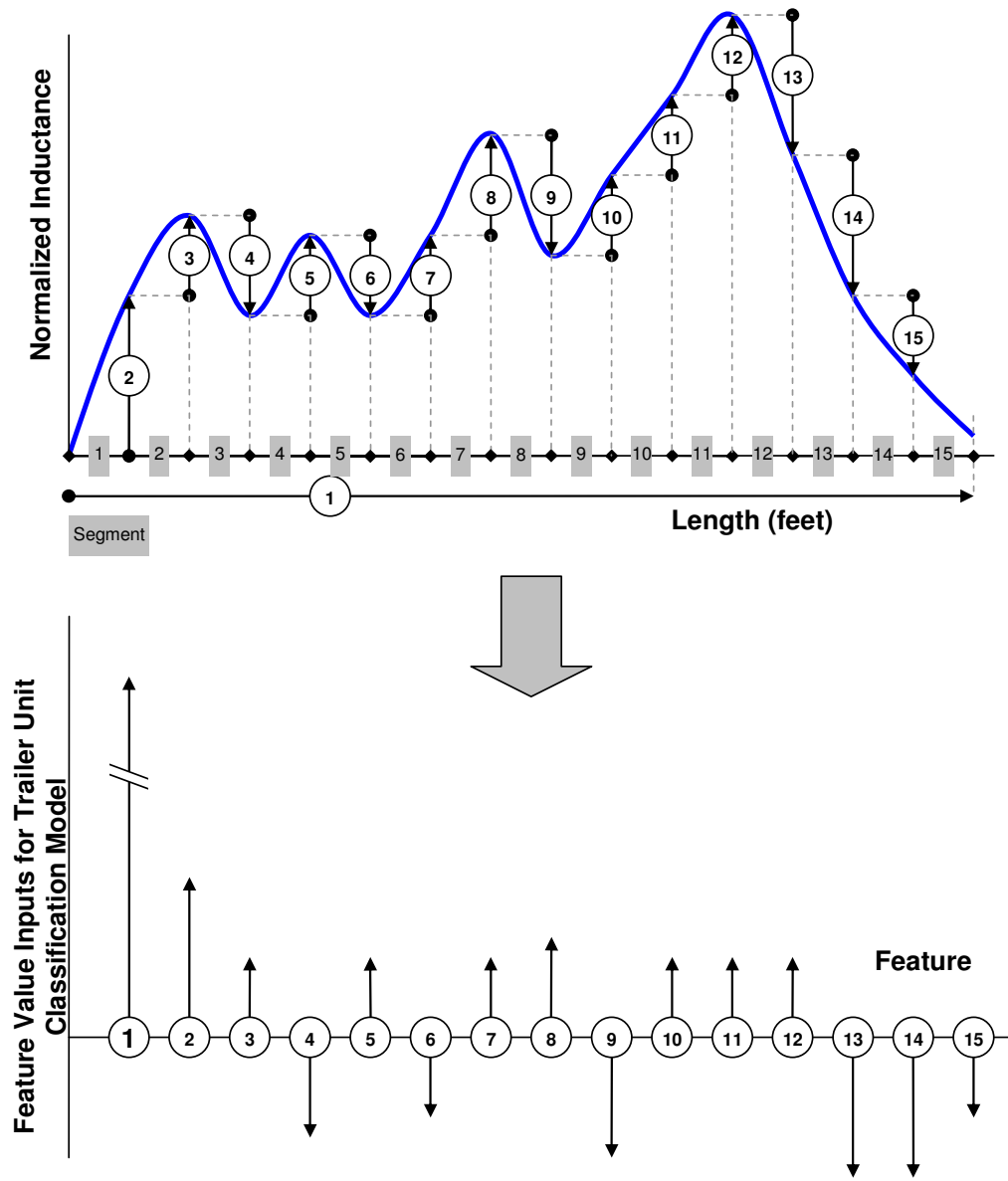


Figure 7.5. Extraction of trailer unit body signature features

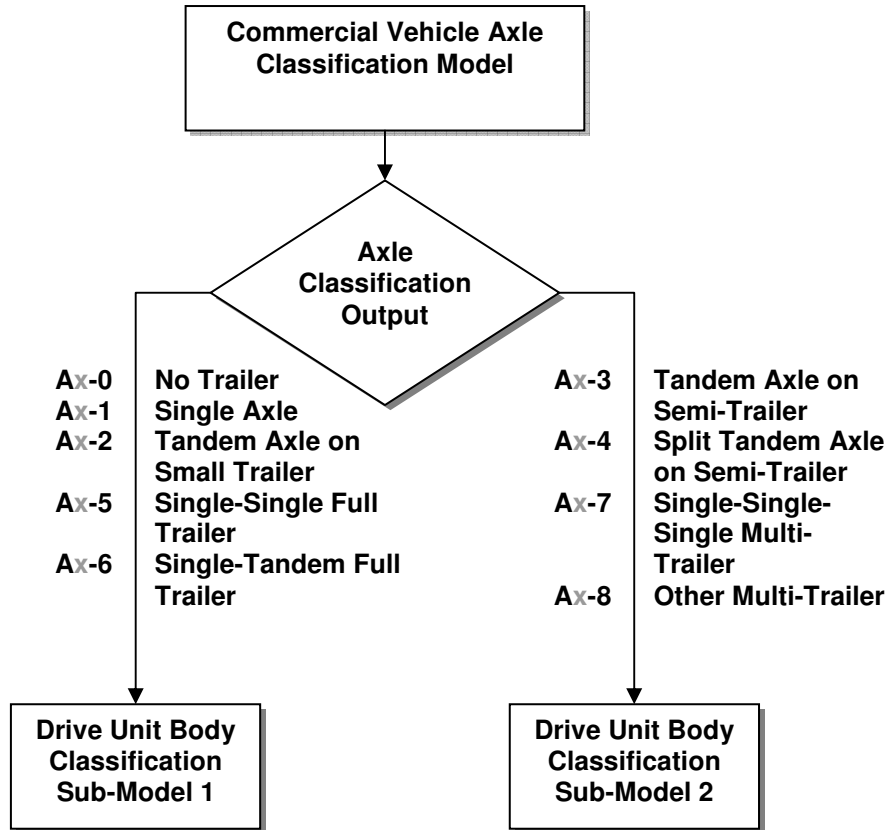


Figure 7.6. Assignment of vehicles to drive unit body classification sub-models by axle classification

Both drive unit body classification sub-models were designed using the Multi-Layer Feedforward (MLF) neural network architecture as described in Section 5.4.3. The trailer unit body classification model consists of a single model which is also based on the MLF neural network architecture. Weight and bias values were updated according to Levenberg-Marquardt optimization using the Levenberg-Marquardt backpropagation training method described in Section 5.4.3. Both drive unit body classification sub-models have nine input neurons in the input layer corresponding to the number of input

features, and nine output layer neurons, with each output neuron representing a Drive Unit Class. The trailer unit body classification model has fifteen input neurons and ten output neurons corresponding to the number of input features and output Trailer Unit Classes respectively. For all models, the number of hidden layers as well as the number of nodes in each hidden layer was varied to determine the best classification model. Nonlinear squashing functions were used as bounds to the neuron outputs. The hyperbolic tangent function was used between the hidden and output layer and the logistic function applied to the output layer.

#### **7.2.4 Data Description and Organization**

The data is made up of columns of input vectors from each vehicle forming the input matrix and a corresponding output representing the drive unit class forming a row vector of target outputs. Prior to training, the vector of target outputs was converted into a target matrix with its column size corresponding to the target vector output, with its row size corresponding to the number of drive unit classes. This resulted in a sparse matrix where each column had only one non-zero entry which equals to one, and the row of that entry corresponds to the actual drive unit class of the vehicle. This matrix was used as the target for training the neural network and evaluating the performance of the trained network.

Of the 1029 commercial vehicles in the overall dataset, 429 and 600 vehicles were used to develop the first and second drive unit body classification sub-models respectively.

664 vehicles out of the overall dataset had attached trailers, and were used to develop the trailer unit body classification model.

Each of the three datasets was sub-divided into three independent sub-sets for drive unit body classification model development: training, validation and testing. The training data was used to calibrate the weights and biases of the neural network to recognize the drive unit classification (target) of the training vehicle data. To maintain flexibility, over-training of the model was avoided. This was achieved by testing the trained model after each batch training iteration against the independent validation data. The training was terminated when the model performance (as determined by the sum squared errors of the model outputs) on the validation data persistently exceeded an acceptable threshold. The most recent model parameters prior to the performance degradation of the validation data were then assigned to the trained model for that training repetition and evaluated on the test dataset to determine model performance.

## **7.3 RESULTS ANALYSIS**

### **7.3.1 Drive Unit Classification Results**

Table 7.1 shows the results summary of the drive unit classification MLF neural network sub model 1 trained using the Levenberg -Marquardt backpropagation learning algorithm. The training data achieved an overall performance of 95.3 percent CCR. Of the nine drive body classes, only two classes did not achieve 100 percent accuracy. The

performance of the trained model was significantly lower on the test dataset, achieving only 73.7 percent CCR. It should be noted that classes with poor classification performance generally reflected a smaller overall data representation. This may have led to under calibration of the classification model parameters for those classes, leading to the unsatisfactory classification rates observed.

Table 7.1. Type I Drive Body Configuration classification results

Drive Unit Body Class	Description	Training Data			Test Data		
		Count	Classified Correct	CCR (%)	Count	Classified Correct	CCR (%)
D1	Platform	61	51	83.6	21	15	71.4
D2	Van	154	154	100.0	53	47	88.7
D3	Concrete Mixer	4	4	100.0	3	2	66.7
D4	Gravel / Dump	3	3	100.0	2	0	0.0
D5	Tank	8	8	100.0	4	1	25.0
D6	Conv. Tractor	7	7	100.0	4	1	25.0
D7	Ext. Cab Tractor	10	10	100.0	4	3	75.0
D8	Cab Over Tractor	1	1	100.0	1	1	100.0
D9	Other	5	3	60.0	3	0	0.0
<b>Overall Performance</b>		<b>253</b>	<b>241</b>	<b>95.3</b>	<b>95</b>	<b>70</b>	<b>73.7</b>

Table 7.2 shows the cross-classification results of sub model 1 on the test dataset. It shows significant cross-classification error between platform type drive units (D1) and van type drive units (D2). The overwhelming representation of the platform type drive units (D1) and van type drive units (D2) in the dataset was the likely cause of cross-classification from other classes to these two drive unit classes.

Table 7.2. Type I Drive Body Configuration test data cross classification results

Drive Units		Predicted Class								
		D1	D2	D3	D4	D5	D6	D7	D8	D9
Actual Class	Platform D1	15	6	0	0	0	0	0	0	0
	Van D2	5	47	0	1	0	0	0	0	0
	Concrete Mixer D3	0	1	2	0	0	0	0	0	0
	Gravel / Dump D4	1	0	1	0	0	0	0	0	0
	Tank D5	1	0	0	0	1	0	2	0	0
	Conv. Tractor D6	0	1	0	0	0	1	0	2	0
	Ext. Cab Tractor D7	0	1	0	0	0	0	3	0	0
	Cab Over Tractor D8	0	0	0	0	0	0	0	1	0
	Other D9	1	1	0	0	0	0	1	0	0

Table 7.3 summarizes the classification results of drive unit classification sub model 2. The training dataset obtained an accuracy of 93.0 percent CCR while the independent test dataset achieved 93.6 percent CCR. The performance of the test dataset is likely attributed to significant representation in three of the four represented classes. Table 7.4 shows the cross classification results based on the test dataset.

Table 7.3. Type II Drive Body Configuration classification results

Drive Unit Body Class	Description	Training Data			Test Data		
		Count	Classified Correct	CCR (%)	Count	Classified Correct	CCR (%)
D1	Platform	1	0	0	2	0	0
D2	Van	0	0	-	0	0	-
D3	Concrete Mixer	0	0	-	0	0	-
D4	Gravel / Dump	0	0	-	0	0	-
D5	Tank	0	0	-	0	0	-
D6	Conv. Tractor	58	46	79.3	20	18	90
D7	Ext. Cab Tractor	251	244	97.2	85	83	97.6
D8	Cab Over Tractor	48	43	89.6	17	15	88.2
D9	Other	0	0	-	0	0	-
<b>Overall Performance</b>		<b>358</b>	<b>333</b>	<b>93.0</b>	<b>124</b>	<b>116</b>	<b>93.6</b>



Table 7.4. Type II Drive Body Configuration test data cross classification results

Drive Units		Predicted Class								
		D1	D2	D3	D4	D5	D6	D7	D8	D9
Actual Class	Platform D1	0	0	0	0	0	1	1	0	0
	Van D2	0	0	0	0	0	0	0	0	0
	Concrete Mixer D3	0	0	0	0	0	0	0	0	0
	Gravel / Dump D4	0	0	0	0	0	0	0	0	0
	Tank D5	0	0	0	0	0	0	0	0	0
	Conv. Tractor D6	0	0	0	0	0	18	1	1	0
	Ext. Cab Tractor D7	0	0	0	0	0	1	83	1	0
	Cab Over Tractor D8	0	0	0	0	0	1	1	15	0
	Other D9	0	0	0	0	0	0	0	0	0

The overall drive unit body classification model correctly classified 186 of 219 vehicle drive units in the test dataset, yielding an aggregate test performance of 84.9 percent CCR.

### 7.3.2 Trailer Unit Classification Results

Table 7.5 shows the results summary of the trailer unit classification MLF neural network model trained using the Levenberg -Marquardt backpropagation learning algorithm. The training data achieved an overall performance of 88.2 percent CCR. The performance of the trained model on the test dataset yielded 84.1 percent CCR. Among the classes, the auto transport trailer units (T7) and chemical / dry bulk trailer units (T8) performed poorest, with accuracies of 0 and 40.0 percent CCR respectively.

Table 7.5. Trailer Body Configuration classification results

Trailer Unit Body Class	Description	Training Data			Test Data		
		Count	Classified Correct	CCR (%)	Count	Classified Correct	CCR (%)
T1	Basic Platform	41	25	61.0	15	9	60.0
T2	Low Boy Platform	13	6	46.2	5	3	60.0
T3	Enclosed Van	202	195	96.5	69	67	97.1
T4	Drop Frame Van	6	5	83.3	3	2	66.7
T5	40' Container	65	59	90.8	23	19	82.6
T6	20' Container	23	22	95.7	9	8	88.9
T7	Auto Transport	6	5	83.3	3	0	0.0
T8	Chemical / Dry Bulk	15	11	73.3	5	2	40.0
T9	Gravel / Dump	5	3	60.0	3	3	100.0
T10	Towed Vehicle / Small Trailer	6	6	100.0	3	3	100.0
<b>Overall Performance</b>		<b>382</b>	<b>337</b>	<b>88.2</b>	<b>138</b>	<b>116</b>	<b>84.1</b>


From Table 7.6, it can be observed that these types of trailer units are likely to be misclassified as enclosed van trailer units (T3). This shows that the training samples for these classes were insufficient to establish proper model recognition of the trailer characteristics. Table 7.6 also shows that most misclassified trailer units are classified as enclosed van trailer units (T3).

Table 7.6. Trailer Body Configuration test data cross classification results

Trailer Units		Predicted Class									
		T1	T2	T3	T4	T5	T6	T7	T8	T9	T10
Actual Class	Basic Platform T1	9	0	5	0	1	0	0	0	0	0
	Low Boy Platform T2	0	3	2	0	0	0	0	0	0	0
	Enclosed Van T3	1	0	67	0	1	0	0	0	0	0
	Drop Frame Van T4	0	0	1	2	0	0	0	0	0	0
	40' Container T5	0	0	2	1	19	1	0	0	0	0
	20' Container T6	0	0	0	0	1	8	0	0	0	0
	Auto Transport T7	0	0	2	0	1	0	0	0	0	0
	Chemical / Dry Bulk T8	1	0	2	0	0	0	0	2	0	0
	Gravel / Dump T9	0	0	0	0	0	0	0	0	3	0
	Towed Vehicle / Small Trailer T10	0	0	0	0	0	0	0	0	0	3

## 7.4 COMBINED CLASSIFICATION PERFORMANCE

The commercial vehicle vector classification system developed in this study is an integration of the axle-configuration model described in Chapter 6 as well as the drive unit body and trailer unit body classification sub-models described in this chapter, which together yields a comprehensive description of each commercial vehicle. Figure 7.7 shows a sample classification output from the commercial vehicle vector classification system.



Classification Type	Output Class	Description
Axle Configuration	A2-3	Single Steering Axle, Tandem Drive Axles on Drive Unit; Tandem Trailer Axles on Single Semi Trailer Unit
Drive Unit Body	D6	Conventional Tractor
Trailer Unit Body	T8	Chemical/Dry Bulk Tank

Figure 7.7. Sample output from the Commercial Vehicle Vector Classification System

The overall model performance was obtained by evaluating the commercial vehicle vector classification model on the combined dataset of 1029 commercial vehicles. The

evaluation of this overall dataset yielded 99.0 percent CCR for axle configuration classification and 81.1 percent CCR for combined drive unit and trailer unit body classification performance (i.e., the model classifies both the drive unit body and trailer unit body type correctly). Overall, the model obtained 80.8 percent CCR in correctly identifying all three commercial vehicle vector class parameters (axle configuration, drive unit body and trailer unit body) in a commercial vehicle.

## **7.5 DISCUSSIONS**

The models presented in this chapter show promising results in identifying body configurations of the drive and trailer units of commercial vehicles. However, many of the classes were under-represented in the model development dataset. As a consequence, the real-world heterogeneity of vehicles within those classes may not be well represented, and may result in high rates of misclassification – an observation already made in drive unit body configuration classes D4, D5, D6 and D9 as well as trailer unit body configuration classes T7 and T8. Hence, these models require further calibration with a larger dataset before implementation.

## **CHAPTER 8 APPLICATIONS**

### **8.1 ACCURATE COMMERCIAL VEHICLE TRAVEL STATISTICS**

The commercial vehicle classification system developed in this dissertation can yield a new paradigm in advanced commercial vehicle exposure statistics. Examples are presented in this section to show the potential of the commercial vehicle classification system developed in this dissertation using data obtained from May 3 2006 at the southbound San Onofre Truck Weigh and Inspection Facility.

#### **8.1.1 Understanding Commercial Vehicle impacts from Port Activities**

Port activities generate significant commercial vehicle trips on a daily basis. The impacts of these generated trips have a profound impact on the environment, freeway traffic performance and infrastructure, and safety. Hence, it is important to obtain accurate measures of port-related commercial vehicle travel to understand their daily and seasonal travel patterns.

Figure 8.1 shows the travel patterns of port-related commercial vehicles by trailer type at the San Onofre study site on May 3 2006. Two types of trailer statistics are available from the model: 40' box container and 20' box container trailers. The figure shows a comparison of actual and predicted 15-minute interval volume counts. It can be observed

that model predicted counts match closely to actual counts for both trailer types across time of day.

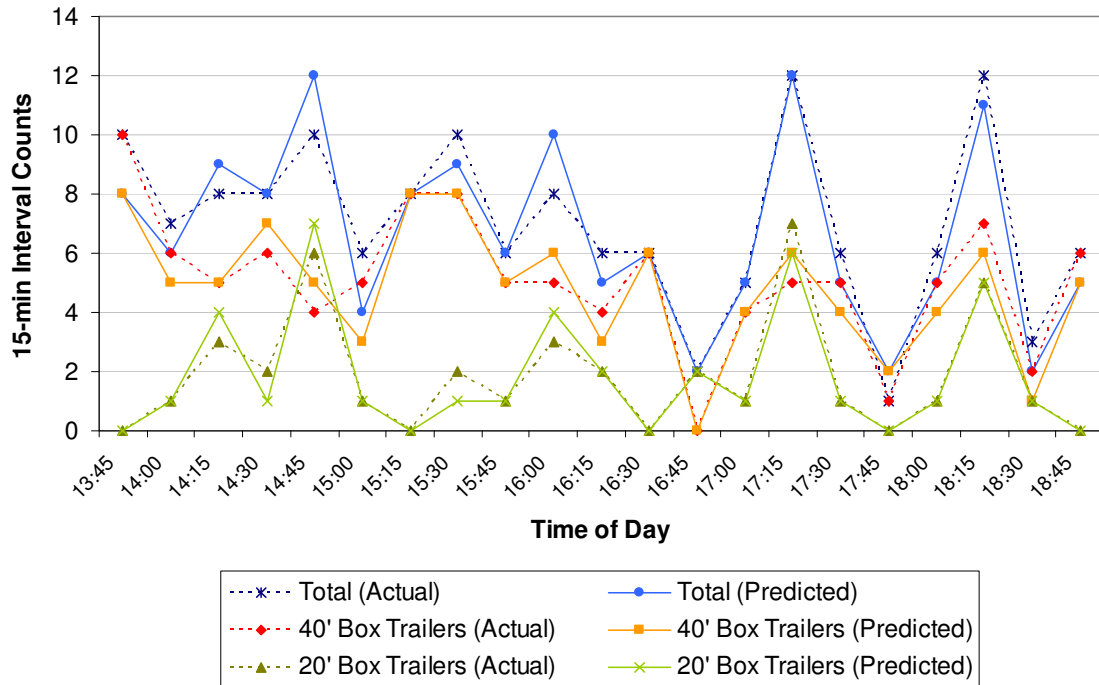


Figure 8.1. Travel patterns of port-related commercial vehicles by trailer type

Figure 8.2 shows further insight into the drive unit configurations of the 40' box trailers. It is observed that extended cab tractors outnumber cab-over tractors for pulling 40' box trailers. The travel patterns between these two drive units also appear different, which is not surprising, since extended cab tractors are more suited for long-haul trips than cab-over tractors. Hence, the classification system may reveal further insight to predicting travel behavior of box trailer movements

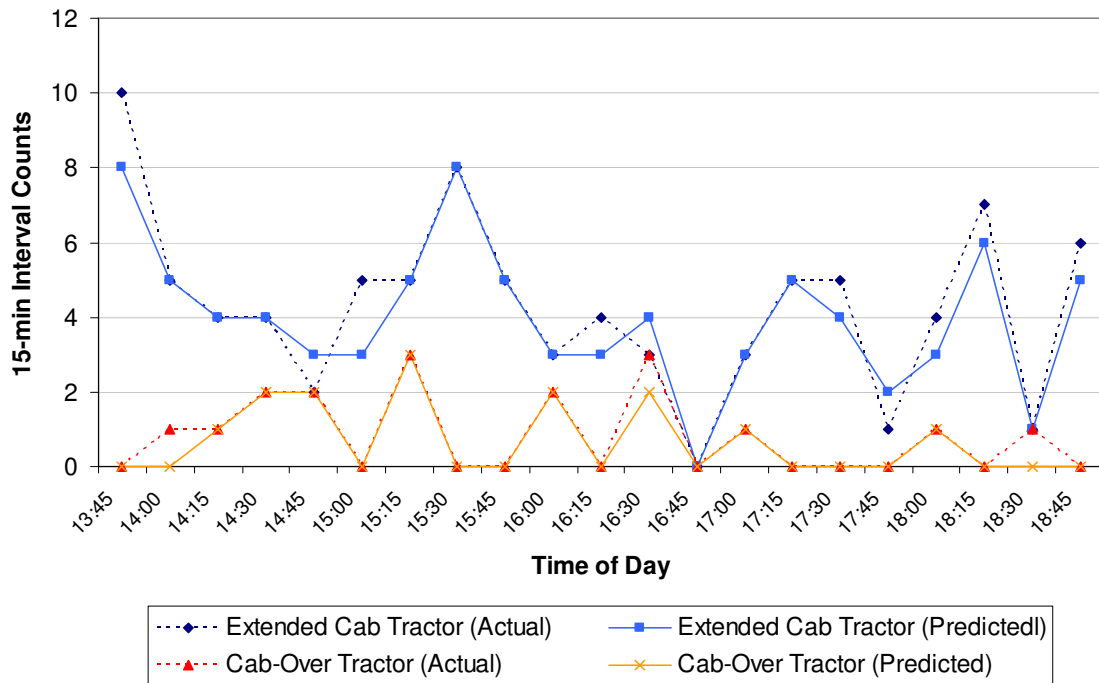


Figure 8.2. Travel patterns of 40' box trailers by drive unit type

### 8.1.2 Non-port Related Freight Movement

Figure 8.3 shows the travel patterns of non-port related freight travel by truck types. Model results follow closely to actual counts. The detailed breakdown of vehicle types can serve several purposes such as determining freight-related impacts on the environment, pavement infrastructure and safety though the analysis of the unique characteristics of each vehicle configuration.

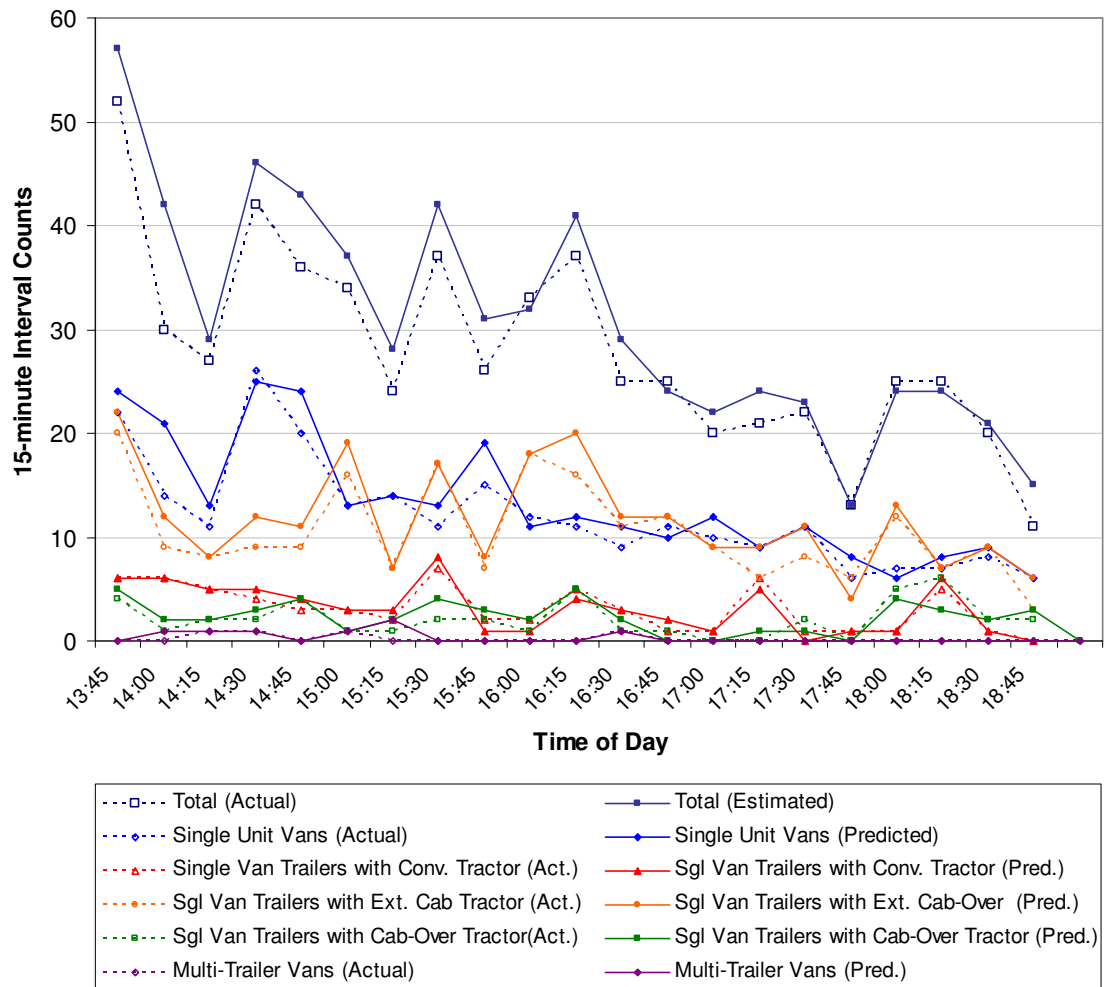


Figure 8.3. Travel patterns of non-port related freight trucks



## **8.2 VEHICLE RE-IDENTIFICATION IN UNSTABLE TRAFFIC CONDITIONS**

### **8.2.1 Background**

The concept of re-identifying vehicles platoons across a section using inductance signatures to obtain section traffic measures was first conceived by Böhnke and Pfannerstill (1986). In their model, inductive vehicle signatures were used as input to a pattern recognition system for re-identification of a vehicle platoon.

Kühne and Immes (1993) developed a model that could re-identify a platoon of vehicles by finding correlation of vehicles feature series at upstream and downstream sites. Kühne et al. (1997) later proposed an improved model that was able to identify individual vehicles as well as vehicle platoons.

Sun et al. (1999) expanded on this framework and developed a lexicographic optimization model that matched individual vehicles traversing between two adjacent detector stations on freeways. In this algorithm, five distinct levels were defined in the lexicographic optimization problem. These are time window determination, vehicle classification by maximum magnitude of inductance signature, vehicle length restriction, vehicle features differences minimization and vehicle matching. The re-identification rates achieved from this study was 75 percent and 78 percent for passenger and non-passenger vehicles respectively along the SR-24 freeway in Lafayette, California. The

model was also able to yield partial origin/destination demands and individual lane changing information in addition to the section measures obtainable from the previous studies.

Abdulhai and Tabib (2003) adopted a waveform warping-reduction process to improve accuracy in re-identification performance. The warping-reduction process consisted of signal magnitude normalization, transformation of the time axis into length (which required a double loop speed trap configuration), and re-sampling of data using a spline interpolation.

Other approaches were also investigated to solve the vehicle re-identification problem. Tawfik et al. (2004) proposed a decision tree model that integrated distance measurements first developed by Abdulhai and Tabib (2002). Jeng et al. (2005) also suggested an interpolation approach that could be applied to both single and dual inductive loop detector configurations. It does away with the need to obtain speed as a feature and was able to obtain comparable results to the lexicographic optimization model first developed by Sun et al. (1999).

Oh and Ritchie (2003) expanded the scope of the re-identification model developed by Sun et al. to signalized arterial networks, introducing a new search space reduction technique and employing probabilistic pattern recognition. Oh et al. (2004) further investigated the feasibility of Blade™ inductive sensors for use in a heterogeneous re-identification detection system with existing round inductance loops.

However, the above studies all require vehicles to traverse the sensors at constant speeds to avoid generating signatures that are distorted by acceleration and deceleration effects.

This section investigates the improvements to the reliability of Blade™ inductive signatures in unstable traffic conditions. Control vehicles traversed the Blade™ inductive sensors multiple times to generate samples of Blade™ inductive signatures, some of which while accelerating and decelerating over the Blade™ inductive sensors to generate distorted signatures simulating adverse traffic conditions.

A comparison of signatures with and without the distortion-correcting SPRINTS transformation method described in section 4.5.2 was made to evaluate the improvement offered by the SPRINTS transformation on the Blade™ inductive signatures.

### **8.2.2 Feature Extraction**

Thirty interpolated data points were extracted from the magnitude normalized Blade™ inductive signatures of each control vehicle for analysis.

### **8.2.3 Repeatability Analysis**

The standard deviation is measured at each corresponding interpolated point across all signature samples from the same control vehicle. The Signature Repeatability Index

(SRI) is then defined as the average of standard deviation measures across all thirty interpolated points. Hence, the SRI represents an aggregate measure for the overall standard deviation across all samples obtained from a control vehicle, where a lower SRI value indicates that the signatures obtained for the vehicle show a greater level of repeatability—an important requirement for performing vehicle re-identification.

$$SRI = \frac{1}{m} \sum_{j=1}^m \sqrt{\frac{1}{n} \sum_{i=1}^n (NormMag_{i,j}^2) - \frac{1}{n} \sum_{i=1}^n (NormMag_{i,j})^2}$$

Where:

- $NormMag_{i,j}$  -  $j^{\text{th}}$  Interpolated Normalized Magnitude Point from  $i^{\text{th}}$  Control Vehicle Sample
- $m$  - total number of control vehicle signature samples
- $n$  - total number of interpolated points

The SRI results obtained for each control vehicle is shown in Table 8.1. Figure 8.4 shows compares the SRI results for each control vehicle ordered by the duration standard deviation across signature samples for each control vehicle. Using the duration standard deviation as a surrogate measure for the presence acceleration-distorted signatures, Figure 8.4 shows that applying the distortion-correcting SPRINTS transformation model results in more significant reduction in SRI for vehicles with acceleration-distorted signature samples. On the other hand, vehicles with low duration standard deviation amongst signature samples show little or no SRI improvement.

Table 8.1. Signature Repeatability Index (SRI) results for control vehicles

Dataset	Control Vehicle No.	Vehicle Description	No. Runs	Duration (sec)				Transformation Method	Signature Repeatability Index (SRI)
				Max	Min	Mean	Std Dev		
3/7/2008	1	Honda Civic	14	1.115	0.292	0.5513	0.290	None SPRINTS	0.043 0.059
	2	BMW 325is-1	19	5.311	0.272	1.2521	1.240	None SPRINTS	0.132 0.060
3/10/2008	1	BMW 325is-2	30	18.138	0.338	1.2722	3.2346	None SPRINTS	0.106 0.053
4/15/2008	1	Alfa Romeo Spider	20	1.502	0.292	0.6851	0.3784	None SPRINTS	0.122 0.100
	2	Toyota Camry V6	18	0.963	0.318	0.499	0.1735	None SPRINTS	0.042 0.042
	3	Toyota Camry	18	0.761	0.298	0.4576	0.1235	None SPRINTS	0.061 0.061
	4	Acura Integra	24	2.538	0.327	0.6853	0.5319	None SPRINTS	0.052 0.047
	5	Hyundai Santa Fe	19	1.543	0.280	0.5287	0.3689	None SPRINTS	0.054 0.056

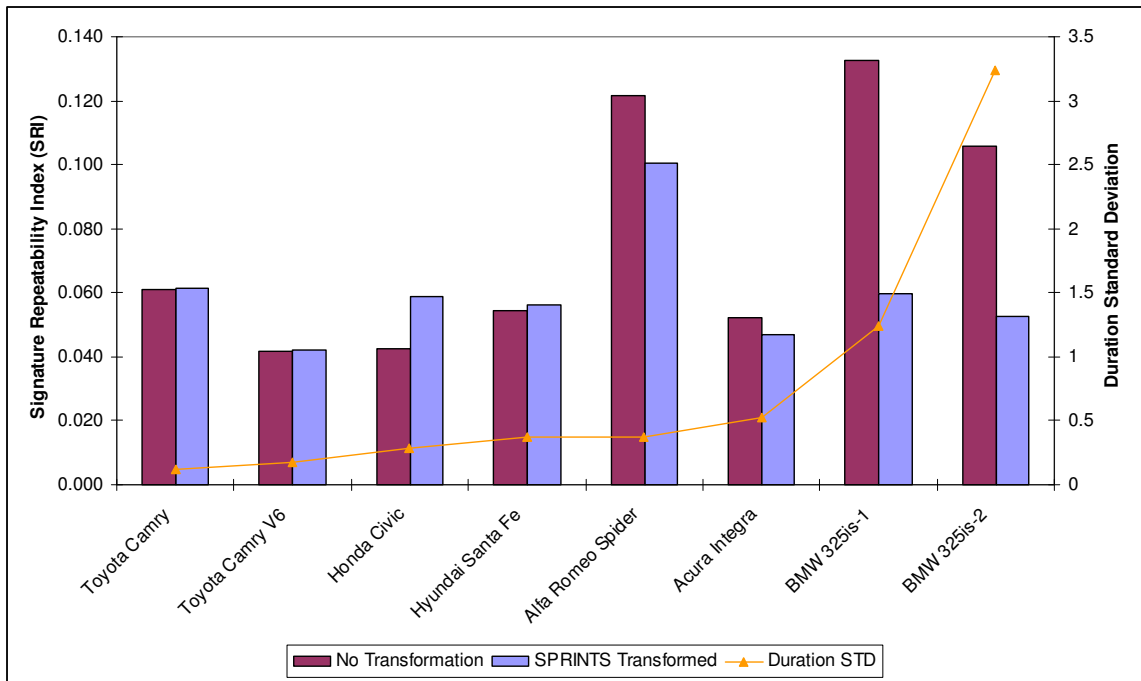
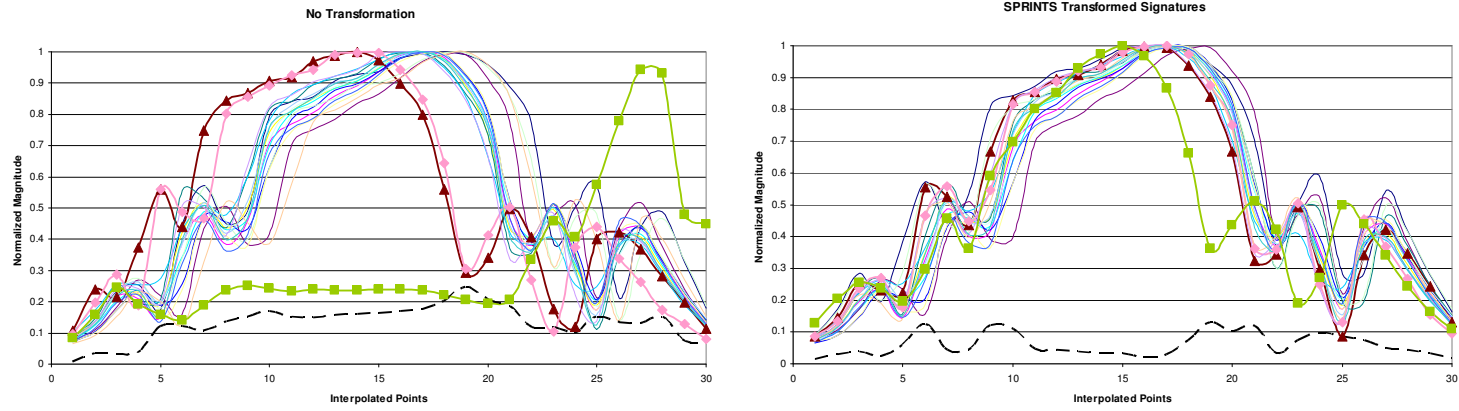
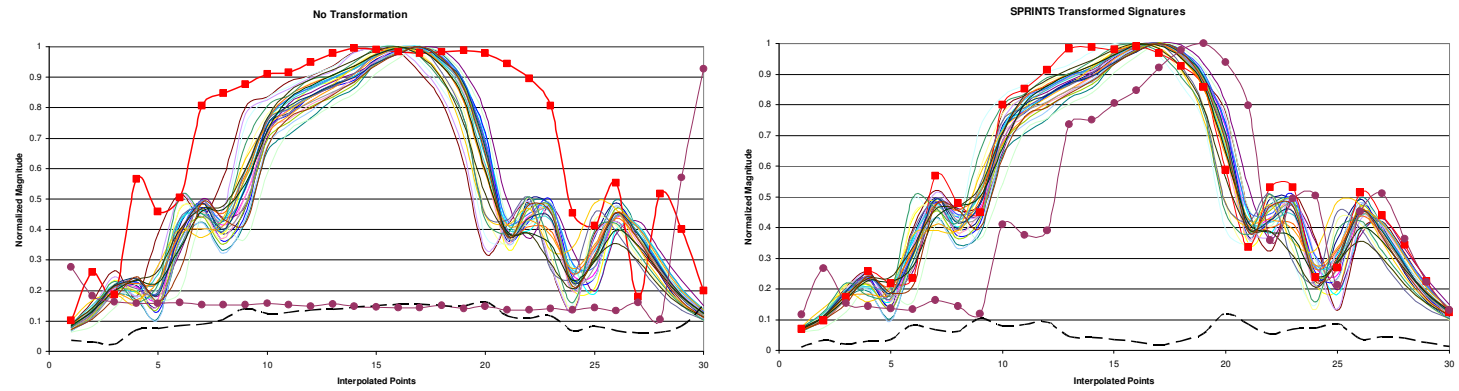


Figure 8.4. Comparison of Signature Repeatability (SRI) Index for each control vehicle ordered by duration standard deviation

Figure 8.5 and Figure 8.6 show comparisons of 30-point interpolated Blade inductive signatures of control vehicles before and after the SPRINTS transformation was applied. Control vehicles containing distorted signature samples were chosen to illustrate the benefits of applying the SPRINTS transformation. Figure 8.5 shows control vehicles BMW 325is-1 and BMW 325is-2. Figure 8.6 shows control vehicles Alfa Romeo Spider and Acura Integra. Distorted signatures in both figures are represented by plots with markers. The standard deviation at each interpolated point is represented by a dashed plot. It can be observed from both figures that the transformed signatures show improved consistency. This is also reflected by the reduced standard deviation at each interpolated point.

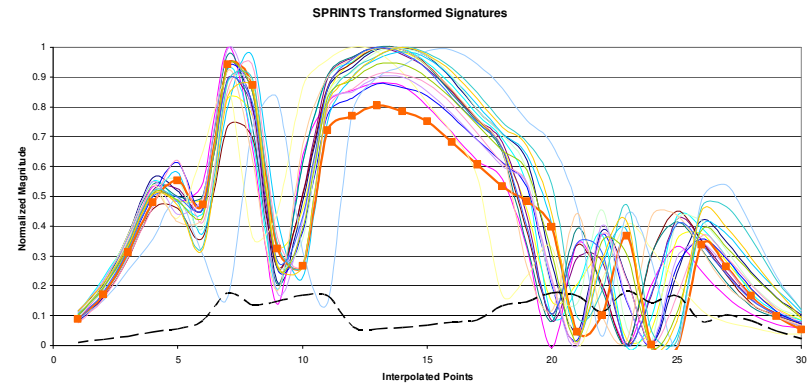
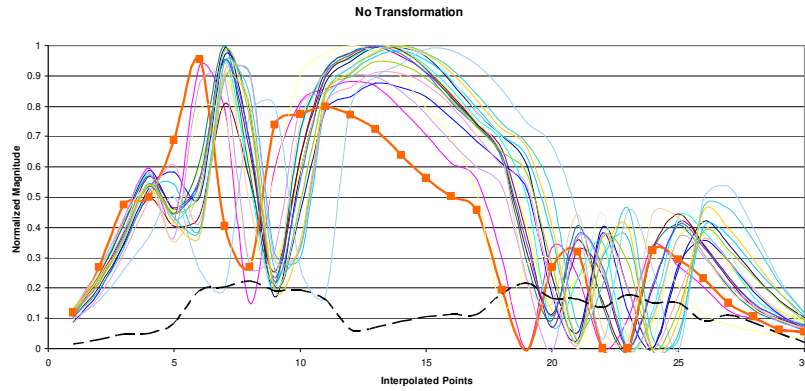


(a) Control vehicle BMW 325is-1

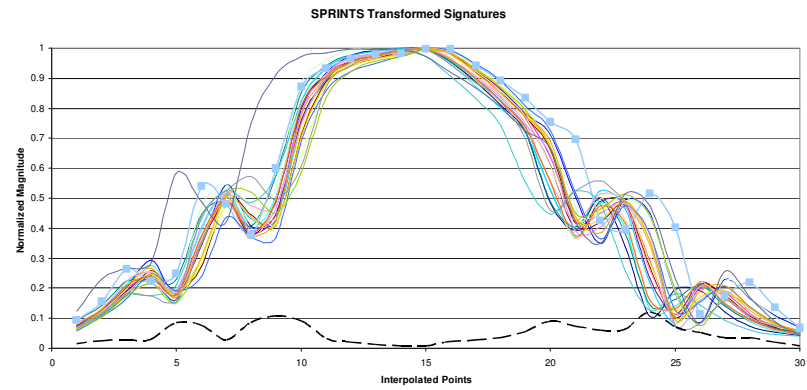
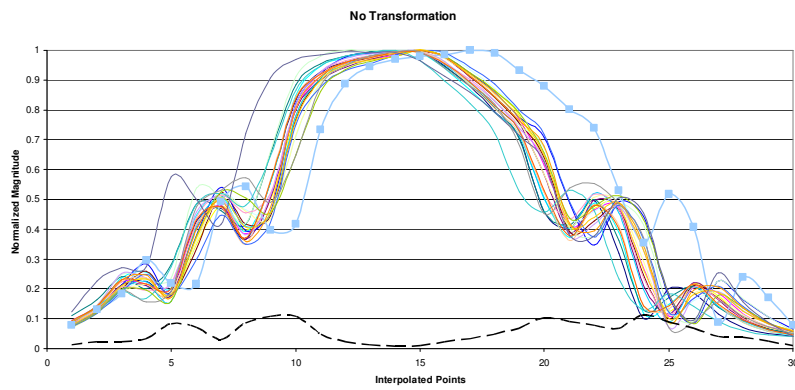


(b) Control vehicle BMW 325is-2

Figure 8.5. Comparison of 30-point interpolated control vehicle signature samples before (left) and after SPRINTS transformation (right) of control vehicles BMW 325is-1 and BMW 325is-2



(a) Control vehicle Alfa Romeo Spider



(b) Control vehicle Acura Integra

Figure 8.6. Comparison of 30-point interpolated control vehicle signature samples before (left) and after SPRINTS transformation (right) of control vehicles Alfa Romeo Spider and Acura Integra



## **8.2.4 Discussion**

The repeatability analysis shows evidence that the Blade™ inductive signature system with the SPRINTS transformation model show potential for vehicle re-identification even in the presence of unstable traffic where vehicles can generate distorted inductive signatures due to acceleration or deceleration over inductive loop sensors.

## **8.3 PORTABLE TRAFFIC SURVEILLANCE SYSTEM**

### **8.3.1 The need for temporary portable traffic surveillance**

Presently, short duration counts are needed to provide roadway segment-specific traffic count information on a cyclical basis and ensure geographic diversity and coverage in the absence of permanent detectors (FHWA, 2001). However, volume counts provide limited information to understand the impacts commercial vehicles can have on localized geographical areas.

### **8.3.2 Proposed solution with surface mounted Blade™ inductive sensors**

The surface-mounted Blade™ inductive sensors investigated in this dissertation can be easily fabricated at a low cost, and show reasonable durability for general traffic surveillance and can be easily implemented as a temporary traffic surveillance system.

Hence, they are an alternative solution to pneumatic traffic counters where more accurate and comprehensive traffic data is desired.

Currently, low-power mini-PCs requiring under 25W operating power are readily available. These processing units can be configured for extended period operations with a modest portable power source. All together, the advanced inductive loop detector cards, a low-power mini-PC, battery and wireless modem can be housed in a compact package for excellent portability as illustrated in Figure 8.7. Such a setup will allow advanced commercial vehicle classification statistics to be measured at multiple locations with little effort without requiring the available of external power sources. The wireless modem allows data collection to be initiated, monitored and terminated off-site, enabling multiple temporary surveillance stations to be concurrently deployed without extensive monitoring effort and logistics.

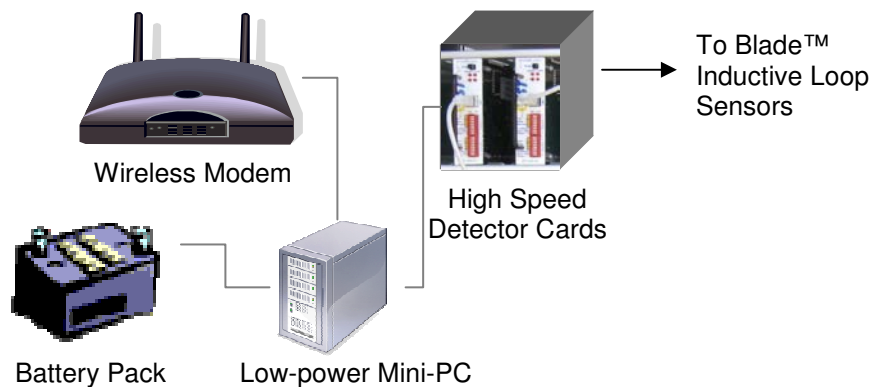


Figure 8.7. Components of a portable advanced inductive loop detector system

## CHAPTER 9 CONCLUDING REMARKS

### 9.1 CONTRIBUTIONS

This dissertation provides two major contributions. First, this study solves the problem of obtaining reliable inductive signature data under adverse traffic conditions, such as those found in peak freeway congestion periods and in arterial streets heavily influenced by intersection delays. Where previously vehicle inductive signatures would be irreversibly distorted by acceleration or deceleration effects, they are now corrected and usable. This is of the essence in freeway applications, as there has been tremendous interest in obtaining accurate freeway performance measures. Yet, accurate performance measures would not have been possible previously under peak congestion periods when the vehicle inductive signature quality degrades due to acceleration-deceleration distortion. The correction is achieved by applying the SPRINTS transformation algorithm developed in this dissertation described in Chapter 4, and paves the way for accurate traffic performance measurements to reveal accurately the severity of congestions and delays experienced on the freeways as well as arterial networks.

The second significant contribution is the development of a comprehensive commercial vehicle classification system. Up till now, the most reliable and detailed classification system is the axle-based FHWA scheme F using automated vehicle classifiers. However, this current system still leaves a void in the comprehensive understanding of commercial

vehicle travel behavior and impacts due to their inherent heterogeneity. This newly developed classification system yields a more detailed axle classification scheme with excellent axle classification performance. More importantly, it introduces new body unit classification schemes that set a new paradigm in classification studies by revealing detailed information regarding the function of the drive and trailer units of each commercial vehicle, with promising results obtained. However, many of the classes were under-represented in the model development dataset. As a consequence, the real-world heterogeneity of vehicles within those classes may not be well represented, and may result in high rates of misclassification – an observation already made in drive unit body configuration classes D4, D5, D6 and D9 as well as trailer unit body configuration classes T7 and T8. Hence, these models require further calibration with a larger and more comprehensive dataset before implementation. The results obtained from this study indicate remarkable potential for providing enhanced commercial vehicle surveillance through the implementation of this system. Such information is critical to reveal exposure rates and travel behavior of specific commercial vehicle types to evaluate the multi-faceted impacts of commercial vehicle impacts as pointed out in Chapter 1. This is critically needed to implement more astute and effective solution policies to minimize the adverse impacts of commercial vehicles and facilities associated with specific commercial vehicle types.

## **9.2 FUTURE RESEARCH**

### **9.2.1 Investigation of Permanent Blade™ Inductive Sensors**

The Blade™ inductive sensors used in this study were of the temporary surface-mounted prototype. Hence, the next logical step in the continuation of this research study is the investigation and feasibility study of permanent Blade™ inductive sensors. A preliminary study is currently in progress to investigate the optimal configuration of the permanent Blade™ inductive sensor at the southbound San Onofre Truck Weigh and Inspection Facility.

### **9.2.2 Arterial Re-identification with Blade™ Inductive Sensors**

The SPRINTS transformation model described in Chapter 4 has shown the ability to yield improved inductive vehicle signatures under stop-and-go arterial traffic conditions. This improves the versatility of the Blade™ inductive signatures to obtain reliable and repeatable Blade™ inductive signatures at different arterial locations. Hence, a natural progression of this study would be the investigation of arterial-based vehicle re-identification using Blade™ inductive sensors. Such a system will be able to provide information of arterial travel times, with further potential for network origin-destination measurement if vehicle re-identification rates within the arterial network are excellent.

## BIBLIOGRAPHY

- Abdulhai, B., Tabib, S.M., 2002. Towards anonymous vehicle tracking via inductance-pattern recognition, in proceedings of the 81<sup>st</sup> Annual Meeting of the Transportation Research Board, Washington, D.C.
- Abdulhai, B., and Tabib, S., 2003. Spatio-temporal inductance-pattern recognition for vehicle re-identification, *Transportation Research Part C: Emerging Technology*, vol. 11 issues 3-4, 2003, pp. 223-239.
- Benekohal, R.F., El-Zohairy, Y.M., Forrler, E., Aycin, M.F., 1999. Truck Delay and Traffic Conflicts Around Weigh Stations, In *Transportation Research Record: Journal of the Transportation Research Board*, No.1653, TRB, National Research Council, Washington, D.C., 1999, pp. 52-60.
- Böhnke, P., Pfannerstill, E., 1986. A system for the automatic surveillance of traffic situations, *Institute of Transportation Engineers Journal*, vol. 56, pp. 41-45.
- Braver, E., Cammisa, M., Lund, A., Early, N., Mitter, E., and Powell, M., 1997. Incidence of Large Truck-Passenger Vehicle Underride Crashes in the Fatal Accident Reporting System and the National Accident Sampling System, In *Transportation Research Record: Journal of the Transportation Research Board*, No., 1595, TRB, National Research Council, Washington, D.C., 1997, pp. 27-33.
- Brown, C., Kennedy, N., Wright, D., Zak, W., 2003. Methodology for estimating vehicle miles traveled for commercial motor vehicles at the state level, In *Transportation Research Record: Journal of the Transportation Research Board*, No. 1830, TRB, National Research Council, Washington, D.C., 2003, pp. 72-76.
- California Department of Transportation (CALTRANS), 2008.  
<http://www.dot.ca.gov/hq/traffops/trucks/datawim/>, Accessed 05/01/08.
- Cheung, S.Y., Coleri, S., Dundar, B., Ganesh, S., Tan, C.W., Varaiya, P., 2004. Traffic measurement and vehicle classification with a single magnetic sensor, In *Transportation Research Record: Journal of the Transportation Research Board*, No. 1917, TRB, National Research Council, Washington, D.C., 2004, pp 173-181.
- Coifman, B, Kim, S, 2007. Speed Estimation and Length Based Vehicle Classification from Freeway Single Loop Detectors, in Proceedings of the 87<sup>th</sup> Annual Meeting of the Transportation Research Board, Washington, D.C.

Crainic T.G., Ricciardi N., Storchi G., 2004. Advanced freight transportation systems for congested urban areas, *Transportation Research Part C: Emerging Technology*, vol. 12, issue 2, pp. 119-137.

Federal Highway Administration (FHWA), 2001. Traffic Monitoring Guide. U.S. Department of Transportation, Washington, D.C.

Federal Highway Administration (FHWA), 2002. Freight Transportation Profile: California Freight Analysis Framework.

Federal Highway Administration (FHWA), 2006. Transportation Air Quality: Selected Facts and Figures.

Federal Motor Carrier Safety Administration (FCMSA), 2007. *Highway/Heavy Vehicle Interaction: A Synthesis of Safety Practice*, 2007. Publication no. FCMSA-MCRRR-07-007. US Department of Transportation, Washington, DC.

Fritsch, F. N. and R. E. Carlson, "Monotone Piecewise Cubic Interpolation," *SIAM Journal on Numerical Analysis*, Volume 17, Number 2, 1980, pp.238-246.

Gupte, S., Masoud, O., Martin, R., Papanikolopoulos, N.P., 2002. Detection and classification of vehicles, *IEEE Transactions on Intelligent Transportation Systems*, vol. 3(1), pp. 37-47.

Hagan, M.T., and H.B. Demuth, "Neural Networks for Control," Proceedings of the 1999 American Control Conference, San Diego, CA, 1999, pp. 1642-1656.

Hallenbeck, M., Kim, S.-G., 1993. Truck Loads and Flows Task A Final Technical Report, Report WA-RD 320.3, Washington State Transportation Research Center (TRAC), Seattle, WA.

Hallenbeck, M., Weinblatt, H., 2004. Equipment for Collecting Traffic Load Data, Transportation Research Board, NCHRP Report 509, Washington, D.C.

Harlow, C., Peng, S., 2001. Automatic vehicle classification with range sensors, *Transportation Research Part C: Emerging Technology*, vol. 9, issue 4, pp. 231-247.

Inductive Signature Technologies (IST), 2006. <http://www.ist-traffic.com/>, Accessed 07/01/2006.

Jeng, S., Ritchie, S.G., 2005. New Inductive Signature Method for Vehicle Reidentification, in Proceedings of the 84<sup>th</sup> Annual Meeting of the Transportation Research Board, Washington, D.C.

Jeng, S., Ritchie S.G., 2006. A New Inductive Signature Data Compression and Transformation Method for On-Line Vehicle Reidentification, in Proceedings of the 85th Annual Meeting of the Transportation Research Board, Washington, D.C.

Jeng, S., Ritchie S.G., 2008. Real-time Vehicle Classification using Inductive Loop Signature Data, in Proceedings of the 87th Annual Meeting of the Transportation Research Board, Washington, D.C.

Jeng S., Ritchie S.G., Tok A., 2007. Freeway Corridor Performance Measurement Based on Vehicle Reidentification, in Proceedings of the 86th Annual Meeting of the Transportation Research Board, Washington, D.C.

Kaufman, L., Rousseeuw, P. J., 1990. Finding Groups in Data: An Introduction to Cluster Analysis. Wiley, New York.

Kruskal, W.H., Wallis, W.A., 1952. Use of ranks in one-criterion variance analysis, *Journal of the American Statistical Association*, vol. 47 no. 260, pp. 583–621.

Kühne, R.D., Immes, S., 1993. Freeway control systems for using section-related traffic variable detection, Pacific Rim TransTech Conference, Seattle, Washington.

Kühne, R.D., Palen, J., Gardner, C., Ritchie, S.G., 1997. Section-related measure of traffic system performance, in proceedings of the 76<sup>th</sup> Annual Meeting of the Transportation Research Board, Washington, D.C.

Kwigizile, V., Mussa, R.N., Selekw, M., 2005. Connectionist approach to improving highway vehicle classification schemes—the Florida case, in proceedings of the 84th Annual Meeting of the Transportation Research Board, Washington, D.C.

Kwon, J., P. Varaiya and A. Skabardonis, 2003. Estimation of Truck Traffic Volume from Single Loop Detectors with Lane-to-Lane Speed Correlation, In *Transportation Research Record: Journal of the Transportation Research Board*, No. 1856, TRB, National Research Council, Washington, D.C., 2003, pp. 106-117.

Laval, J.A., 2007. Delays Caused by Trucks on Multilane Freeways: Impacts of Overtaking Bans for Trucks, in proceedings of the 86<sup>th</sup> Annual Meeting of the Transportation Research Board, Washington, D.C., paper no. 07-2090, 12pp.

Levene, H. , 1960. In Contributions to Probability and Statistics: Essays in Honor of Harold Hotelling, I. Olkin et al. eds., Stanford University Press, pp. 278-292.

Lu, Y.; Hsu, Y.; Maldague, X. , 1992. Vehicle Classification Using Infrared Image Analysis, *Journal of Transportation Engineering*. vol. 118, no. 2, pp. 223-240.



Lyles., R.W., Wyman, J.H., 1983. An operational view of traffic data collection systems, *Institute of Transportation Engineers Journal*, (Dec.), pp. 18-24.

Lyman, S., Braver, E., 2003. Occupant Deaths in Large Truck Crashes in the United States: 25 Years of Experience. *Accident Analysis and Prevention*, 35, 731-739.

Newell G. F., 1998. A moving bottleneck, *Transportation Research Part B: Methodological*, vol. 32, issue 8, November 1998, pp. 531-537.

Nooralahiyan, A.Y., Dougherty, M., McKeown, D., Kirby, H.R., 1997. A field trial of acoustic signature analysis for vehicle classification, *Transportation Research Part C: Emerging Technology*, vol. 5, issues 3-4, 1997, pp. 165-177.

Oh, C., Ritchie, S.G., 2003. Anonymous vehicle tracking for real-time traffic surveillance and performance on signalized arterials, In *Transportation Research Record: Journal of the Transportation Research Board*, No. 1826, TRB, National Research Council, Washington, D.C., 2003, pp. 37-44.

Oh, C., Ritchie, S.G., 2007. Recognizing vehicle classification information from blade sensor signature, *Pattern Recognition Letters*, vol. 28, issue 9, 2007, pp. 1041-1049.

Oh, C., Ritchie, S.G., Jeng, S., 2004. Vehicle reidentification using heterogeneous detection systems, in proceedings of the 83<sup>rd</sup> Annual Meeting of the Transportation Research Board, Washington, D.C.

Oh, C., Tok, A., Ritchie, S.G., 2005. Real-Time Freeway Level of Service Based on Anonymous Vehicle Reidentification, *IEEE Transactions on Intelligent Transportation Systems*, vol. 6(2), pp 138 – 146.

Oh, S., Ritchie, S.G., Oh, C., 2002. Real time traffic measurement from single loop inductive signatures, in proceedings of the 81<sup>st</sup> Annual Meeting of the Transportation Research Board, Washington, D.C.

Oh, S., Ritchie, S.G., Oh, C., 2007. An Innovative Single-Loop Speed Estimation Model with Advanced Loop Data, in proceedings of the 86<sup>th</sup> Annual Meeting of the Transportation Research Board, Washington, D.C.

Park, U., Silva, F., Hou, M., Heidemann, J., Guiliano, G., Wang, X., Prashar, N., 2006. Single- and Multi-Sensor Techniques to Improve Accuracy of Urban Vehicle Classification. Technical Report ISI-TR-2006-614, USC/Information Sciences Institute.

Peeta, S., Zhou, W., Zhang, P., 2004. Modeling and Mitigation of Car-Truck Interactions on Freeways, In *Transportation Research Record: Journal of the Transportation Research Board*, No. 1899, TRB, National Research Council, Washington, D.C., 2004 , pp 117-126.

Pursula, M., Pikkarainen, P., 1994. A neural network approach to vehicle classification with double induction loops, Proceedings of the 17<sup>th</sup> ARRB Conference.

Ritchie, S.G., Park, S., Oh, C., Jeng, S., Tok, A., 2005. Anonymous vehicle tracking for real-time freeway and arterial street performance measurement, California PATH Research Report, UCB-ITS-PRR-2005-9.

Shin, P., Jasso, H., Tilak, S., Cotofana, N., Fountain, T., 2007. Automatic Vehicle Type Classification using Strain Gauge Sensors, Proceedings of the Fifth IEEE International Conference on Pervasive Computing and Communications Workshops, pp. 425-428.

Stamatiadis, N., Allen, D., 1997. Seasonal factors using vehicle classification data, In *Transportation Research Record: Journal of the Transportation Research Board*, No. 1593, TRB, National Research Council, Washington, D.C., 1997, pp. 23–28.

Sun, C., 1998. Use of Vehicle Signature Analysis and Lexicographic Optimization for Vehicle Re-identification on Freeways. 170 pp. Ph.D., Civil Engineering, UC Irvine.

Sun, C., Ritchie, S. G., Tsai, W., Jayakrishnan, R., 1999. Use of vehicle signature analysis and lexicographic optimization for vehicle re-identification on freeways. *Transportation Research Part C: Emerging Technology*, vol. 7, issue 4, pp. 167–185.

Sun, C, Ritchie, S G. and Oh, S. 2003. Inductive Classifying Artificial Network for Vehicle Type Categorization. *Computer-Aided Civil and Infrastructure Engineering*, vol. 18, No 3, pp. 161-172.

Tawfik, A.Y., Abdulhai, B., Peng, A., Tabib, S.M., 2004. Improving the Accuracy of Vehicle Signature Re-identification Using Decision Trees, In *Transportation Research Record: Journal of the Transportation Research Board*, No. 1886, TRB, National Research Council, Washington, D.C., 2004, pp 24-33.

Tok, A., Ritchie, S.G., Jeng, S., 2007. Understanding Commercial Vehicle Travel through New High Fidelity Inductive Sensors, in proceedings of the 86th Annual Meeting of the Transportation Research Board, Washington, D.C.

Tok, A., Jeng, S., Liu, H., Ritchie, S.G., 2008. Design and Initial Implementation of an Inductive Signature-Based Real-Time Traffic Performance Measurement System, accepted for presentation at the 11th International IEEE Conference on Intelligent Transportation Systems (ITSC2008), Beijing, China.

U.S. Department of Transportation (USDOT, 2003), Bureau of Transportation Statistics and U.S. Department of Commerce, Census Bureau, 2002 Commodity Flow Survey: United States (Preliminary) (Washington, DC: December 2003), tables 1b and 1c.

Washington Asphalt Pavement Association (WAPA), 2002. Asphalt Pavement Guide, [http://www.asphaltwa.com/wapa\\_web/modules/04\\_design\\_factors/04\\_loads.htm](http://www.asphaltwa.com/wapa_web/modules/04_design_factors/04_loads.htm)

Wasserman, P. D., 1989. Neural Computing, Theory and Practice. New York: Van Nostrand Reinhold.

Yun, S., White, W. W., Lamb, D. R., Wu, Y., 2005. Accounting for the Impact of Heavy Truck Traffic in Volume-Delay Functions in Transportation Planning Models. In *Transportation Research Record: Journal of the Transportation Research Board*, No. 1931, TRB, National Research Council, Washington, D.C., 2005, pp 8-17.

Zhang, G., Wang, Y., Wei, H., 2006. Artificial neural network method for length-based vehicle classification using single-loop outputs. In *Transportation Research Record: Journal of the Transportation Research Board*, No. 1945, TRB, National Research Council, Washington, D.C., 2006, pp 100-108.